Tampere University

Anna Rekonen

EFFECT OF A-TYPE LAMINS ON NUCLEUS MORPHOLOGY IN EPITHELIAL CELLS

A-tyypin lamiinien vaikutus tuman muotoon epiteelisoluissa

Faculty of Medicine and Health Technology
Master's thesis
07/2020

ABSTRACT

Anna Rekonen: Effect of A-type lamins on nucleus morphology in epithelial cells
Master's thesis
Tampere University
Master's degree programme in Biomedical Technology, specialization in Cell Technology
07/2020

Background and aims: Mechanical forces are known to play essential roles in tissue homeostasis and development. Recently, it has been established that physical forces can travel from the extracellular matrix through the cytoskeleton into the nucleus and deform DNA-associated structures potentially altering gene expression. Lamins are type V intermediate filament proteins that form the nuclear lamina and establish the physical connection between the nucleus and the cytoskeleton. Their functions are not fully understood, but they contribute to nucleus morphology and several cellular processes. Altered nucleus morphology is often a sign of a disease. A-type lamins encoded by the LMNA gene are mainly responsible for nucleus stiffness and morphology, and their mutations are linked to several diseases. The different A-type lamin isoforms result from the alternative splicing of the LMNA gene product pre-lamin A. CRISPR/Cas9 is a novel genome editing tool that can be used to generate knock-out cell models to study the importance of specific genes, such as LMNA. In this thesis, the aims were to establish LMNA knockout cell line and to study the importance of A-type lamins on nucleus morphology. The working hypothesis was that the depletion of A-type lamins leads to irregular nucleus shape.

Methods: LMNA knockout cell line was established using CRISPR/Cas9. In-house pre-designed gRNAs were produced in a liquid bacterial culture and co-transfected into MDCK II cells with a transiently expressed fluorescent Cas9 endonuclease. The fluorescent cells were FACS-sorted, and the knockout was verified by western blot and immunostaining. The effect of pre-lamin A depletion on nucleus morphology was then studied by using wild type (wt) and stably fluorophore-conjugated lamin-A expressing cell lines including lamin A-mutant unable to incorporate into the nuclear lamina as controls. To this end, immunostaining followed by confocal microscopy imaging and data analysis in ImageJ distribution Fiji and Microsoft Excel. A customized ImageJ macro was used to measure the morphological features i.e. aspect ratios of the nuclei, and cell density was analysed by calculating the nuclei in microscopy images. Cell proliferation rate was determined by culturing equal numbers of cells and counting them. Student's T-test with a significance level 0.05 was used as a statistical measure in all the analyses.

Results: LMNA knockout cell line was successfully established by CRISPR/Cas9. The analysis of the nuclear aspect ratio showed, that the pre-lamin A -depleted nuclei were mostly crescent- or donut-shaped, and that their circularity, roundness and solidity differed significantly from those of the wt cells. In addition, N-terminal deletion mutation of 20 amino acids or fluorophore tags in the lamin A protein delayed cell proliferation but didn't remarkably affect the nucleus morphology. Endogenous lamin A expression was mostly unaffected by the LMNA modifications. In support of the hypothesis, the results showed that the depletion of A-type lamins led to an irregular nucleus shape.

Conclusions: To conclude, the results support the hypothesis and demonstrate the importance of A-type lamins on nucleus morphology. The results suggest that the successfully established pre-lamin A knock-out cell line can serve as a model of laminopathies and can be used to study the importance of A-type lamins in cellular processes. It can be speculated if the depletion of A-type lamins affects the nuclear mechanotransduction. Further studies are needed to elucidate the mechanisms of the phenomena as well as the effects of lamin knock-out on other cellular processes, such as mechanical force transmission and gene expression.

Keywords: *LMNA, lamin A, nuclear lamina, CRISPR/Cas9, mechanobiology, nucleus morphology*

The originality of this thesis has been checked using the Turnitin OriginalityCheck service.

TIIVISTELMÄ

Anna Rekonen: A-tyypin lamiinien vaikutus tuman muotoon epiteelisoluissa
Pro gradu -tutkielma
Tampereen yliopisto
Bioteknologian maisteriohjelma, erikoistumissuunta soluteknologia
07/2020

Tutkimuksen tausta ja tavoitteet: Mekaanisten voimien tiedetään olevan tärkeitä kudosten normaalille homeostaasille ja kehitykselle. Viime aikoina mekaanisten voimien on havaittu välittyvän solun ulkopuolelta solutukirangan kautta tumaan asti ja muokkaavan DNA:han sitoutuneita proteiineja, mikä saattaa vaikuttaa geenien ilmentymiseen soluissa. Lamiinit ovat tyypin V välikokoisia säikeitä, jotka muodostavat tumalevyn ja mahdollistavat mekaanisen linkin tuman ja solutukirangan välille. Lamiinien toimintaa ei vielä täysin ymmärretä, mutta niiden tiedetään vaikuttavan tuman muotoon ja useisiin solun toimintoihin. Muutokset tuman muodossa ovat usein merkki sairaudesta. LMNA-geenin tuottamien A-tyypin lamiinien on ajateltu olevan pääasiassa vastuussa tuman jäykkyydestä ja muodosta. Niiden toimimattomuus liittyy useisiin sairauksiin. Eri A-tyypin lamiinit muodostuvat LMNA-geenin tuottaman pre-lamiini A:n vaihtoehtoisen silmukoinnin seurauksena. CRISPR/Cas9 on uusi perimän muokkaustyökalu, jonka avulla voidaan tutkia halutun geenin toimintaa hiljentämällä kyseinen geeni soluista. Tässä pro gradu -tutkielmassa tavoitteina oli perustaa solulinja, josta LMNA-geeni on hiljennetty CRISPR/Cas9 menetelmällä, ja lopulta tutkia A-tyypin lamiinien merkitystä tuman muodolle. Työn hypoteesina oli, että A-tyypin lamiinien puuttuminen johtaa epäsäännölliseen tuman muotoon.

Tutkimusmenetelmät: LMNA-geeni hiljennettiin soluista CRISPR/Cas9-menetelmää hyödyntäen. Etukäteen suunnitellut g-RNA:t tuotettiin bakteeriviljelmässä ja transfektoitiin soluihin elektroporaatiolla yhdessä väliaikaisesti ilmennettävän, fluoresoivan Cas9-endonukleaasin kanssa. Fluoresoivat solut lajiteltiin FACS-menetelmällä, ja LMNA-geenin hiljentyminen varmistettiin western blot - ja immunoleimausmenetelmällä. Lopulta A-tyypin lamiinien vaikutusta tuman muotoon tutkittiin vertailemalla tuman muotosuhteita villin tyypin sekä fluoroforiin liitettyjä lamiini A:ta ilmentäviä solulinjoja kontrollina käyttäen. Analyysi tehtiin immunoleimatuista ja konfokaalimikroskoopilla kuvatuista näytteistä käyttäen ImageJ:n Fiji-ohjelmistoa sekä Microsoft Excel -taulukkolaskentaohjelmaa. Itse tehtyä ImageJ-makroa käytettiin tuman muotomääreiden mittaamisessa, ja solutiheyttä analysoitiin laskemalla tumien määrä mikroskoppikuvista. Solujen kasvunopeutta tutkittiin viljelemällä samat määrät soluja ja laskemalla ne. Studentin T-testiä (p-arvo 0,05) käytettiin kaikissa analyyseissä statistisen merkitsevyyden selvittämiseen.

Tulokset: LMNA -geenin hiljentäminen ja pre-lamiini A -negatiivisen solulinjan luominen onnistui CRISPR/Cas9 menetelmää käyttäen. Hypoteesin mukaisesti pre-lamiini A -negatiivisissa soluissa tumat olivat epäsäännöllisen muotoisia. Ne muistuttivat muodoltaan kuunsirppiä tai donitsia, ja useat niiden muotomääreet, kuten korkeus ja pyöreys, erosivat merkittävästi kontrollisoluista. Sen sijaan fluoroforiin liitettyjä tai N-terminaalisen 20 aminohapon deleetion seurauksena tumalevyyn yhdentymättömän lamiini A:ta ilmentävien solujen tumissa ei juurikaan havaittu muotomuutoksia, mutta solut kasvoivat selvästi hitaammin kuin villityypin solut. Huolimatta mutatoidun tai fluoroforiin liitetyn lamiini A:n ilmentämisestä solujen oman LMNA-geeni-ilmentyminen oli normaalia. Työn tulokset tukivat hypoteesia osoittaen, että A-tyypin lamiinien puutos vaikuttaa tuman muotoon merkittävästi.

Johtopäätökset: Yhteenvetona, työn tulokset tukevat hypoteesia osoittaen A-tyypin lamiinien tärkeyden tuman muodolle. Työ osoittaa, että onnistuneesti perustettu LMNA-negatiivinen solulinja voi toimia tautimallina tutkittaessa A-tyypin lamiinien merkitystä solujen eri toiminnoille. Voidaankin pohtia, vaikuttaako LMNA:n hiljentäminen tuman kykyyn aistia mekaanista voimaa. Lisätutkimuksia tarvitaan sekä A-tyypin lamiinien ja tuman muodon säätelyn välisten mekanismien selvittämiseksi että niiden hiljentämistä seuraavien vaikutusten kartoittamiseksi solun muissa toiminnoissa, kuten mekaanisen voiman välittymisessä ja geenien ilmentymisessä.

Avainsanat: *LMNA, lamiini A, tumalevy, CRISPR/Cas9, mekanobiologia, tuman muoto*

Tämän julkaisun alkuperäisyys on tarkastettu Turnitin OriginalityCheck –ohjelmalla.

ACKNOWLEDGEMENTS

This study was conducted in the research group of Cellular Biophysics in BioMediTech, Faculty of Medicine and Health Technology, Tampere University. First, I would like to thank the group leader and my supervisor Title of Docent Teemu Ihalainen for this opportunity to conduct my thesis work in the group. It was interesting to see what kind of research is carried out in your group as the group name “Cellular Biophysics” doesn’t actually tell very much. I guess I have a better insight of your work now.

Next, I would sincerely like to thank my principal supervisor, PhD Elina Mäntylä for her guidance both during the laboratory work and writing. I really don’t know where you found enough time to guide me as you have so many projects going on, but I’m thankful that you did. You really seem to be motivated on your research which is honorable.

I would also like to thank my friends and family for listening my complaints about my thesis. I guess you have all helped me by simply not getting mad at me even though I’m pretty talented to annoy people. Thank you and my apologies.

Finally, I would like to thank a wooden cottage in Ylläsjärvi for serving as a place to write my thesis when my neighbours made it impossible in my home.

This thesis is dedicated to introverts.

Tampere, 15th July 2020

Anna Rekonen

CONTENTS

ABBREVIATIONS

dN20-LA-EGFP	delta20-lamin A-EGFP cell line
AAV	adeno-associated virus
AFM	atomic force microscopy
AR	aspect ratio
BSA	bovine serum albumin
Cas9	crispr-associated nuclease 9; crispr-associated protein 9
CB	chromobody
cLAD	constitutive lamin-associated domain
Col-I	collagen-I
CRISPRa	CRISPR activation
CRISPRi	CRISPR interference
CRISPR/Cas9	clustered regularly interspaced short palindromic repeats/CRISPR-associated nuclease 9
crRNA	crispr RNA
DBS	double strand break
dCas9	dead Cas9 (catalytically inactive Cas9)
DCM	dilated cardiomyopathy
DNA	deoxyribonucleic acid
ECM	extracellular matrix
EDMD	Emery-Dreifuss muscular dystrophy
EGFP	enhanced green fluorescent protein
EMT	epithelial-to-mesenchymal transition
EPHA2	Ephrin A receptor 2
ERK	extracellular signal-regulated kinase
FACS	fluorescence-activated cell sorting
F-actin	filamentous actin
FBS	fetal bovine serum
fLAD	facultative lamin-associated domain
FPLD	familial partial lipodystrophy
gRNA	guide RNA
HGPS	Hutchinson–Gilford progeria syndrome
HR	homologous recombination
indels	insertions and deletions
INM	inner nuclear membrane
KASH	Klarischt, ANC-1, and SYNE homology
KO	knock-out
LA-CB	lamin A-chromobody cell line
LAD	lamin-associated domain
LA-EGFP	lamin A-EGFP cell line
LA-KO	LMNA knock-out cell line
LA-KO ctrl	wt cells of the LA-KO cell line
LA-KO KO	knock-out cells of the LA-KO cell line
LAP2	lamin-associated protein 2
LAP2α	lamin-associated polypeptide 2α
LBR	lamin B receptor
LINC	linker of the nucleoskeleton and cytoskeleton
MDCK II	Madin-Darby canine kidney II (cell line)
MEM	Minimum Essential Medium
MET	mesenchymal-to-epithelial transition
MTOC	microtubule-organizing center
nCas9	nickase Cas9 with no endonuclease activity
NE	nuclear envelope

nesprin	nuclear envelope spectrin-repeat protein
NET	nuclear envelope transmembrane protein
NHEJ	non-homologous end-joining
NL	Nuclear lamina
NPC	nuclear pore complex
ONM	outer nuclear membrane
PAM	protospacer-adjacent motif
PBS	Phosphate-Buffered Saline
PLA	proximity ligation assay
PS	penicillin-streptomycin
RNA	ribonucleic acid
RNAi	RNA interference
RNP	ribonucleoprotein
Sa Cas9	Cas9 from *Staphylococcus aureus*
sgRNA	single guide RNA
Sp Cas9	Cas9 from *Streptococcus pyogenes*
SUN	Sad1p-UNC-84 protein
TALEN	transcription activator-like effector nuclease
TBST	Tris-buffered saline supplemented with 0.1 % Tween20
tracrRNA	trans-activating crRNA
WT	the studied wild type cell line (passage 9)
wt	wild type cells in general
YAP	yes-associated protein
ZFN	zinc finger nuclease

1. INTRODUCTION

Cells in tissues are exposed to different kind of physical stimuli, e.g. tensile and compressive forces, and environment topographies and rigidities. The mechanical forces are known to play essential roles in both development and tissue homeostasis (Weaver et al. 2009). In a process called mechanotransduction, cells convert external mechanical stimuli into intracellular biochemical signaling (DuFort et al. 2011, Martins et al. 2012). Among the most studied mechano-sensory complexes are the focal adhesions, through which the cytoskeleton is connected to the extracellular matrix (ECM) via integrins, their ligands, and adaptor and signaling proteins (DuFort et al. 2011). Via these mechanical nodes physical forces can influence the cell structure and function. As an example, they can induce reorganization of the actin cytoskeleton resulting in reorganization of cell surface receptors (Weaver et al. 2009, DuFort et al. 2011). It is now emerging that mechanical stress can induce changes in intranuclear structures including the nuclear envelope (NE) -associated proteins and nuclear lamina, and result in nuclear deformation (Dahl et al. 2008, Thorpe & Lee 2017). However, it has remained unclear how these intranuclear mechanosensitive structures contribute to nucleus morphology.

During the recent years it has been established that physical forces are transduced from the ECM through the cytoskeleton into the nucleus and deform DNA-associated proteins potentially leading to changes in gene expression (Martins et al. 2012). The nucleus is tightly mechanically associated with the cellular cytoskeleton via several NE-embedded proteins (Lelièvre 2009, Tytell et al. 2009). These proteins form, among others, the linker of the nucleoskeleton and cytoskeleton (LINC) complex which mediates mechanical forces from the ECM and cytoskeleton through the NE into the nucleus (Martins et al. 2012, Burke & Stewart 2013). The LINCs thus provide a direct mechanical link between the cytoskeleton and the nucleus (Méjat 2010, Martins et al. 2012, Burke & Stewart 2013). The LINC contributes to cellular processes such as cell division, cytoskeleton organization and organelle positioning (Méjat 2010). Mammalian LINC-complexes are composed of nesprins in the outer nuclear membrane and SUN proteins in the inner nuclear membrane (INM) connecting at the perinuclear space and interact with lamins in the nuclear lamina among a number of lamin- and chromatin -associated proteins (Méjat 2010).

Nuclear lamina is a network composed mainly of type V intermediate filaments, called nuclear lamins, and their associated proteins and is located beneath the INM (Méjat 2010, Martins et al. 2012, Burke & Stewart 2013). The nuclear lamins are divided into A- and B-type (Burke & Stewart 2013, Osmanagic-Myers et al. 2015). The A-type lamins are coded by the LMNA gene, and the major A-type lamins expressed in somatic cells are lamin A and lamin C (Burke & Stewart 2013). The nuclear lamina is one of the major components responsible for the nucleus stiffness (Martins et al. 2012). Lamins and their associated proteins interact with the chromatin and have been suggested to participate in controlling gene expression (Martins et al. 2012, Burke & Stewart 2013). Although their functions are not fully understood, lamins are known to be mechanosensitive (Ihalainen et al. 2015) and to contribute to nucleus morphology, DNA replication, RNA transcription, cell cycle regulation, cell differentiation and apoptosis (Méjat 2010).

Altered nucleus morphology is commonly used as a marker of a disease (Dahl et al. 2008, Uhler & Shivashankar 2018). On the other hand, defects in the mechanosensitive structures of the nucleus such as mutations in lamins and their associated proteins are known to cause several diseases, called laminopathies often characterized by muscle defects (Méjat 2010, Martins et al. 2012). In addition, A-type lamin expression is often reduced in cancer (Martins et al. 2012). Although lamins are associated to altered structural features of the nucleus, it is not known what structures actually orchestrate nucleus form and morphology.

By studying nuclear lamins, it is possible to develop disease models and to improve understanding of the lamin-associated diseases. Several cell and animal models with lamin mutations have been developed to study e.g. muscle dystrophies (Kang et al. 2018, Nicolas et al. 2019), aging disorders (Sui et al. 2019, Kristiani et al. 2020) and cancer (Urciuoli et al. 2020). Lamin functionality can be disrupted by creating deletions to the lamin gene leading to the gene knockout, and a novel genome editing tool, CRISPR/Cas9, has been effectively used in this kind of approaches (Chiang et al. 2016, Mattioli et al. 2019, Sui et al. 2019). CRISPR/Cas9 is one of the most rapidly developing genome-editing tools based on factors of the bacterial immune system that enable to cleave the DNA of invading bacteriophages (Hsu et al. 2014). Bacterial CRISPR loci contains repeat sequences known as CRISPR (clustered regularly interspaced short palindromic repeats) and genes associated to them (CRISPR-associated genes = cas genes) (Hsu et al. 2014). The CRISPR repeats are transcribed into RNA molecules that guide crispr-associated protein 9 (Cas9) endonuclease to the genome to cleave its DNA resulting in a frame shift

inactivating the gene (Hsu et al. 2014). Similarly, the engineered CRISPR/Cas9 system consists of a Cas9 endonuclease and a specific guide RNA (gRNA) guiding the endonuclease to a desired location (Wang et al. 2016). CRISPR/Cas9 is a versatile method as it can be easily targeted to multiple sites by changing the gRNA sequence (Wang et al. 2016). As the DNA-binding interaction arises from the Watson-Crick base pairing between the gRNA and the target DNA, CRISPR/Cas9 is a highly specific compared to other endonucleases (Wang et al. 2016).

Previous work has shown that LMNA gene can be knocked out in several human cells using CRISPR/Cas9, and this knockout leads to the misshapen nuclei and altered chromatin organization (Chiang et al. 2016). CRISPR/Cas9 has also been successfully used in Madin-Darby canine kidney II (MDCK II) cells which are the applied model system in this thesis (Karlgren et al. 2017). In this thesis, the importance of A-type lamins for nucleus morphology was investigated. LMNA knockout cell line was established using CRISPR/Cas9 technology, and the effects of the depletion of A-type lamins on nucleus morphology were investigated. Several additional cell lines with different LMNA expression were compared with the knock-out (KO) and wild type (wt) cells in their nucleus morphology. In addition, the effects of LMNA modifications on nucleus morphology and cell growth were investigated.

2. LITERATURE REVIEW

2.1 Nucleus structure and mechanics

2.1.1 Structure of nucleus

The eukaryotic nucleus is physically and functionally separated from the cytoplasm by the NE, a membrane consisting of two continuous lipid bilayers (Dahl et al. 2008, Méjat 2010, Martins et al. 2012, Holaska 2016, Adam 2017). The outer layer of the NE, called outer nuclear membrane (ONM), is directly associated with the endoplasmic reticulum (ER), while the INM surrounds the chromatin (Dahl et al. 2008, Méjat 2010, Martins et al. 2012, Holaska 2016, Adam 2017). Between the two nuclear membranes is the perinuclear space (Martins et al. 2012, Hah & Kim 2019). The NE and nuclear interior, called nucleoplasm, are both structurally and functionally distinct regions (Dahl et al. 2008). In addition to comprising the genome, the nucleoplasm contains several subnuclear bodies, including nucleoli and Cajal bodies (Dahl et al. 2008, Martins et al. 2012). Nucleoli are responsible for ribosomal RNA synthesis and processing (Martins et al. 2012), while Cajal bodies produce enzymatic backbone responsible for the catalysis of the RNA splicing (Sawyer et al. 2016). Nuclear pore complexes (NPCs) are large protein complexes responsible for bidirectional macromolecule exchange between the cytoplasm and the nucleus (Dahl et al. 2008, Méjat 2010, Martins et al. 2012, Holaska 2016, Adam 2017, Hah & Kim 2019). **Figure 1** shows a schematic of the structure of a eukaryotic nucleus.

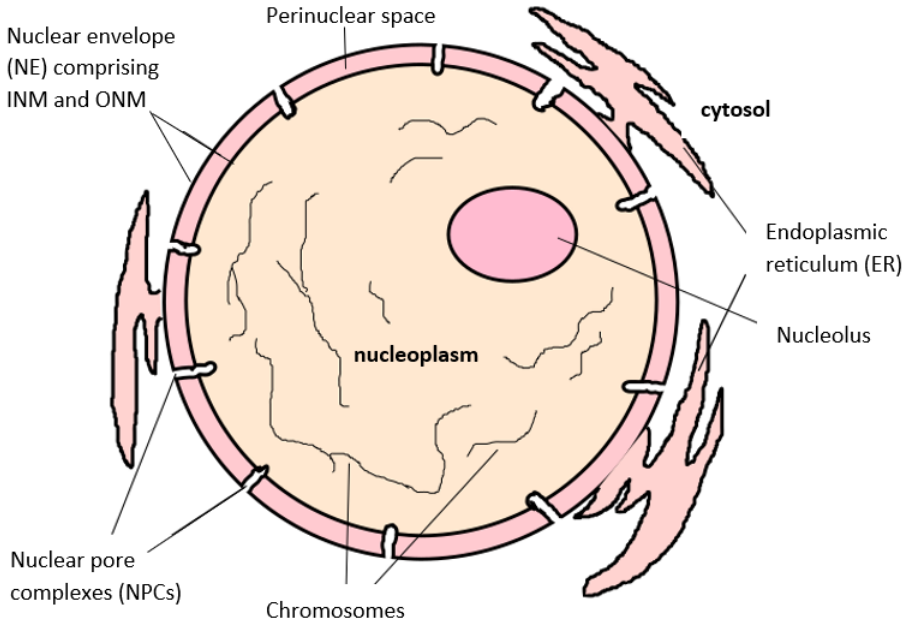

Figure 1. A schematic of the structure of an animal cell nucleus. The nucleus is surrounded by the double-layered nuclear envelope (NE) consisting of inner and outer nuclear membranes (INM and ONM). Nuclear pore complexes (NPCs) span the NE and transport molecules between the cytoplasm and the nucleoplasm. The ONM is continuous with the endoplasmic reticulum (ER) in the cytoplasm. Nucleolus is responsible for ribosomal RNA synthesis and processing. (Redrawn and modified from https://www.earthslab.com/physiology/nucleus/)

2.1.1.1 Nuclear folds

Some cells exhibit smooth-surfaced nuclei, but in the other cells, the nuclei appear as folded (Abe et al. 2004). These folds or invaginations seem to be formed during mitosis when NE breaks down and microtubules penetrate into the nucleus and tear the nuclear lamina (Abe et al. 2004). Sometimes these folds can be formed by other cytoskeletal filaments: actin and intermediate filaments (Jorgens et al. 2017). The significance of nuclear folds is somewhat unclear, but they are suggested to participate in calcium metabolism (Abe et al. 2004, Mauger 2012, Drozdz & Vaux 2017), mRNA export (Abe et al. 2004, Cornelison et al. 2019), nucleo-cytoplasmic transport (Abe et al. 2004) and determination of nuclear morphology (Mauger 2012).

2.1.2 Nuclear mechanics

2.1.2.1 Mechanotransduction and mechanoreciprocity

Mechanotransduction refers to a process in which mechanical stimuli are translated into biochemical and/or electrophysiological signalling in cells (Dahl et al. 2008, Tytell et al.

2009, DuFort et al. 2011, Boyle & Samuel 2016, Thorpe & Lee 2017, Martino et al. 2018, Hah & Kim 2019). The physical forces sensed by the cell can be either external, from the extracellular matrix (ECM), such as shear stress, compression or tension (Dahl et al. 2008, Weaver et al. 2009, DuFort et al. 2011), or hydrostatic pressure (Weaver et al. 2009, DuFort et al. 2011), or internal responses to changes in ECM stiffness (Dahl et al. 2008, Weaver et al. 2009, Helvert et al. 2018). Cells respond to these forces at subcellular, cellular and multicellular levels through ECM-cell surface interactions (Miroshnikova et al. 2017, Helvert et al. 2018). ECM controls tissue boundaries and cell shape, and more specifically, integrin organization, signal transport and adhesion assembly which then influence cell behaviour (Weaver et al. 2009, DuFort et al. 2011). The mechanical properties of the ECM have an impact on cell differentiation and migration (Lelièvre 2009, Weaver et al. 2009, DuFort et al. 2011). The ability of the cell to sense its mechanical microenvironment, including substrate topography, adhesiveness and rigidity along with stress and strain, is called mechanosensing (DuFort et al. 2011, Osmanagic-Myers et al. 2015, Martino et al. 2018). In addition to the cell-ECM connectivity, cell-cell signalling is a critical part of mechanotransduction (Tytell et al. 2009, DuFort et al. 2011). As cells are constantly interacting with their surroundings, their response to physical forces depend on the signals rising from the ECM, neighbouring cells and microenvironment (DuFort et al. 2011). Thus, the intrinsic mechanosensory mechanisms of the cells together with the spatial and physical context from the surroundings determine the response to mechanical stimuli (DuFort et al. 2011). Alterations in the physical environment can lead to significant changes in cell phenotype and behaviour (Lelièvre 2009, DuFort et al. 2011, Osmanagic-Myers et al. 2015).

Mechanical forces are known to be important in tissue development, shaping and homeostasis (Weaver et al. 2009, DuFort et al. 2011, Helvert et al. 2018) as well as in gene expression, cell motility and survival (Weaver et al. 2009). For example, osmotic stress can alter nucleo-cytoplasmic transport which in turn alters cellular signalling because molecular exchange between the nucleus and the cytoplasm is critical in many signalling pathways (Martins et al. 2012). Also, failures in force sensing can give rise to several diseases, including atherosclerosis, arthritis, Hutchinson–Gilford progeria syndrome (HGPS), osteoporosis and cancer (DuFort et al. 2011).

Mechanoreciprocity is a concept closely related to mechanotransduction and refers to a process in which cells respond to physical forces by exerting reciprocal forces, i.e. by actomyosin contractions and cytoskeleton remodelling (Weaver et al. 2009, Boyle &

Samuel 2016, Helvert et al. 2018). Cells exhibit visco-elastic behaviour and will deform time-dependently in response to a physical force and, if the force is removed, return to their original form (Weaver et al. 2009, DuFort et al. 2011, Martins et al. 2012). Thus, mechanoreciprocity is an adaptive process occurring at different magnitudes and time- and length scales, leading to local or global changes in tissue mechanics (Helvert et al. 2018). Mechanoreciprocity is critical for tissue-specific differentiation and development as it maintains tensional homeostasis, and disturbances in mechanoreciprocity can lead to the development of diseases (Weaver et al. 2009, Boyle & Samuel 2016, Helvert et al. 2018).

Mechanical signals from the cell surroundings are essential in determining cell function and gene expression, but cell signalling is, in turn, important regulator of the ECM structure and mechanics (Osmanagic-Myers et al. 2015, Helvert et al. 2018). Physical properties of the ECM can be tuned by the cells in several ways, including alignment of the ECM networks, altering the nanotopography and porosity of the ECM and densification of the ECM (Helvert et al. 2018). Also, force transmission between the cells and the ECM can cause conformational changes in ECM, adhesion and cytoskeletal proteins, revealing novel binding sites and altering protein function, such as signalling status or enzymatic activity (Helvert et al. 2018).

2.1.2.2 Force transmission into nucleus

Cells have specific mechanoreceptors through which they can sense force and respond to it by cytoskeletal contractions, and this response is independent of the type of the force (Weaver et al. 2009). Primary mechanosensors, including integrins, cell-cell adhesion molecules, mechanosensory complexes and stretch-activated ion channels on the cell surface mediate force transformation to biochemical signalling (Dahl et al. 2008, Tytell et al. 2009, DuFort et al. 2011, Osmanagic-Myers et al. 2015, Thorpe & Lee 2017, Martino et al. 2018). Some force-sensing mechanisms are universal, such as stretch-activated potassium channels and transmembrane integrins, while others are tissue-specific, such as primary cilia in the inner ear cells and calcium-gated ion channels in cardiac muscle cells (Weaver et al. 2009). Lately, novel force sensing receptors have been found, including nonselective cation channels Piezo1 and Piezo2 (Lim et al. 2018, Lin et al. 2019). Piezo1 seems to organize endothelial cells in vascular system, while Piezo2 guides mechanical activity in some neuronal cells (Lim et al. 2018). Piezo channels are also necessary for bone formation (Zhou et al. 2020).

Cellular mechanoresponse can be usually induced either via signalling molecules and transcriptional regulators at the plasma membrane causing the activation of stretch-induced cell-adhesion complexes and cytoskeletal filaments or via straight force propagation to the nucleus (Dahl et al. 2008, Martins et al. 2012, Osmanagic-Myers et al. 2015, Miroshnikova et al. 2017, Thorpe & Lee 2017). Some genes can potentially be activated solely via mechanotransduction, whereas others need additional biochemical signalling (Lelièvre 2009, Thorpe & Lee 2017). Mechanoresponsive transcription factors involve MAL-SRF and YAP/TAZ proteins which activity is are regulated by actin (Miroshnikova et al. 2017, Thorpe & Lee 2017). Specific proteins can act as mechanotransducers and shuttle to the nucleus in response to mechanical stimuli, including ZO-1 and β-catenin (Martino et al. 2018). Some of these proteins are physically connected to the focal adhesions in the absence of mechanical stimuli (Martino et al. 2018).

Focal adhesions are one of the most well-known mechanosensory complexes consisting of integrins and several adaptor and signalling proteins, such as vinculin and talin (Tytell et al. 2009, DuFort et al. 2011, Martino et al. 2018). Focal adhesions are responsible for connecting cytoskeletal actomyosin complexes and the ECM (Tytell et al. 2009, DuFort et al. 2011, Martino et al. 2018) External mechanical forces can directly alter the shape, composition and size of these protein complexes, as integrins and other proteins undergo conformational changes, pointing out the correlation between force sensing and biochemical signal transduction (Tytell et al. 2009, DuFort et al. 2011, Martino et al. 2018). Focal adhesion assembly can also be stimulated by the conformational changes of the ECM components in response to a force (Weaver et al. 2009, DuFort et al. 2011, Martino et al. 2018). Whereas the cell-ECM connectivity is mainly mediated by actin and integrins, cell-cell signalling is believed to be cadherin-mediated (Tytell et al. 2009, Thorpe & Lee 2017, Helvert et al. 2018).

Adhesion proteins mechanically bridge the ECM to the cytoskeleton that conveys forces forward to the nuclear envelope (DuFort et al. 2011, Martino et al. 2018, Harris et al. 2018). Similarly, adhesions mediate the signal transmission between neighbouring cells by connecting their cytoskeletons together (Harris et al. 2018). Cytoskeleton is a dynamic protein network consisting of filamentous actin (F-actin), microtubules, intermediate filaments and crosslinking proteins (Martino et al. 2018). Cytoskeleton regulates cellular tensional homeostasis as well as cell motility and shape (Martino et al. 2018). F-actin is a critical component in the cytoskeleton as it is responsible for cytoskeletal contractility together with the myosin, with which if forms complexes called stress fibers

(Martino et al. 2018, Harris et al. 2018). These fibers pull on adhesions and propagate forces from and to the cell interior (Martino et al. 2018). Mechanical forces can activate the cytoskeleton by altering the conformation or polymerization kinetics of the actin-binding proteins, in addition to directly changing actin conformation (Harris et al. 2018).

Most of the characterized cell surface receptors are able to react to biochemical cues, and force-responding receptors, i.e. integrins and cadherins, seem to be a minority (DuFort et al. 2011). However, due to the importance of force sensing in development and homeostasis, many force-sensing receptors remain to be recognized, and some chemically responding receptors may also be able to respond to physical forces (DuFort et al. 2011). Studies have demonstrated the critical role of mechanical environment in organizing cell surface receptors: for example, actin organization, which is influenced by almost all physical forces, ultimately determines the spatial organization of EPHA2 (Ephrin A receptor 2) receptors on the cell membrane, and probably affects the organization of other receptors as well (DuFort et al. 2011). Many molecules involved in biochemical signalling can be also activated by mechanical cues (Lelièvre 2009).

The effect of biochemical signalling in cell fate is well-studied, but the contribution of physical forces to the function and development of tissues is largely unknown (Dahl et al. 2008, Weaver et al. 2009, DuFort et al. 2011). Cells are known to sense mechanical forces and environmental changes on the molecular level, but the force-sensing mechanisms are not yet fully understood (Dahl et al. 2008, Tytell et al. 2009). Due to the crucial role of surface receptors and focal adhesions in the process, studies of mechanotransduction mainly focus on mechanical signalling on the cell surface (Tytell et al. 2009). However, in addition to initiating cell surface signalling cascades, mechanical forces can be conducted from the cell surface along the cytoskeleton into the nucleus (Dahl et al. 2008, Lelièvre 2009, Tytell et al. 2009, Osmanagic-Myers et al. 2015, Thorpe & Lee 2017). In recent years, it has been shown that the NE serves as a mechanosensitive communication interface between the cytoplasm and the nucleoplasm. When cells in tissues are exposed to mechanical force, the NE can change its composition and deform. Nuclear remodeling in response to mechanical cues has been indicated to be important co-regulator in cellular and tissue physiology, and essential driver of cell behavior, development, and disease (Paszek et al. 2005, Engler et al. 2006, Hahn & Schwartz 2009). Studies have demonstrated that extracellular forces applied to the cell surface can induce changes in nucleus, e.g. remodelling of chromatin (Tytell et al. 2009, Weaver et al. 2009, Martino et al. 2018). For example, osmotic stress can induce chromatin condensation and increased nuclear

stiffness (Thorpe & Lee 2017). Chromatin, especially heterochromatin, can also itself be a source of mechanical signalling as it undergoes topological changes particularly during replication and chromosome condensation (Miroshnikova et al. 2017). Mechanical signal transduction is much faster than biochemical signalling which makes nuclear mechanotransduction particularly interesting (Tytell et al. 2009). It appears that mechanosignalling into the nucleus is a critical determinant of the nucleus shape and position (Dahl et al. 2008, Lele et al. 2018).

2.1.2.3 Nucleoskeleton in force sensing

The role of the cytoskeleton as a cellular organizing structure responsible for regulating cellular functions such as mechanics, locomotion and organelle distribution is well-studied, but the concept of nucleoskeleton as an organizer of the nucleus is less familiar (Adam 2017). The idea of the nucleoskeleton or "nuclear matrix" responsible for regulating gene expression and organizing the genome was proposed in 1970s (Adam 2017) and, nowadays, a peripheral nucleoskeleton is known to exist in animal cells, bordering the chromatin mass (Dahl et al. 2008, Adam 2017). This nucleoskeleton is composed of lamins and their associated proteins (Dahl et al. 2008, Adam 2017, Hah & Kim 2019). However, the existence of a load-bearing internal nucleoskeleton throughout the nucleus has not been validated, although many cytoskeletal proteins have lately been identified in eukaryotic nuclei (Dahl et al. 2008, Adam 2017). These proteins include e.g. actin, myosin and spectrin, but it is unclear whether they function as nucleoskeletal structures or have other functions (Dahl et al. 2008, Adam 2017). However, these cytoskeletal proteins are known to participate in genome organization and gene expression regulation in the nucleus (Dahl et al. 2008, Adam 2017). Often, the word "nucleoskeleton" refers to the peripheral nucleoskeleton comprising lamins and other proteins they interact with.

2.1.3 Mechanical linking of nucleus

2.1.3.1 Structural components of the LINC-complex

A protein complex responsible for transducing mechanical signals between the nucleus and the cytoskeleton is called LINC (linker of nucleoskeleton and cytoskeleton), and it is composed of a set of NE embedded proteins including nesprins and SUN proteins (Dahl et al. 2008, Tytell et al. 2009, Adam 2017, Hah & Kim 2019). Nesprins (nuclear envelope

spectrin-repeat proteins) are located in the ONM where their carboxyl-terminal KASH (Klarischt, ANC-1, and SYNE homology) domain binds to SUN (Sad1p-UNC-84) proteins which reside in the INM (Dahl et al. 2008, Tytell et al. 2009, Méjat 2010, Martins et al. 2012, Adam 2017). The SUN proteins in turn bind lamin A in the nuclear lamina (Tytell et al. 2009, Méjat 2010, Martins et al. 2012, Holaska 2016, Adam 2017) and are also bound to the NPCs and chromatin (Tytell et al. 2009, Martino et al. 2018, Hah & Kim 2019). The correct positioning of the SUN proteins is mediated by nuclear lamins (Hah & Kim 2019). Nesprins establish the connection between the nucleus and cytoskeleton by binding to cytoskeletal actin filaments (Tytell et al. 2009, Méjat 2010, Martins et al. 2012, Adam 2017, Hah & Kim 2019), microtubule-associated kinesin and dynein or intermediate filaments (Martins et al. 2012, Hah & Kim 2019) via their amino-terminal domain. Thus, the LINC-complex physically connects the nucleoskeleton, especially nuclear lamins, to the cytoskeleton enabling the transduction of mechanical signals straight to the nucleus (Dahl et al. 2008, Méjat 2010, Holaska 2016, Adam 2017). The importance of LINC-complex in nuclear morphology is indisputable, as it establishes a physical connection between the nucleus and the cytoskeleton and enables signal transmission between the nucleus and cell membrane. Still, short-term activation of mechanosensitive genes is possible even in LINC-deficient cells, indicating that the necessity of LINC-complex in mechanotransduction is still somewhat unknown (Osmanagic-Myers et al. 2015). However, defects in LINC-complex are known to hamper cell migration, polarisation and responsiveness to shear stress (Osmanagic-Myers et al. 2015), and disturb cell division, chromatin dynamics and organelle positioning, among others (Martino et al. 2018). LINC-complex is also responsible for organizing the perinuclear actin cap in nuclear shaping (Khatau et al. 2009). As several variants of LINC proteins have been found in cells, composition of the LINC-complex may be tissue-specific or dependent on the developmental status (Méjat 2010). There is also partial redundancy in LINC components: if individual proteins are mutated, they can sometimes be replaced by the others LINC proteins (Méjat 2010). A schematic of the structure of the lamin and LINC-mediated mechanical linking of the nucleus is shown in **Figure 2**.

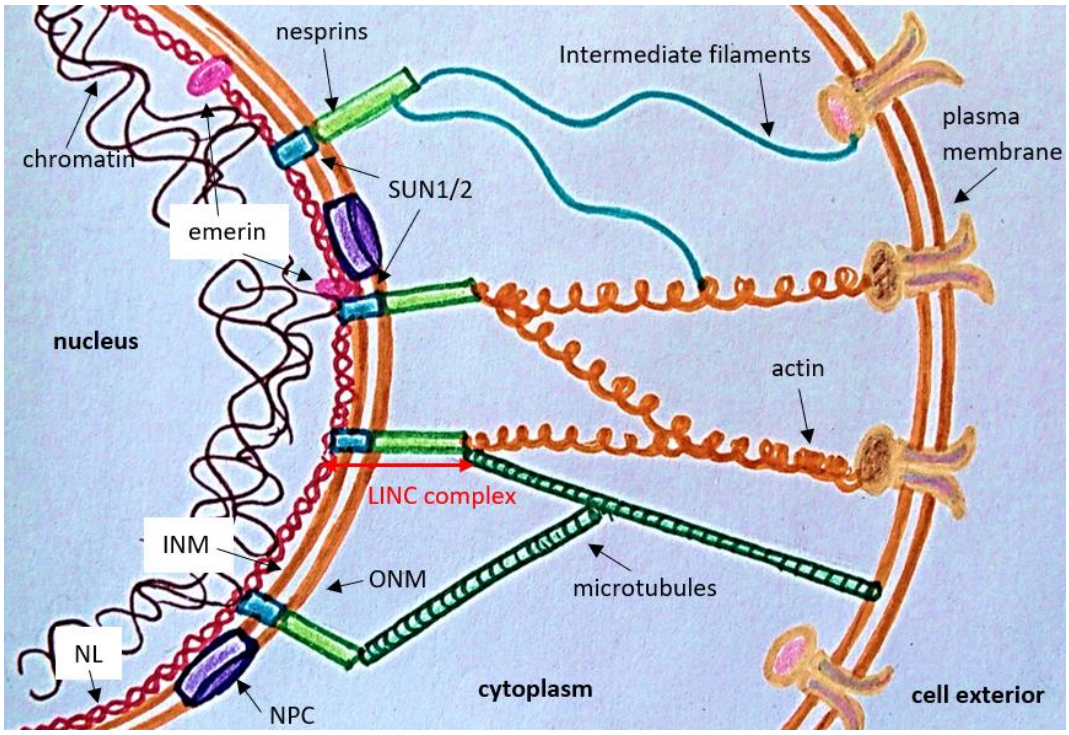

Figure 2. Mechanical linking of nucleoskeleton to the cytoskeleton enables mechanical signalling into nucleus. LINC is composed of SUN proteins on the inner nuclear membrane (INM) and nesprins on the outer nuclear membrane (ONM). Nesprins are attached to the cytoskeletal filaments: actin, intermediate filaments, and microtubules, which are further connected to the plasma membrane of the cell. The SUN proteins interact with nuclear lamins and chromatin within the nucleus enabling transmission of mechanical signals through the cell surface receptors along the cytoskeleton straight to the nucleus (mechanical signalling). Chemically, signals are conveyed to the nucleus through the nuclear pore complexes (NPCs). As demonstrated in the figure, chromatin is directly connected to the nuclear lamina at some points, enabling direct modification of the chromatin structure by the lamina. (Redrawn and modified from Liu et al. 2016)

2.1.4 Nuclear lamina

The peripheral nucleoskeleton is called nuclear lamina (Adam 2017), and it is composed of lamins and lamin-associated proteins (Dahl et al. 2008, Holaska 2016, Adam 2017, Thorpe & Lee 2017). It is a complex protein meshwork located at the INM (Dahl et al. 2008, Osmanagic-Myers et al. 2015, Holaska 2016, Adam 2017, Hah & Kim 2019), and it can be considered as a part of NE (Dahl et al. 2008). The lamina is responsible for nuclear strength, elasticity and rigidity (Osmanagic-Myers et al. 2015, Holaska 2016, Miroshnikova et al. 2017, Hah & Kim 2019), and it's the major load-bearing component of the nucleus (Dahl et al. 2008, Hah & Kim 2019). The lamina can act as a buffer against

physical stimuli originating both from the inside or outside the nucleus (Osmanagic-Myers et al. 2015, Miroshnikova et al. 2017). Lamina also contributes to the integrity of the NE (Martins et al. 2012, Osmanagic-Myers et al. 2015, Helvert et al. 2018, Hah & Kim 2019) and mediates the positioning of NPCs (Thorpe & Lee 2017, Adam 2017). Overall, nuclear response to any mechanical stress is dependent on the structure of the nuclear lamina (Hah & Kim 2019).

2.1.4.1 Structure of nuclear lamins

Nuclear lamins are the main components of the lamina, and they are type V intermediate filament proteins divided into two subtypes, A and B (Dahl et al. 2008, Osmanagic-Myers et al. 2015, Holaska 2016, Adam 2017, Hah & Kim 2019) based on their biochemical nature (Osmanagic-Myers et al. 2015, Adam 2017), sequence similarities, expression patterns and structural features (Osmanagic-Myers et al. 2015). All A-type lamins are encoded by LMNA gene, whereas B type lamins are products of two separate genes, LMNB1 and LMNB2 (Dahl et al. 2008, Méjat 2010, Osmanagic-Myers et al. 2015, Holaska 2016, Hah & Kim 2019). Lamins are the only intermediate filament proteins present inside the nucleus (Adam 2017), and they are found only in metazoan organisms (Osmanagic-Myers et al. 2015, Adam 2017). The expression of lamin isoforms varies between different cell types, but in most cells, both A- and B-type lamins are expressed (Adam 2017, Thorpe & Lee 2017).

Structurally lamins resemble other intermediate filament proteins: they have a tripartite structure with an α-helical rod domain lined by globular N-terminal head and C-terminal tail with an immunoglobulin-like motif that is probably involved in protein-protein interactions (Dittmer & Misteli 2011, Osmanagic-Myers et al. 2015, Holaska 2016). In vitro, lamins interact with each other through their rod domains to form coiled-coil dimers which further organize into polar head-to-tail polymers (Méjat 2010, Dittmer & Misteli 2011, Adam 2017). In in vitro assembly experiments, the polymers constitute paracrystalline arrays, but this organization hasn't been detected in living cells, and the cellular lamin assembly is somewhat unclear (Osmanagic-Myers et al. 2015, Adam 2017). Still, the ability to form higher-order structures seems to be critical for most lamin functions (Osmanagic-Myers et al. 2015). In vivo, A- and B-type lamins seem to form separate but interconnected networks (Dahl et al. 2008, Osmanagic-Myers et al. 2015, Holaska 2016, Adam 2017, Nmezi et al. 2019), even though heterodimerization of the different types of

lamins is possible in vitro (Dittmer & Misteli 2011, Osmanagic-Myers et al. 2015, Holaska 2016, Adam 2017). Albeit A-type lamins and B2 lamins seem to be dependent on B1 lamins in their assembly, each type of lamin can form lamina on their own if the lamin concentration is high enough (Osmanagic-Myers et al. 2015). Still, it is somewhat unclear how lamins are organized in the nuclear lamina at the molecular level (Burke & Stewart 2013, Osmanagic-Myers et al. 2015, Adam 2017).

2.1.4.2 Function of nuclear lamins

Lamins have several important functions in cells: they play a role in DNA replication and repair by supporting protein complexes related to these processes (Dahl et al. 2008, Méjat 2010, Dittmer & Misteli 2011, Osmanagic-Myers et al. 2015, Adam 2017). Lamins are also involved in gene expression (Dahl et al. 2008, Martins et al. 2012, Osmanagic-Myers et al. 2015), nuclear positioning and aging (Dahl et al. 2008, Hah & Kim 2019), cell proliferation, signalling and differentiation (Dittmer & Misteli 2011, Osmanagic-Myers et al. 2015) and apoptosis (Hah & Kim 2019). Lamins can influence several universal and tissue-specific signalling pathways directly or indirectly (Osmanagic-Myers et al. 2015). The direct effects can be either enhancing or attenuating as nuclear lamina can both "trap" the signalling molecules to prevent signalling or serve as a scaffold for efficient signalling reactions (Osmanagic-Myers et al. 2015). Indirectly, lamins can affect cellular signalling by binding to and regulating INM proteins, such as MAN1 and emerin, which are involved in signalling pathways (Osmanagic-Myers et al. 2015). Also, lamins can regulate epigenetic pathways and organize chromatin, e.g. by anchoring heterochromatin to the lamina to hamper its transcription (Osmanagic-Myers et al. 2015, Shevelyov & Ulianov 2019). The interaction between lamins and chromatin can occur via DNA-binding proteins or directly (Thorpe & Lee 2017, Hah & Kim 2019). Cells lacking all nuclear lamins exhibit ruptures in the nuclear membrane and DNA damage, indicating the critical role of functional lamina in nuclear morphology (Chen et al. 2018).

2.1.4.3 Significance of the lamins in nuclear morphology

A- and B-type lamins have different effects on nuclei: A-type lamins are responsible for nuclear viscosity and stiffness, whereas B type lamins confer nuclei with elasticity (Osmanagic-Myers et al. 2015, Thorpe & Lee 2017, Hah & Kim 2019). The importance of A-type lamins comes out mainly during postnatal development, whereas B-type lamins influence cellular processes already during embryogenesis (Dittmer & Misteli 2011, Osmanagic-Myers et al. 2015). Based on a recent study, A-and B-type lamins have only

18% colocalization, demonstrating their different spatial organization (Nmezi et al. 2019). According to the same study, lamin B1 seems to form a sparser meshwork close to the INM, whereas the lamin A/C network beneath it is denser and stiffer. Still, as the different A-type lamins were not separated in the study, the higher stiffness may result from the combination of distinct lamin A and lamin C networks. However, it seems that lamin A/C network tends to form outward protrusions, so called nuclear blebs, and the curvature-dependent and more stress-responsive LB1 network prevents these protrusions (Nmezi et al. 2019). As the effects of A-type lamins on nucleus morphology are the topic of this thesis, they will be discussed further.

2.1.4.4 LMNA gene and A-type lamins

2.1.4.4.1 A-type lamin isoforms

As already mentioned, all A-type lamin isoforms result from the alternative splicing of the LMNA gene product pre-lamin A. Lamin A and lamin C are the predominant isoforms, but two other isoforms also exist: LAΔ10 and another lamin C isoform LC2 which is specific for the germ-line cells (Dittmer & Misteli 2011, Holaska 2016, Adam 2017). Lamin A has been traditionally assumed to influence the most to cellular mechanics, but recently the correlation between lamin C expression and cellular viscoelastic properties has been demonstrated (González-Cruz et al. 2018). Currently, little seems to be known about the minor isoform LAΔ10. However, LAΔ10 expression seems to be inhibited by the expression of progerin, a farnesylated lamin which expression is usually associated with diseases (Al-Qahtani et al. 2019). In this study, genetic depletion of LMNA -guided pre-lamin A was used to create a cell line deficient of A-type lamins.

2.1.4.4.2 Expression and location of A-type lamins

A-type lamins are usually expressed in differentiated cells of vertebrates and Drosophila, but small amounts of them can also be found in mouse embryonic stem cells and preimplantation embryos, indicating that they are present already at the early stages of development (Osmanagic-Myers et al. 2015). However, based on recent studies, A-type lamins are necessary only during postnatal development and not required for the differentiation and proliferation of embryonic cells (Osmanagic-Myers et al. 2015). Even if A-type lamins are expressed in almost all differentiated cells, their expression is pronounced in car-

diac and skeletal muscle (Dahl et al. 2008), and they are completely absent in some terminally differentiated hematopoietic cells (Dittmer & Misteli 2011). In addition, despite the partial colocalization of A- and B-type lamins, lamin B1 is not necessary for lamin A/C network construction (Nmezi et al. 2019).

In addition to comprising nuclear lamina, A-type lamins are also found in the nuclear interior (Dahl et al. 2008, Dittmer & Misteli 2011, Osmanagic-Myers et al. 2015, Holaska 2016, Adam 2017). They are fairly mobile and probably don't polymerize as in the nuclear lamina (Dittmer & Misteli 2011, Adam 2017). These nucleoplasmic lamins form a complex with lamina-associated protein 2α (LAP2α) proteins and regulate pRb/E2F signalling to determine the cell fate, i.e. to affect the differentiation and proliferation of tissue progenitor cells (Osmanagic-Myers et al. 2015, Vidak et al. 2018). Both nucleoplasmic and lamina-associated A-type lamins seem to affect chromatin organization, gene expression and cell signalling, and thus, the cellular phenotype can be significantly altered following changes in the ratio of these two lamin pools (Dahl et al. 2008, Osmanagic-Myers et al. 2015). However, the functions, assembly and regulation of these nucleoplasmic lamins are still mostly unknown (Osmanagic-Myers et al. 2015).

2.1.4.5 Lamin-associated defects

2.1.4.5.1 Laminopathies in general

Defects in the genes encoding NE proteins have been associated with several human diseases, and especially mutations in the LMNA gene coding for A-type lamins cause a variety of tissue-specific diseases (Dahl et al. 2008, Méjat 2010, Hah & Kim 2019). Lamin-related diseases are collectively referred as laminopathies (Dahl et al. 2008, Méjat 2010, Martins et al. 2012, Holaska 2016, Adam 2017, Hah & Kim 2019), and they include around 14 different diseases caused by over 400 identified mutations (Osmanagic-Myers et al. 2015). In contrast, only a few pathogenic mutations have been identified in lamin B genes, probably because mutations in these genes usually lead to embryonic death (Dahl et al. 2008, Osmanagic-Myers et al. 2015). LMNA mutations that lead to disease development are usually autosomal dominant and result in changes in single amino acids in A-type lamins (Dahl et al. 2008, Osmanagic-Myers et al. 2015, Adam 2017). These mutations can disturb lamin folding, assembly and stability or alter its biochemical properties (Osmanagic-Myers et al. 2015, Martino et al. 2018).

Most laminopathies damage especially muscle tissue (Méjat 2010, Osmanagic-Myers et al. 2015, Adam 2017, Martino et al. 2018, Hah & Kim 2019). These kinds of diseases include e.g. Emery-Dreifuss muscular dystrophy (EDMD) and dilated cardiomyopathy (DCM) which harm striated muscle tissue (Méjat 2010, Osmanagic-Myers et al. 2015, Holaska 2016, Martino et al. 2018). In addition to cardiac and skeletal muscle defects, laminopathies can affect neurons, adipocytes and other tissues (Méjat 2010, Osmanagic-Myers et al. 2015, Holaska 2016, Martino et al. 2018). Some non-muscle tissue -related diseases include a lipodystrophic disorder called familial partial lipodystrophy (FPLD) and an aging disorder HGPS (Méjat 2010, Osmanagic-Myers et al. 2015, Holaska 2016, Adam 2017, Martino et al. 2018).

Two hypotheses have been traditionally proposed to explain the nature of laminopathies, referred as structural hypothesis and gene regulation hypothesis (Dahl et al. 2008, Méjat 2010, Osmanagic-Myers & Foisner 2019). According to the structural hypothesis, dysfunctionality of A-type lamins increases nuclear fragility leading to cell death in load-bearing tissues, while altered transcription regulation is seen as the disease-causing factor in gene regulation hypothesis (Dahl et al. 2008, Méjat 2010, Osmanagic-Myers & Foisner 2019). Nowadays, these two hypotheses can be combined into a single disease model as the nuclear organization and gene expression regulation are known to be connected through mechanotransduction (Osmanagic-Myers & Foisner 2019).

2.1.4.5.2 Typical features of laminopathies

Despite the versatility and tissue-specificity of laminopathies, they usually share some common features including nuclear instability, abnormal cytoskeletal structure, and defects in force transmission between nucleoskeleton and cytoskeleton (Dahl et al. 2008, Martins et al. 2012, Thorpe & Lee 2017, Hah & Kim 2019) as well as altered cellular and nuclear stiffness and heterochromatin organization (Martins et al. 2012, Thorpe & Lee 2017). This leads to defects in loadbearing at the nuclear level which decreases the tolerance of the cells against physical forces (Dahl et al. 2008, Martino et al. 2018, Hah & Kim 2019). Lamin A/C deficiency can also cause mislocalization of NPCs (Holaska 2016, Thorpe & Lee 2017) and fragility of the NE (Miroshnikova et al. 2017). Thus, disturbations in the nucleo-cytoskeletal connectivity are the key factor altering nuclear mechanics and leading to an abnormal behaviour in cells (Martino et al. 2018, Hah & Kim 2019).

The wide variety of laminopathies can be explained by the key roles lamins have in general nuclear morphology and several essential cell processes including cell differentiation, apoptosis and cell cycle regulation (Méjat 2010). Abnormal production of A-type lamins disturbs mechanotransduction signalling and makes the nuclei sensitive to mechanical stress (Méjat 2010, Osmanagic-Myers et al. 2015, Thorpe & Lee 2017, Martino et al. 2018, Hah & Kim 2019) and impairs overall cell survival (Tytell et al. 2009, Méjat 2010, Miroshnikova et al. 2017, Thorpe & Lee 2017). Lamin-deficient cells exhibit altered shape, size, dynamics and nuclear stiffness (Hah & Kim 2019). Therefore, studies on nucleus morphology and the regulation of nucleus size are important and provide information for design of related therapies.

2.1.4.5.3 Lamin deficiencies and cancer

Abnormalities in nuclear morphology and defects in the expression of nuclear proteins are many times indicators of cancer (Dahl et al. 2008, Weaver et al. 2009, Martins et al. 2012, Uhler & Shivashankar 2018). The expression of A-type lamins is reduced in several cancers leading to more deformable nuclei, which facilitates metastasis (Martins et al. 2012). Altered nuclear stiffness is often manifest of metastasis potential in tumor cells (Dahl et al. 2008, Weaver et al. 2009, Helvert et al. 2018, Martino et al. 2018), and integrin expression is often altered in cancers (Dahl et al. 2008, DuFort et al. 2011, Martino et al. 2018). Disturbances in mechano-reciprocity may lead to continuous mechanosignalling, which facilitates the formation of mechano-responsive cancers, e.g. breast and skin cancer (Weaver et al. 2009, Boyle & Samuel 2016). High stiffness of the ECM promotes events such as growth factor signalling, invadopodia formation and cell migration, contributing to stemness and survival potentially leading to cancer progression (Helvert et al. 2018).

2.1.4.5.4 Other lamin-mediated defects

As lamins are in close contact with other LINC proteins, mutations in lamin-associated proteins, such as emerin or other proteins in the LINC-complex, often cause similar disease phenotypes to LMNA-related diseases (Méjat 2010, Osmanagic-Myers et al. 2015, Holaska 2016). For example, lamin A/C deficiency and defects in LINC-complex both cause similar defects in 3D cell migration, probably by actin network re-organization (Khatau et al. 2012). Alterations in the ECM structure may result from the defective lamin expression, compatible with the increased collagen production as a typical feature in several laminopathies (Osmanagic-Myers et al. 2015). Due to the interconnection between

lamins and LINC-complex, the effects of lamin depletion are often far-reaching. As the positioning of Sun2 is dependent on A-type lamins, defective lamin signalling can lead to Sun2 mislocalization, which further causes nesprin-1 mislocalization, as Sun2 is responsible for nesprin-1 positioning (Méjat 2010, Martino et al. 2018). This suppression of nucleo-cytoskeletal connectivity can cause overexpression of Sun1 proteins in the NE and Golgi apparatus leading to cellular toxicity and herniation (Hah & Kim 2019). Lamins are needed for the correct localization of emerin: if the interaction with lamins is absent, emerin mislocalizes to the ER instead of the INM (Holaska 2016). Specific LMNA mutations also cause clustering of NPCs leading to defective nuclear transport which can contribute to pathological conditions (Holaska 2016). Defects in lamin function also disrupt the desmin meshwork causing nuclear deformation and contractile dysfunction (Hah & Kim 2019). The perinuclear actin cap is missing in lamin A/C deficient cells, indicating the critical role of A-type lamins in nuclear shaping (Khatau et al. 2009). Similar effects can be detected if the LINC-complex is disrupted, highlighting the interaction between the LINC-complex and nuclear lamina (Khatau et al. 2009). Thus, the effects of LMNA deficiency are not restricted to the nuclear lamina and nucleus shape but affect all mechanical interactions in the cell.

2.2 Nucleus morphology

2.2.1 Cytoskeleton and nucleus morphology

Cytoskeletal filaments, especially actin and microtubules, participate in the maintenance of nuclear morphology (Osmanagic-Myers et al. 2015, Thorpe & Lee 2017, Uhler & Shivashankar 2018, Hah & Kim 2019). Contractile forces originate from actomyosin activity, while microtubules are the source of compressive forces (Uhler & Shivashankar 2018). Microtubules seem to be of specific importance in maintaining normal nuclear morphology in the presence of A-type lamins, and the abnormalities resulting from LMNA knockout seem to be executed by microtubules (Tariq et al. 2017, Arias-Garcia et al. 2019). They also push against NE, and these pushing forces can alter chromatin organization and probably gene expression as well, but this hasn't been validated (Martins et al. 2012).

Cytoskeletal actin is also important for correct nuclear morphology as it controls the nuclear shape in a perinuclear actin cap which is composed of actin filament bundles and phosphorylated myosin II (Khatau et al. 2009). This cap is connected to the lamina via

nesprins and SUN proteins and seems to be regulated by different pathways than the basal actin stress fibers (Khatau et al. 2009). In addition to nuclear shaping, the cap seems to also have a role in stem cell differentiation, cellular 3D migration and ECM remodelling (Khatau et al. 2012). The cap prevents nuclear deformation in the presence of A-type lamins but fails to protect nuclei in LMNA-deficient cells (J. Kim, Louhghalam, Lee, Schafer et al. 2017). In general, nuclear shape is correlated with the cell shape, indicating that the cell shape regulates nuclear shaping (Khatau et al. 2009, Lelièvre 2009). The ability of the actin cap to control nuclear shape depends critically on actin assembly, but the actomyosin contractility has also an effect on the nuclear shape regulation (Khatau et al. 2009), and sometimes the abnormal nucleus morphology of the LMNA-deficient cells seems to be induced by actin instead of microtubules (Takaki et al. 2017). Cytoskeletal actin influences nuclear membrane tension and volume (Helvert et al. 2018). Thus, the nucleus morphology is determined by both the nuclear lamina and cytoskeletal filaments.

2.2.1.1 Nuclear actin in controlling nucleus force response

Lately, the role of nuclear actin in maintaining the integrity of the nucleus by forming a visco-elastic network stabilizing nuclear bodies and ribonucleoprotein droplets, such as nucleoli, has begun to emerge (Miroshnikova et al. 2017). Nuclear actin seems to facilitate mRNA transcription, processing and export, and nuclear actin and myosin may regulate gene expression by moving the chromosomes, but the role of nuclear actin is still somewhat unclear (Adam 2017). Nuclear lamins and nuclear actin seem to work together in tuning nuclear response to mechanical forces (Miroshnikova et al. 2017). During cell migration through narrow pores, lamin A expression is reduced to make the cell more deformable, but simultaneously leaving it more susceptible to mechanical damage (Miroshnikova et al. 2017). Actin assembly seems to compensate lamin A loss in these situations and offering enough mechanical protection for the migrating cells (Miroshnikova et al. 2017). The balance between actin and lamin A expression is important, as reduced lamin A expression can lead to decreased cell survival in long period and excessive deformability can cause cancer (Miroshnikova et al. 2017).

2.2.2 Lamins and nucleus morphology

The mechanical response of the nucleus in mostly regulated by A-type lamins, and the more expressed A-type lamins are, the stiffer is the tissue (Lammerding et al. 2006, Dahl et al. 2008, Helvert et al. 2018, Hah & Kim 2019). A-type lamins participate in epigenetic

regulation and organization of higher-order chromatin structure, e.g. by anchoring heterochromatin to the lamina (Webster et al. 2009, Osmanagic-Myers et al. 2015, Ranade et al. 2019). They are involved in DNA replication and probably stabilize the replication fork (Adam 2017). The interaction between lamin A and chromatin can be either direct or mediated by other proteins like emerin (Tytell et al. 2009, Martino et al. 2018, Ranade et al. 2019). A-type lamins are also involved in gene expression modulation and maintenance of the nuclear structure, shape and stability (Dahl et al. 2008, Webster et al. 2009). They are critical in nuclei repositioning and centrosome polarization (Osmanagic-Myers et al. 2015), and overall, they seem to mediate interactions between the microtubules and the nucleus (Tariq et al. 2017). As the expression of A-type lamins regulates nuclear stiffness, A-type lamins are important in cell migration: the lower the lamin A expression levels, the more deformable nuclei and the higher the cell migration speed (Helvert et al. 2018). Enhanced lamin A expression prevents migration but protects the DNA from mechanical damage (Helvert et al. 2018). Especially, the A-type lamins are important in 3D migration, whereas they don't seem to have a lot of effect on 2D migration (Khatau et al. 2012). Also, muscle function seems to be critically dependent on lamin A/C expression (Hah & Kim 2019), and A-type lamins have a role in cell cycle regulation and apoptosis (Méjat 2010).

Alterations in the mechanical properties of A-type lamins may have several consequences: changes in chromatin organization, which may lead to chromatin accessibility for regulators, detachment of the transcriptionally silent chromatin from the nuclear periphery and signalling alterations between the A-type lamins and other molecules (Osmanagic-Myers et al. 2015). A-type lamins are critical for the localization of emerin in the INM, and this further regulates actin assembly (Osmanagic-Myers et al. 2015). Emerin, on the other hand, controls the expression of ECM components, standing for the fact that mutations in A-type lamins lead to mislocalization of emerin and thus alter the ECM composition (Osmanagic-Myers et al. 2015). The A-type lamins are of particular importance in the maintenance of nucleus morphology (Lammerding et al. 2006, Dahl et al. 2008, Lele et al. 2018, Hah & Kim 2019) which is again demonstrated in this thesis.

2.3 CRISPR/Cas9 genome editing

To study the importance of A-type lamins on nucleus morphology, LMNA gene needs to be either mutated to hamper its activity or knocked out to completely block its function. CRISPR/Cas9 is a novel genome editing tool that has been effectively used to generate KO cell and animal models (Shinmyo et al. 2016, Khan et al. 2018, Nicolas et al. 2019), and the method has been used to study laminopathies, including muscle dystrophies (Kang et al. 2018, Nicolas et al. 2019), aging disorders (Sui et al. 2019, Kristiani et al. 2020) and cancer (Urciuoli et al. 2020). CRISPR/Cas9 has been used both to diminish lamin A expression (Beyret et al. 2019, Santiago-Fernández et al. 2019) and to completely knock out the LMNA gene (Chiang et al. 2016, Mattioli et al. 2019, Sui et al. 2019).

In this thesis, CRISPR/Cas9 is used to knock out the LMNA gene in canine MDCK II cell line. Previously, the method has been successfully used to knock out different genes in this cell line (Simoff et al. 2016, Karlgren et al. 2017, Van Itallie et al. 2018).

2.3.1 Genome engineering

Genome engineering is a process in which genomes, epigenetic marks or transcripts are modified by targeting mutations to specific areas (Hsu et al. 2014). It can be used to study how specific gene contributes to the phenotype of an individual or what happens if the gene is not functional (Hsu et al. 2014, Wang et al. 2016, Chira et al. 2017). Besides basic research, genome editing has potential to be used in therapeutic medicine as well to treat genetic disorders (Hsu et al. 2014, Wang et al. 2016, Carroll 2017, Khan et al. 2018) or to model cancer (Chira et al. 2017). Outside medical research and therapeutical applications, genome engineering can be used e.g. to produce new synthetic materials, to produce pathogen-resistant agricultural crops or to develop sustainable biofuels (Hsu et al. 2014).

Different genome editing strategies have been developed to create KO and knock-in animal and cell models to study the functions of the genes, the first of which being homologous recombination (HR) -mediated mutation targeting based on DNA repair with exogeneous repair template (Hsu et al. 2014, Carroll 2017). Although precise method of manipulating germline cells, the method is very inefficient (Hsu et al. 2014, Carroll 2017) and thus cannot be effectively used in large scale (Hsu et al. 2014).

2.3.2 Programmable nucleases

One of the basic tools of genome engineering are so called programmable nucleases which are often originating from bacteria (Chira et al. 2017). These nucleases can overcome the challenges associated with HR-mediated gene editing: they can be used to edit eukaryotic and mammalian cells with high efficiency (Hsu et al. 2014). All programmable nucleases take an advantage of the fact that by generating targeted double strand breaks (DBSs) in the DNA, it is possible to utilize cellular DNA repair machinery to induce mutations to the genome (Hsu et al. 2014, Khan et al. 2018). When the target DNA has been cleaved by the nuclease, the DNA repair occurs either via HR, if another copy of the DNA template is present, or via non-homologous end-joining (NHEJ) in the absence of the template DNA (Hsu et al. 2014, Hryhorowicz et al. 2017, Carroll 2017, Khan et al. 2018). DNA repair via NHEJ is more error-prone than HR, and thus, random insertions and deletions (indels) are likely to emerge (Hsu et al. 2014, Carroll 2017, Hryhorowicz et al. 2017, Khan et al. 2018). The principles of HR- and NHEJ-mediated DNA repair are shown in **Figure 3**.

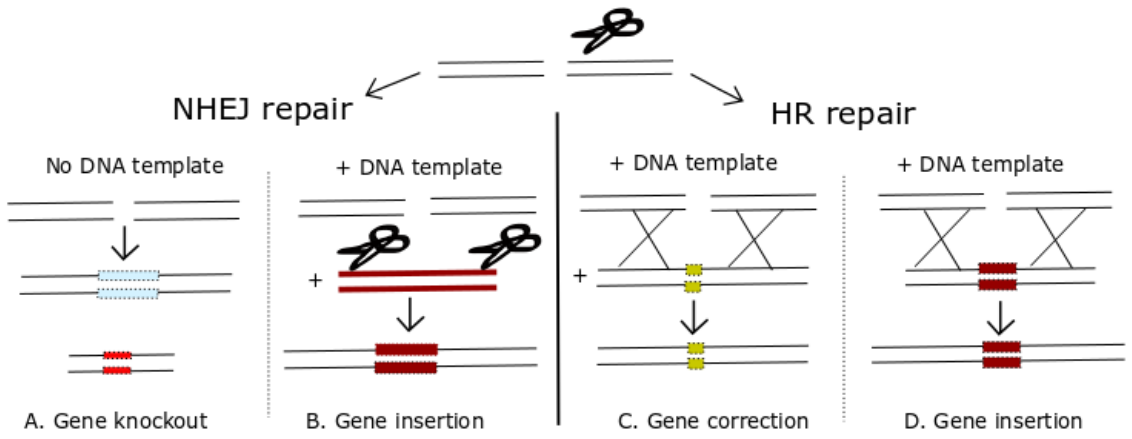

Figure 3. Principles of HR- and NHEJ-mediated DNA repair. If donor DNA template is present, DNA damage is corrected by homologous recombination (HR) leading to original DNA sequence (C.). If no DNA template is available, repair occurs via non-homologous end-joining (NHEJ) leading to insertions and deletions (indels) and possibly gene knockout (A.). Both HR- and NHEJ-mediated DNA repair can be used in genome editing: NHEJ to generate gene knockouts (A.) or to insert functional genes into the genome (B.), and HR to correct genetic errors/mutations (C.) or to insert new functional genes into the genome (D.). (Redrawn and modified from Khan et al. 2018)

Several programmable nucleases have been developed to efficiently modify eukaryotic genomes, including meganucleases, zinc finger nucleases (ZFNs), transcription activator-

like effector nucleases (TALENs) and, most recently, a system called clustered regularly interspaced short palindromic repeats (CRISPR)/CRISPR-associated nuclease 9 (Cas9), abbreviated as CRISPR/Cas9 (Hsu et al. 2014, Wang et al. 2016, Khan et al. 2018). Meganucleases, ZFNs and TALENs recognize their target DNA through protein-DNA interactions (Hsu et al. 2014, Khan et al. 2018). Although efficient tools, these nucleases have some limitations, including laborious manufacturing (Wang et al. 2016, Khan et al. 2018), context-dependent specificity (Hsu et al. 2014) and possible cytotoxicity (Khan et al. 2018). CRISPR/Cas9 is superior to the other nuclease systems in its programmability and simplicity (Chira et al. 2017, Khan et al. 2018) and compared to the other nuclease systems in **Table 1**.

Table 1. CRISPR/Cas9 compared to other nuclease systems (information collected from Wang et al. 2016, Chira et al. 2017, Khan et al. 2018)**.** Each endonuclease system has its limitations, but CRISPR/Cas9 system is the most easily targeted and its costs are low. PAM = protospacer adjacent motif, a short nucleotide sequence near the target DNA.

System	CRISPR/Cas9	ZFNs	TALENs	Meganucleases
Nuclease	Cas9	FokI	FokI	I-SceI
Recognition	RNA-DNA	Protein-DNA	Protein-DNA	Protein-DNA
Cytotoxicity	Low	Low	Variable to high	Low
Cost	Low	High	Moderate/High	Low
Limitations	Off-targets	Constructing expensive and time-consuming	Constructing time-consuming	Limited targeting possibilities
Targeting limitations	PAM needed	Difficult to target non-G-rich regions	T in the start and A in the end of the sequence	Limited versatility in targeting
Design and retargeting	Simple design by altering crRNA sequence; Easy to re-target	Complex molecular cloning required; time-consuming and labor-intensive re-targeting	Protein engineering required; labor-intensive re-targeting	Protein engineering required; Difficult to re-target

2.3.3 CRISPR/Cas9

CRISPR/Cas9 is a relatively new endonuclease system for genome engineering applications. It outshines the other nuclease-based genome engineering platforms by its programmability and cost (Zhang et al. 2016, Khan et al. 2018). The system can be used in basic research to study the functionality of specific genes or in disease modelling, and it has potential to be used in therapeutic applications as well (Zhang et al. 2016, Wang et al. 2016). CRISPR/Cas9 has already been used to manipulate the genomes of several cells, including stem cells, and organisms, including rodents and mammals (Zhang et al. 2016). Many preclinical studies targeting the system to treat human diseases are already ongoing, but some challenges remain to be overcome before the method can be utilized in clinical applications (Zhang et al. 2016).

2.3.3.1 CRISPR/Cas9 as a bacterial immune system

CRISPR/Cas9 is a part of prokaryotic adaptive immune system (Hsu et al. 2014, Wang et al. 2016, Hryhorowicz et al. 2017, Khan et al. 2018). It is composed of the CRISPR locus and crispr-associated genes (Cas genes) (Hsu et al. 2014, Wang et al. 2016, Hryhorowicz et al. 2017, Khan et al. 2018). The components of CRISPR/Cas system were found already in 1987, but its function as a prokaryotic immune defence mechanism was figured out only in 2007 (Hsu et al. 2014, Hryhorowicz et al. 2017). The mechanism was initially found in *Escherichia coli*, but nowadays it is known to be present in around 40 % of sequenced bacterial and 90 % of sequenced archaeal genomes (Hsu et al. 2014, Hryhorowicz et al. 2017).

As a prokaryotic immune defence, CRISPR/Cas works by inserting short DNA sequences of invading viruses or plasmids into the host genome to be transcribed into RNA molecules to direct the elimination of the invaders (Hsu et al. 2014, Wang et al. 2016, Hryhorowicz et al. 2017, Khan et al. 2018). The CRISPR/Cas systems can be divided into two (Wang et al. 2016, Khan et al. 2018) or three (Hsu et al. 2014, Hryhorowicz et al. 2017) classes, and the mostly used CRISPR/Cas system, CRISPR/Cas9, belongs to the second class (Hsu et al. 2014, Wang et al. 2016, Khan et al. 2018) and is mainly discussed here as it is utilized in this study. Whereas several effector proteins are needed for class 1 CRISPR systems to function, only one RNA-guided nuclease is enough to cleave the DNA in the class 2 systems (Wang et al. 2016). The different CRISPR/Cas systems can be further divided into six types (Khan et al. 2018).

The three critical components for the DNA cleavage in CRISPR/Cas9 system and, in other class 2 CRISPR systems (Hsu et al. 2014, Wang et al. 2016), include CRISPR RNA (crRNA) which targets the system to specific location, i.e. to the complementary nucleic acid sequence of the foreign bacteria, Cas9 protein that cleaves the target DNA, and trans-activating crRNA (tracrRNA) which is responsible for the maturation of the crRNA and the formation of Cas9-crRNA complex (Hsu et al. 2014, Wang et al. 2016, Hryhorowicz et al. 2017). DNA recognition is based on Watson-Crick base pairing between the crRNA and its complementary nucleotide sequence in the target DNA (Hsu et al. 2014, Wang et al. 2016, Khan et al. 2018).

The function of CRISPR/Cas system can be divided into different steps (**Figure 4.**) (Hsu et al. 2014, Wang et al. 2016, Hryhorowicz et al. 2017, Khan et al. 2018). In the adaptation or acquisition step, the invader DNA is incorporated into the host CRISPR array (Hsu et al. 2014, Wang et al. 2016, Hryhorowicz et al. 2017, Khan et al. 2018). The foreign DNA segments that are introduced into the host DNA are called protospacers (Hsu et al. 2014, Wang et al. 2016, Hryhorowicz et al. 2017, Khan et al. 2018). In the following crRNA biogenesis step, the genes of the CRISPR locus are expressed to produce a pre-crRNA which matures into a final crRNA with a single spacer (Wang et al. 2016, Hryhorowicz et al. 2017, Khan et al. 2018). In the last interference step, mature crRNA guides the Cas nuclease to the correct location, and the nuclease cleaves the target DNA (Hsu et al. 2014, Wang et al. 2016, Hryhorowicz et al. 2017, Khan et al. 2018).

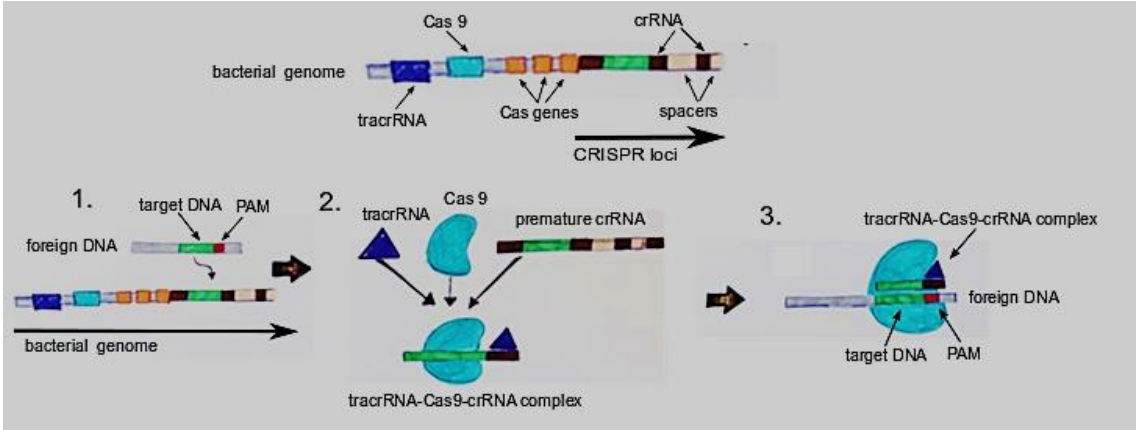

Figure 4. The function of bacterial CRISPR/Cas9 system. CRISPR/Cas9 is a bacterial adaptive immune system which functionality can be divided into three steps. *1. Adaptation:* The target DNA sequence of the foreign invader is inserted into the crispr locus of the bacterial genome. *2. crRNA biogenesis:* The CRISPR genes are expressed, leading to the production of premature crRNA, tracrRNA and Cas9. The tracrRNA mediates the maturation of crRNA, and the complex of mature crRNA, tracRNA and Cas9 is formed. *3.*

Interference: The tracRNA-Cas9-crRNA complex pairs with its target sequence in the foreign invader DNA and cleaves it. The DNA binding is mediated by crRNA and is based on the complementary sequences between the crRNA and the target sequence. The cleavage is mediated by Cas9 nuclease. PAM = protospacer-adjacent motif, crRNA = CRISPR RNA, tracrRNA = trans-activating crRNA, Cas9 = crispr-associated protein 9. (Redrawn and modified from Arora & Narula 2017)

Many CRISPR systems need a sequence-specific protospacer-adjacent motif (PAM) next to the crRNA target site to work properly, and this also applies to the CRISPR/Cas9 system (Hsu et al. 2014, Wang et al. 2016, Zhang et al. 2016, Hryhorowicz et al. 2017, Khan et al. 2018). The PAM sequence is absent in the host DNA and thus, the host genome is protected from self-cleavage (Hsu et al. 2014, Wang et al. 2016, Hryhorowicz et al. 2017). The PAM regions differ between the Cas9 orthologs, and they can be few or several nucleotides in length (Hsu et al. 2014, Wang et al. 2016, Hryhorowicz et al. 2017).

2.3.3.2 CRISPR/Cas9 in genome engineering

CRISPR/Cas9 system is easily programmable and can be targeted to any nucleotide sequence of around 20 nucleotides in size whenever suitable PAM sequence is adjacent the target site (Hsu et al. 2014, Wang et al. 2016, Zhang et al. 2016, Hryhorowicz et al. 2017). Sp Cas9 from *Streptococcus pyogenes* is the mostly used Cas9 in genomic engineering although other Cas9 proteins, e.g. Sa Cas9 from *Staphylococcus aureus*, are sometimes also used (Wang et al. 2016). The Sp Cas9 has a simple PAM region: either NGG or NAG, where N can be any nucleotide, making the targeting of the system easy (Hsu et al. 2014, Wang et al. 2016). The two RNA components of the CRISPR/Cas9 system, crRNA and tracrRNA, can be joined together to construct a single gRNA (sgRNA), and this is often done in genome engineering and other Cas9-utilizing technologies to further simplify the system (Hsu et al. 2014, Wang et al. 2016, Hryhorowicz et al. 2017).

Although the wild type CRISPR/Cas9 machinery works quite well in genome engineering, the system can be modified to enhance its genome editing capabilities (Hsu et al. 2014, Wang et al. 2016, Zhang et al. 2016, Hryhorowicz et al. 2017, Khan et al. 2018). Often, CRISPR systems are used to generate mutations in the target cells to generate knockout cell lines or model organisms (Hsu et al. 2014, Wang et al. 2016, Hryhorowicz et al. 2017). Sometimes, the DNA cleavage and HR-mediated DNA repair are used to knock-in genes to e.g. correct mutations in diseased cells or animals (Wang et al. 2016, Zhang et al. 2016, Hryhorowicz et al. 2017).

One or both nuclease domains of Cas9 can be mutated to modify the functionality of the CRISPR/Cas9 system (Hsu et al. 2014, Wang et al. 2016, Hryhorowicz et al. 2017, Khan et al. 2018). Mutation of one cleavage domain creates nickase Cas9 (nCas9) which only cuts one strand of the target DNA, leaving the other strand intact (Hsu et al. 2014, Wang et al. 2016, Hryhorowicz et al. 2017). This mechanism can be used to enhance the specificity of the DNA cleavage: both strands of the target DNA need their own specific nCas9s for the cleavage to occur, and the probability of having an appropriate DNA sequence for both nCas9s several times in the genome is very small (Hsu et al. 2014, Wang et al. 2016, Hryhorowicz et al. 2017). This process is called double-nicking strategy, and it enhances the specificity and minimizes off-target activity of the DNA cleavage (Hsu et al. 2014, Hryhorowicz et al. 2017).

If both nuclease domains are inactivated, Cas9 loses its DNA cleaving ability, but can still specifically bind to its target DNA when used together with the sgRNA (Hsu et al. 2014, Wang et al. 2016, Hryhorowicz et al. 2017, Khan et al. 2018). This catalytically inactive dead Cas9 (dCas9) system can be utilized in site-specific epigenetic and genetic regulation without the DNA cleavage (Hsu et al. 2014, Wang et al. 2016, Hryhorowicz et al. 2017, Khan et al. 2018). This is useful as it enables transient activation or inhibition of gene expression without any permanent changes to the genome. For example, dCas9 can be combined with transcriptional activators, such as VP64, to enhance transcription of a specific gene (CRISPR activation, or CRISPRa) or with transcriptional repressors to prevent transcription of a selected gene (CRISPR interference, or CRISPRi) (Hsu et al. 2014, Wang et al. 2016, Hryhorowicz et al. 2017, Khan et al. 2018). CRISPRi functions similarly to RNA interference (RNAi) and inhibits gene expression by preventing the RNA polymerase from reading the DNA (Hsu et al. 2014, Wang et al. 2016, Hryhorowicz et al. 2017, Khan et al. 2018). CRISPRi works as such in prokaryotic cells without additional modifications, but efficient knock-down of gene expression in eukaryotic cells usually requires fusion with repressor domains (Hsu et al. 2014, Wang et al. 2016, Khan et al. 2018). CRISPR/Cas9 system can also be utilized in live cell imaging to study the genomic organization in living cells or in chromatin immunoprecipitation to study specific protein-genome interactions (Hsu et al. 2014, Wang et al. 2016). Even though the CRISPR system is mostly used to target DNA, the system seems to be suitable for RNA targeting as well: at least, the system can recognize some mRNAs that are used to construct bacterial lipoproteins and cleave them (Wang et al. 2016).

2.3.3.3 Delivery of CRISPR/Cas system

CRISPR/Cas9 system can be delivered into the target cells by several viral and non-viral mechanisms, and the best delivery method depends on the target cell type and the assay (Hsu et al. 2014, Wang et al. 2016, Campenhout et al. 2019). The viral methods include lentiviruses, adenoviruses and adeno-associated viruses (AAVs) (Khan et al. 2018). In non-viral delivery, possible methods include electroporation, lipid-mediated transfection, hydrodynamic delivery and induced osmocytosis, among others (Wang et al. 2016, Khan et al. 2018). If non-viral delivery is used, the CRISPR/Cas9 components can to be packed into non-viral plasmids or delivered as ribonucleoprotein (RNP) complexes (Wang et al. 2016, Khan et al. 2018, Campenhout et al. 2019).

AAV-based vectors are ideal viral vectors for gene therapy as they are non-pathogenic and cause only mild immune response (Hsu et al. 2014, Wang et al. 2016). In addition, they can be also targeted to non-dividing cells (Wang et al. 2016). However, the CRISPR/Cas9 system is large in size and thus not easily packaged into AAV vectors (Hsu et al. 2014, Wang et al. 2016). Of the non-viral delivery methods, microinjections, lipid-mediated transfections and electroporation work usually well, and electroporation enables the delivery of CRISPR/Cas9 system also into primary cells and stem cells (Wang et al. 2016). By electroporation, targeted mutations can be induced into the cells with minimal off-target activity (Wang et al. 2016). RNP-based delivery is another non-viral method to deliver the endonuclease with high fidelity and low toxicity (Wang et al. 2016).

2.3.3.4 Design and current limitations of CRISPR/Cas9 systems

Although a very promising technology, CRISPR/Cas9 still has some limitations that need to be considered. One major issue is the safety: as the target DNA sequence together with its corresponding PAM may exist several times in the genome, there's a possibility of off-target cleavage (Hsu et al. 2014, Wang et al. 2016, Zhang et al. 2016, Hryhorowicz et al. 2017, Khan et al. 2018). Cas9 can tolerate some mismatches, so the off-target activity doesn't even require exact sequence similarities (Zhang et al. 2016, Hryhorowicz et al. 2017). This off-target activity can be decreased e.g. by optimizing sgRNA design, using paired Cas9 nucleases instead of just one nuclease, optimizing Cas9-sgRNA concentration or by controlling Cas9 activity (Zhang et al. 2016, Wang et al. 2016, Hryhorowicz et al. 2017). However, reduction of the off-target activity many times deteriorates the efficiency of the genome editing (Wang et al. 2016, Hryhorowicz et al. 2017). Spatiotemporal

control of Cas9 activity can be achieved by transcriptional or post-translational regulation, e.g. by using light-inducible systems or by chemically activating the inactivated Cas9 (Hsu et al. 2014, Wang et al. 2016, Zhang et al. 2016), but in these approaches the nuclease activity can't be turned off after the activation (Wang et al. 2016). By splitting the Cas9 into smaller pieces which need to be combined before the cleavage can occur, it is also possible to control Cas9 activity and, besides that, to overcome some size limitations associated with the Cas9 delivery (Hsu et al. 2014, Wang et al. 2016). However, by using the split Cas9, the cleavage efficiency often decreases (Wang et al. 2016).

Although the off-target activity is one of the major challenges of CRISPR/Cas9, other problems and limitations remain. Safe and efficient delivery of the CRISPR/Cas9 system is one challenge even though many viral and non-viral delivery methods are available (Hsu et al. 2014, Wang et al. 2016, Campenhout et al. 2019). Also, for more efficient and targeted genome engineering, DNA repair should occur via HR instead of the error prone NHEJ (Hsu et al. 2014, Wang et al. 2016). Different strategies to overcome this problem and to increase HR:NHEJ ratio in cells include e.g. modification of DNA repair machinery and optimization of the delivery of the CRISPR/Cas9 system (Wang et al. 2016). However, especially in some cell lines, DNA repair tends to occur via NHEJ, and only limited success has been gained in modifying the HR:NHEJ ratio (Carroll 2017).

Based on a previous study, the efficiency of CRISPR/Cas9-mediated knockout is not significantly dependent on the copy number of the target gene, but the potency of the sgRNA is primarily responsible for efficient DNA cleavage (Yuen et al. 2017). The efficiency of CRISPR/Cas9-mediated cleavage is also dependent on the target DNA sequence and sgRNA secondary structure (Zhang et al. 2016). Thus, the sgRNAs need to be carefully planned to get optimal gene editing results. The knockout efficiency is affected by both the sgRNA and Cas9 expression (Yuen et al. 2017). PAM requirements also limit the usage of CRISPR/Cas9: for example, there's no identified PAM which could span any whole genome sequences (Zhang et al. 2016). In summary, several things need to be considered for efficient and specific genome engineering by CRISPR/Cas9.

2.3.3.5 CRISPR/Cas9 as a tool to study the effects of the depletion of A-type lamins on nucleus morphology

The nucleus shape is an important determinant of the cellular function and varies between different cell types (Skinner & Johnson 2017, Thorpe & Lee 2017). Changes in nuclear

shape alter cellular function and genome organization (Jevtić et al. 2014, Thorpe & Lee 2017), and they are often associated with pathological conditions (Jevtić et al. 2014, Mukherjee et al. 2016, Skinner & Johnson 2017). Nucleus morphology is regulated by several factors, including nucleo-cytoplasmic transport, ER, cell cycle and lamins (Mukherjee et al. 2016). Cytoskeletal stiffness is also known to correlate with the nucleus shape, but the mechanisms behind this nucleo-cytoskeletal interplay are unclear (Thorpe & Lee 2017). However, nucleus shape is known to be influenced by cytoskeletal forces, transmitted to the inner nucleus via the LINC-complex and lamina (Lele et al. 2018). Although the mechanisms of nuclear shape regulation are not fully understood, alterations in nuclear shape can possibly induce changes in gene expression and can cause cancer progression (Jevtić et al. 2014).

Lamins are one of the major determinants of the nuclear shape, and their depletion can cause significant alterations in the nuclear morphology (Dahl et al. 2008, Mukherjee et al. 2016, Chen et al. 2018, Hah & Kim 2019). Especially A-type lamins are important for the correct nucleus morphology as they are mainly responsible for nuclear stiffness and response to mechanical forces (Dahl et al. 2008, Osmanagic-Myers et al. 2015, Helvert et al. 2018, Hah & Kim 2019). Several studies have demonstrated that cells without or with mutated A-type lamins exhibit abnormal nucleus morphology (Chiang et al. 2016, Tariq et al. 2017, Hah & Kim 2019) and NE defects (Bank et al. 2011, Capo-chichi et al. 2011, Earle et al. 2020).

CRISPR/Cas9 can be used to specifically knock out genes to study their function, and this method has been successfully used in LMNA knock out (Chiang et al. 2016). KO cell lines have been established by this method to serve as disease models (Roy et al. 2014, Giuliano et al. 2019). In this thesis, epithelial LMNA KO cell line was established by CRISPR/Cas9 to study the importance of A-type lamins on correct nucleus morphology. In addition, the effects of different LMNA modifications on nucleus morphology were investigated by comparing the cell lines with modified LMNA gene to the wt and LMNA KO cells.

As A-type lamins are involved in cellular signalling, proliferation (Dittmer & Misteli 2011, Osmanagic-Myers et al. 2015, Hah & Kim 2019) and DNA replication (Dittmer & Misteli 2011, Osmanagic-Myers et al. 2015, Adam 2017), they can be assumed to affect the proliferation rate and growth density in cells, which can further influence the nucleus morphology (Skinner & Johnson 2017). Nucleoplasmic A-type lamins seem to be particularly important in cell growth regulation (Vidak et al. 2018). Thus, the effects of LMNA

KO or modifications on cell growth density and proliferation rate were also studied in this thesis.

3. OBJECTIVES

The purpose of this study was to establish an epithelial LMNA KO cell line using CRISPR/Cas9 technology and importantly, to study the importance of A-type lamins on nucleus morphology. In addition, the effects of different modifications of the LMNA gene on nucleus morphology were investigated. Also, the growth density and proliferation rate in the cell lines with different lamin A/C expressions were studied.

The aims of the study were:

I. **To construct epithelial A-type lamin knockout cell line using CRISPR/Cas9**
II. **To study the effect of A-type lamin KO on nucleus morphology**

The hypothesis of the study was:

I. **Depletion of A-type lamins leads to irregular nucleus shape in epithelial cells.**

4. MATERIALS AND METHODS

4.1 Cell lines

In this study, Madine Darby Canine Kidney (MDCK) type II cells (generous gift from Prof. Aki Manninen, University of Oulu) were used. From this cell line, CRISPR/Cas9 LMNA KO cell line (abbreviated as LA-KO) was established. In addition, three additional MDCK II cell lines stably expressing fluorescent fusion proteins had been previously established and were studied in this thesis. These included EGFP-tagged lamin A and lamin A mutant cell lines. These cell lines are abbreviated as follows: lamin A -EGFP (LA-EGFP), lamin A chromobody (LA-CB), deltaN20-lamin A -EGFP (dN20-LA-EGFP) and wild type (WT). In this thesis, WT with capital letters refers to the wt cells of this study (passage 9), while the wt refers to the wild type MDCK II cells in general. The features of each cell line are summarized in **Table 2**.

Table 2. The MDCK2 cell lines of this thesis. The LA-KO cell line was established in this thesis and doesn't have freezing information. The rest of the cell lines had been established earlier and were thawed for this thesis work.

Cell line	LA-EGFP	LA-CB	dN20-LA-EGFP	WT	LA-KO
Initial passage	12	14	15	9	14
Date of freezing	14.7.2017, Teemu.I.	21.4.2016, Teemu I.	22.5.2017, Teemu I.	17.11.2019, Elina M.	-
Characteristics	EGFP tag at the C-terminus of the LMNA gene	Lamin A -binding single-chain camelid antibody continuously produced (single H+L chain)	EGFP tag at the C-terminus and 20 amino acids removed from the N-terminus of the LMNA gene.	Wild-type cell line	LMNA gene knock-out

4.2 Cell culture

All cell lines were incubated at 37 °C in a humidified atmosphere containing 5 % CO2. WT cells were cultured in Minimum Essential Medium (MEM; Thermo Fisher Scientific, Waltham, Massachusetts, United States) with 10 % fetal bovine serum (FBS; Thermo Fisher Scientific) and 1 % penicillin-streptomycin (PS; Thermo Fisher Scientific). Other

cell lines were cultured in MEM supplemented with 0.25 mg/ml geneticin (G418; Sigma-Aldrich, Saint Louis, Missouri, USA). All cell lines were passaged once a week, and their media were changed twice a week. In passaging, the cells were washed once with 1X Phosphate-Buffered Saline (PBS; Thermo Fisher Scientific), detached 10-20 min in 0.25% trypsin-EDTA (Thermo Fisher Scientific) and seeded 1:8.

4.3 Establishment of LMNA knockout cell line

4.3.1 In silico analysis of gRNA sequences

Targets for the CRISPR/Cas9 knockout were designed by Elina Mäntylä, Teemu Ihalainen and Eric Dufour against canine LMNA1 gene *(https://www.ncbi.nlm.nih.gov/nuccore/NM_001287151.1,* GeneID:480124). The design of constructs was aimed to produce minimal likelihood of off-target cleavage with the use of an online guide design tool (CRISPR.MIT.EDU). The tool was used to scan the entire canine reference genome (CanFam 3.1) for the presence of sequences similar to each gRNA target site and to score the potential gRNA targets. This was done by assessing the likelihood of off-targets determined by scoring using the total number of mismatches, the position of the mismatch in the gRNA sequence, and the distance between the mismatches. The highest scoring gRNA primer sequences used in gRNA design and abbreviated here as D04 (CACGGTCGATGTAGACCGCC) and D07 (CAAAGCGCGCAATACCAAGA) were selected for the use in CRISPR/Cas9 experiments.

4.3.2 gRNA production

The designed gRNAs were produced in liquid bacterial culture mainly according to the Addgene's protocol (*https://www.addgene.org/protocols/inoculate-bacterial-culture/*). The L-solution for the culture was prepared by diluting LB Broth (Sigma-Aldrich) tablets into distilled water (dH2O) such that 1 tablet was diluted into 48.3 mL of dH2O and autoclaved before usage (121 ̊C, 20 min). Ampicillin (100 ug/mL) (Invivogen, San Diego, California, United States (USA)) was used as a selective antibiotic. The two gRNA cultures were kept in a shaking incubator o/n (37 °C, 250 rpm). As no growth was detected after the o/n incubation, the bacterial growth plates had probably dried, and 50 ul of bacterial glycerol stocks were added to the cultures and the incubation was continued for two more days (200 rpm, 37 °C). The sufficient bacterial growth was ensured by measuring the OD_{600} values with Eppendorf Biophotometer.

Plasmid purification was done according to the Macherey-Nagel's Endotoxin-free plasmid DNA purification (NucleoBond® Xtra Midi EF/Maxi EF) protocol (*https://www.takarabio.com/assets/documents/User%20Manual/Nucleo-Bond%20Xtra%20Endotoxin-Free%20Plasmid%20DNA%20Purification%20User%20Manual%20(PT4042-1)_Rev_06.pdf*) with the following exceptions: in the harvest step, the centrifugation was done using 4300 rpm, 10 min, 4 °C, and the same rotational speed was used in each centrifugation step as it was the maximum speed of the table top centrifuge. The purified plasmids were kept o/n at 4 °C, after which their RNA concentrations were measured with Nanodrop (Thermo Fisher Scientific).

4.3.3 gRNA Transfections

For expression in target cell line, D04 gRNA (nucleotide sequence CAC-GGTCGATGTAGACCGCC) and Cas9 (pCas9-GFP, Addgene, Watertown, Massachusetts, United States (USA)) with transient endonuclease- and GFP-activity were transfected by electroporation with the Neon TM system (Thermo Fisher Scientific). Several transfections with different gRNAs, gRNA concentrations and Cas9 concentrations were used to optimize the protocol, and Thermo Fischer's transfection guidelines (*https://www.thermofisher.com/fi/en/home/life-science/genome-editing/genome-editing-learning-center/genome-editing-resource-library/crispr-validated-protocols/general-crispr-rnp-transfection-guidelines.html*) were utilized in the optimization. For the final transfections, four different transfection mixtures with different number of cells and different amounts of gRNA and pCas9 were prepared (**Table 3**).

Table 3. Optimized transfection mixtures for the establishment of LA-KO cell line. Equal amount of gRNA was used in all transfections, but the number of cells and the amount of Cas9 varied. The LA-KO cell line was established by pooling of transfected cells followed by FACS-sorting.

Tube/mixture	Mix 1	Mix 2	Mix 3	Mix 4
N (cells) *10^6	0.6	1.2	0.6	1.2
m (pCas9) µg	1.5	1.5	2.5	2.5
m (D04 gRNA) ng	300	300	300	300

The cells were trypsinized and counted in a Bürker chamber to obtain 1.2 x 10^6 cells for each transfection. The cells were pelleted (1000 rpm, 4 min, room temperature (RT) 20 ˚C) and resuspensed in R-buffer (Thermo Fischer Scientific; 120 µl buffer/1.2*10^6 cells). Cas9 and gRNA were added to the transfection mixtures as shown in **Table 3**.

Electroporation was performed with the Neon device by using a customised program (1650 V, 20 ms, 1 pulse). The cells were plates into 6-well plates, incubated 24 h and supplemented with a selective antibiotic G418 (0.25 mg/ml, Sigma-Aldrich).

One day post-transfection, the cells were observed under the light microscope to verify the GFP expression (i.e. the succeeding in transfection). Two days post-transfection, the cells were FACS-sorted (BD FACSAria Fusion, BD Biosciences) in the university FACS core (*https://biomeditech.fi/research-infra/flow-cytometry/*) and all the GFP-positive cells were pooled. Following confluency, the cells were subcultured to 6-well plates until full confluency was reached again. After the FACS sorting, medium was changed twice a day and concentration of P/S was increased temporally to 2 % for 1 week to cure possible contaminations.

4.4 Analysis of pre-lamin A expression and nucleus morphology

4.4.1 Validation of knockout and pre-lamin A expression status by western blotting

To analyze for the success of pre-lamin A knockout in LA-KO cells or lamin A expression in LA-EGFP, LA-CB and dN20-LA-EGFP cell lines, these and WT cells grown in similar manner were subcultured 1:3 on 6-wells. Next, the total lysate of each cell line was produced by following the Bio-Rad's protocol (*www.bio-rad.com/webroot/web/pdf/lsr/literature/Bulletin_6376.pdf*). The cells were washed with 1X PBS (Thermo Fisher Scientific), lysed with ice-cold RIPA buffer supplied with HALT protease inhibitor (Thermo Fischer Scientific; 1:1000) and collected into pre-cooled tubes. They were kept in constant agitation (30 min, 4 °C) and centrifuged (16 000 g, 20 min, 4 °C), and protein concentrations were measured with Nanodrop (Thermo Fisher Scientific). The lysates were mixed with dH2O and sample buffer (NuPAGE LDS Sample buffer, Thermo Fisher Scientific; dilution 1:4) to adjust their protein concentrations (1ug/ul) and denaturated (95 °C, 5 min).

Proteins were separated by gel electrophoresis using Invitrogen's Mini Gel Tank system and SDS-PAGE gradient gels (Bolt™ 4-12 % Bis-Tris Plus, Thermo Fisher Scientific). Precision Plus Protein Western C standard (Bio-Rad Laboratories, Hercules, California, United States (USA)) was used as a molecular weight marker (10-250 kDa). Two identical gels (the other used to confirm equal loading of proteins enabling quantification of the results) were run with two parallel samples of each cell line. The gels were run in 1X Bolt buffer (Bolt MES SDS Running Buffer 20X stock solution, dilution 1:20, Thermo Fisher Scientific, 90 V (for the first couple of minutes) and 180 V (for the rest of the run), 400 mA, 35 min) Proteins were transferred to membranes with Bio-Rad's Trans-Blot® Turbo™ Transfer System by using a mixed MW program (7 min, 1.3 A, 25 V).

The membranes were blocked in 3 % bovine serum albumin (BSA) in Tris-buffered saline supplemented with 0.1 % Tween®20 (TBST) (4 °C, o/n, constant mixing) and stained with epitope specific primary antibodies (Lamin A+C, [EP4520] rabbit polyclonal antibody (rPAb, # ab133256), dilution 1:20 000, Abcam, Cambridge, United Kingdom (UK)) and beta-actin [AC-15] mouse monoclonal antibody (mMAb), dilution 1:5000, Abcam) for 1h at RT, followed by incubation with horseradish preroxidase –-conjugated species specific secondary antibodies (goat anti-rabbit IgG (#ab6721), Abcam, and goat anti-mouse IgG-HRP H+L (#62-6520), Thermo Fischer Scientific) (dilution 1:2000). The membranes were rinsed with TBST (3 times, á 5 min) between and after the antibody incubations and stored in dH2O until the detection.

The membranes were incubated (2 min) in detection reagent mixture (Western-Bright™ ECL, K-12045-DN20, advansta reagents, mixed 1:1, 0.1 ml/cm2) and imaged with Bio-Rad's ChemiDoc™ XRS+ Molecular Imager® and Image Lab™ Software. Blot images of the fluorescent lamin A and lamin mutant cell lines were processed with Inkscape, their band intensities were measured with ImageJ and their mean intensities with the corresponding standard deviations were calculated with Microsoft Excel. The values were normalized by dividing them by a specific normalizing factor between 0 and 1. The normalizing factor for each replicate was calculated by dividing the control (beta actin) intensity values by the biggest control intensity value. For the LA-KO cells, the intensity analysis was not done due to corona-virus epidemy and laboratory lockdown.

4.4.2 Validation of knockout and lamin A/C expression status by immunostaining

4.4.2.1 Cell culturing and fixation

Zeiss high-performance 18x18 mm coverslips (0.170±0.005 mm) were coated with collagen-I (ColI; 150 ul/ml, in 0.2 N acetic acid) by using the following protocol: the coverslips were rinsed with dH2O and absolute ethanol and dried in laminar flow hood. Coverslips were incubated with 200 µl ColI in the laminar hood (45-60 min, first 20 min in UV light), rinsed with 1X PBS and stored o/n at 4 ℃. Cells were grown for 7 days on the coated coverslips, and two parallel samples of each cell line were included. Cells were fixed with 4 % paraformaldehyde (20 % PFA, Electron Microscopy Sciences, Hatfield, Pennsylvania, United States (US)); dilution 1:5 into the cell culture medium) for exactly 10 minutes, washed twice with 1X PBS and stored protected from the light at 4 °C until the staining.

4.4.2.2 Immunostaining

Cells were permeabilized in the permeabilization buffer (0.5 % Triton-X, 0.5 % BSA in 1X PBS) for 10 min at RT and incubated with primary antibodies (Lamin A/C mouse monoclonal antibody (#sc-376248, 200µg/ml), dilution 1:500, Santa Cruz Biotechnology, Santa Cruz, California, United States (US); and Lamin B1 rabbit (#ab16048), dilution 1:500, Abcam for the LA-KO samples and Lamin A+C,[EP4520] rabbit polyclonal antibody (rPAb, #ab133256), dilution 1:50, Abcam, for the rest of the samples) for 1h at RT. They were washed three times for 10 minutes: first with the permeabilization buffer, then with the 1X PBS and again with the permeabilization buffer. Secondary antibodies (Alexa Fluor™ 647, goat anti-rabbit (#A21244), ThermoFisher Scientific, and Alexa Fluor™ 488, goat anti-mouse (#A11029), ThermoFisher Scientific, for the LA-KO samples and Alexa Fluor™ 647, goat anti-rabbit (#A21244), ThermoFisher Scientific, for the rest of the samples) (dilution 1:200) were added together with phalloidin (phalloidin-Atto 565 (#94072), dilution 1:50, Sigma, for all samples), and the samples were incubated for 1h at RT in dark. The samples were washed twice with 1X PBS (10 min/wash). LA-KO samples were counterstained with DAPI (1 ug/ml, dilution 1:1000 in dH2O; incubation 10 min), washed (dH2O, 5 min) and mounted with Prolong Antifade (Thermo Fisher Scientific) staining reagent. The rest of the samples were washed (dH2O, 10 min) and

mounted with Prolong Diamond Antifade mounting media with DAPI (Thermo Fisher Scientific). All samples were incubated o/n in dark at RT and stored at 4 °C (in dark) until imaging.

4.4.2.3 Microscopy imaging and deconvolution

The samples were imaged with A1R confocal microscope (image size = 1024x1024, pin-hole = 57.5 µm, optical resolution = 0.26 µm, averaging mode). Z-stacks were taken with 100X oil objective (SR Apo TIRF, NA = 1.5, WD = 120 µm) with the pixel size 0.04 µm and field images with 60X oil objective (Plan Apo VC 60X Oil DIC N2, NA = 1.4, WD = 130 µm) with the pixel size 0.10 µm. One of the two samples of each cell line was imaged per each replicate. Single nuclei were imaged as z-stacks (15 pcs), and field images (5 pcs) with several nuclei were taken of each imaged sample. The LA-KO field images contained around as much the KO and wt control cells which were both present in the cell line in approximately equal portions. The z-stacks were taken from the KO cells and their wt controls separately for correct morphology analysis. The images were taken as single or as multipoint, and deconvoluted with Hyugen's Essential deconvolution program (Scientific Volume Imaging) and saved as single-channel tiff images. The deconvolution templates were customized.

4.4.3 Data analysis with ImageJ and Excel

The number of total and folded nuclei in all field images of the three replicates were calculated manually with Image J. For the field images of LA-KO cell line, the KO and wt cells were first analysed separately (data not shown) but pooled as the LMNA knock-out didn't affect nuclei count or folding (data not shown). The results were collected into Excel, and the percentages of folded and unfolded nuclei were calculated. Two-tailed Student´s T-test with a significance level 0.05 was used to compare nuclei counts between LA-KO, LA-EGFP, LA-CB, dN20-LA-EGFP and WT cells.

To study the morphology of the nuclei, a customised ImageJ macro analysing nucleus shape, circularity and XY/ZY aspect ratios (written by Teemu Ihalainen) was used. For each sample in each replicate, 10 of the 15 z-stack images were analysed resulting in 30 parallel samples for each cell line in total. Mean and standard deviation for each morphological feature in each cell line were calculated in Excel, and bar graphs were drawn

showing the mean as bars and standard deviation as error bars. Student´s T-test with a significance level 0.05 was used as a marker of statistical significance. In the morphology analysis, the KO and wt cells in LA-KO cell line were analysed separately.

4.5 Cell growth density analysis

To determine the growth density of fluorescent lamin A and lamin mutant cell lines, equal numbers of LA-EGFP, LA-CB, dN20-LA-EGFP, and WT cells were cultured for 7 days and counted with Bürker chamber. Two parallel samples of each cell line were included. Averages and standard deviations of the parallel samples were calculated with Excel, and a bar graph was drawn about the results.

5. RESULTS

5.1 Establishment of LMNA knockout cell line by CRISPR/Cas9

The LMNA KO cell line was successfully established by CRISPR/Cas9. The gRNA sequences for pre-lamin A with minimal off-target activity were designed by scanning the canine reference genome and scoring the possible gRNA targets based on their off-target likelihood such that those with the smallest off-target potential got the highest scores. The two highest scoring gRNA primer sequences, abbreviated as D04 and D07, were chosen for the knockout experiments. The selected gRNAs were produced in liquid bacterial culture and purified. MDCKII wt cells were transfected with the pCas9-GFP and gRNA plasmids by electroporation.

Several transfections were needed to optimize the knockout. The transfection efficiency of pCas9 was low, around 12 %, while the Cas9-GFP expression was good and the fluorescence was easy to detect. The GFP activity lasted around 4 days, and even after that, some fluorescent cells could be detected. The construct seemed to localize correctly into the nucleus.

At first, only a few positive cells were detected 24 h post transfection, and their viability was low. Some of the transfected cells were still seeded as single cells in 24-well plate to obtain clones, but very few unhealthy-looking GFP-positive cells were observed one day post-transfection, and even they weren't properly attached. Some of the transfected cells were FACS sorted, but, as the transfection efficiency was low, no GFP-positivity was detected in the cells after the sorting, indicating that the few positive cells were lost during the sorting.

After the optimization of the gRNA and Cas9 amount utilizing the Thermo Fischer's protocol, the transfection efficiency increased, and it was possible to assort enough GFP-positive cells in FACS. Around 200 cells were collected in the sorting, but their well-being remained somewhat obscure. To enhance cell viability and to cure possible contaminations originating from the FACS machinery, the medium was changed twice a day and the antibiotic concentration was increased temporally to 2%. The cells were treated this way a couple of days after the sorting until they seemed healthy.

To validate the success of knockout, the sorted cells were grown for the western blot analysis. In this analysis, the lamin A expression levels of the WT and the LA-KO cells were quantified. The lamin A band of LA-KO cells was lighter than that of the WT cells, which evidenced that the lamin A expression was lowered compared to the WT controls (data not shown). This indicated that the pre-lamin A had been knocked out in LA-KO cells, but the fraction of LA-KO cells remained unknown. To answer this question, the cells were immunostained with lamin A/C and lamin B1 antibodies followed by confocal microscopy imaging. Next, their morphology and expression of lamin A was compared to that of the the WT cells (**Figure 7B**). This revealed the presence of pre-lamin A negative cells with only lamin B expression. The percentage of knockout cells was around 50.62%. Many of the cells were still pre-lamin A positive, but this was determined to be acceptable as they could serve as an endogenous control for quantifying the nucleus shape in these cells.

The knockout cells were passaged successfully, and they stayed viable and could be cultured almost as normal wt cells. The viability of KO cell clones started to decrease after a week's culture period when the cells became more confluent, but the clones were rescued by trypsinising the colonies and spreading the cells. After the colony dispersion, the cells could be cultured as normal wt cells, indicating that the pre-lamin A knock-out didn't significantly decrease cell viability.

Based on this study, LMNA knockout cell line can be established by CRISPR/Cas9 by targeting the N-terminus of the LMNA gene. Electroporation was a suitable transfection method for the Cas9- and gRNA delivery, but optimisation was needed to get the proper transfection efficiency. The LMNA knock-out didn't decrease cell viability but led to significant changes in nucleus morphology.

5.2 Lamin A expression in different cell lines

Western blotting was used to compare lamin A expression between LA-EGFP, LA-CB, dN20-LA-EGFP and WT cells. The blots were stained with lamin A/C antibody and imaged, and the mean lamin A intensities were calculated. Despite the fluorescence tags or other modifications of the LMNA gene in LA-EGFP, LA-CB and dN20-LA-EGFP cells, endogenous lamin A was still effectively expressed in all these cell lines (**Figure 5**). In LA-EGFP and dN20-LA-EGFP cells, an additional band composed of EGFP-tagged lamin A was also visible.

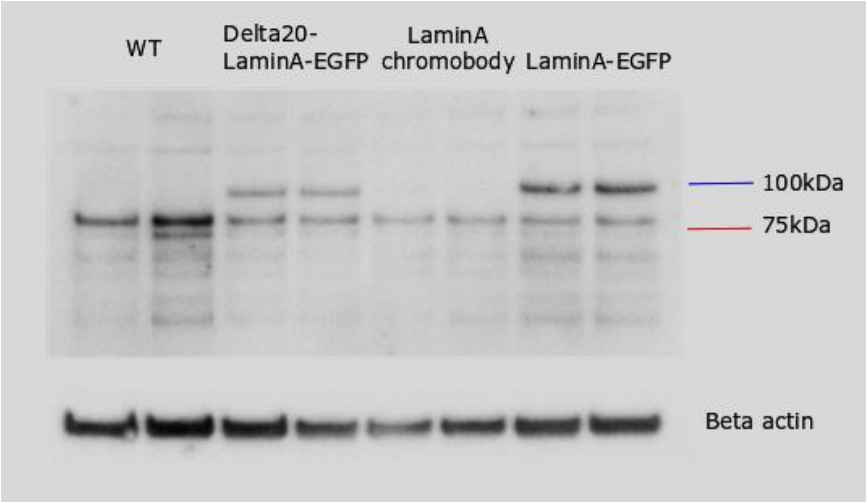

Figure 5. Expression of lamin A in WT, dN20-LA-EGFP, LA-CB and LA-EGFP cell lines. The proteins were detected with lamin A/C antibody to study the lamin A expression. Beta actin was used as a control, and the blotting was done as triplicate with two parallel samples of each cell line in each blot. The lamin A band of size 74 kDa is visible in all cell lines, indicating that the lamin A is expressed in all cell lines despite any modifications of the LMNA gene. Additional band of around 100 kDa in size visible in the dN20-LA-EGFP and LA-EGFP cell lines comprises the EGFP tag (size around 32 kDa) bound to the lamin A. The figure shows the second of the three parallel blots, but similar results were obtained in all blots.

Western blotting showed that the lamin A expression was not affected as a result of the expression of the mutated or GFP-tagged LMNA gene. The differences in beta actin intensities indicate that there are differences in the amount of loaded protein. Sometimes, the intensities of both the beta actin and the lamin A are high, indicating high protein loading, which is the case in the WT samples, especially in the rightmost WT sample (**Figure 5**). However, the intensities of the beta actin don't always correlate with the lamin A intensities. For example, the lamin A intensities of the two dN20-LA-EGFP samples don't seem to significantly differ, but their beta actin intensities do (**Figure 5**). To study whether there were any statistically significant differences in lamin A expression between the cell lines, the band intensities of each sample in the three parallel blots were measured with ImageJ. In the LA-EGFP and dN20-LA-EGFP cell lines, only the endogenous lamin A expression intensity was measured. The intensity values were normalized and collected into the table (**Appendix 1A-B**). The mean normalized intensity values were calculated for each cell line together with the corresponding standard deviations (**Figure 6**).

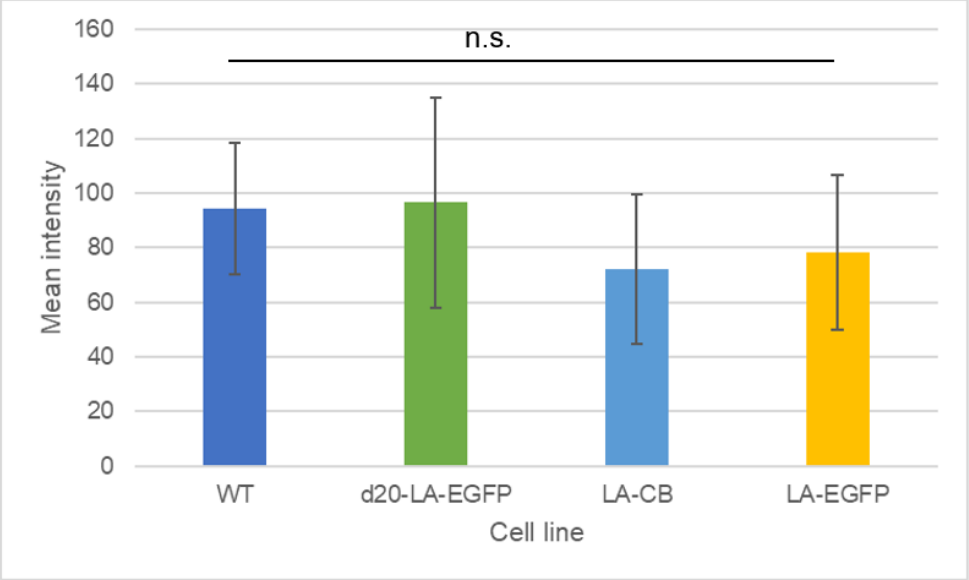

Figure 6. Mean lamin A intensities in different cell lines. The intensity values were calculated as means of three parallel blots, each having two parallel samples. The bars represent the mean normalized intensities and the error bars represent the corresponding standard deviations. There were no statistically significant differences in lamin A expression between any of the samples, indicated here as n.s. ($p \geq 0.05$, Student's T-test, 2-tailed).

Compared to the WT cells, the mean lamin A intensity of LA-CB and LA-EGFP cells was 30.5 % and 20.8 % lowered, respectively. In dN20-LA-EGFP cell line, lamin A intensity was around 2.35 % higher than that of the WT cells, possibly due to lamin A overexpression. However, the deviation within individual samples was high, as indicated by the long error bars in **Figure 6**. Student´s T-test with a significance level 0.05 was used to study whether the differences in lamin A expression between any of the cell lines were statistically significant (**Appendix 1C**). Despite the high percentage differences in lamin A expression, there were no statistically significant deviations in lamin A expression between any of the cell lines. This verified that lamin A expression was not significantly affected by fluorophore-tagging or LMNA gene mutations. Surprisingly, the overexpression of lamin A in LA-EGFP and dN20-LA-EGFP cells didn't reduce the endogenous lamin A expression, contrary to the expectations.

5.3 Effects of lamin A/C expression on nucleus morphology

In order to study the effects of lamin A/C on nucleus morphology, the aforementioned cell lines (LA-EGFP, LA-CB, dN20-LA-EGFP, WT and LA-KO) were fixed and immunostained with lamin A/C antibodies and phalloidin. To study the presence of knock-out cells in LA-KO cell line, these cells were stained with an additional LB1 antibody. Next, the cells were imaged and the nuclear shape descriptors including area, circularity, aspect ratio (AR), roundness and solidity were determined.

Immunostaining was used to visualize lamin A/C expression and nuclei phenotype differences between all the cell lines (**Figure 7**). Based on the immunostaining, there seemed to be differences in both the nucleus size and epithelial maturity.

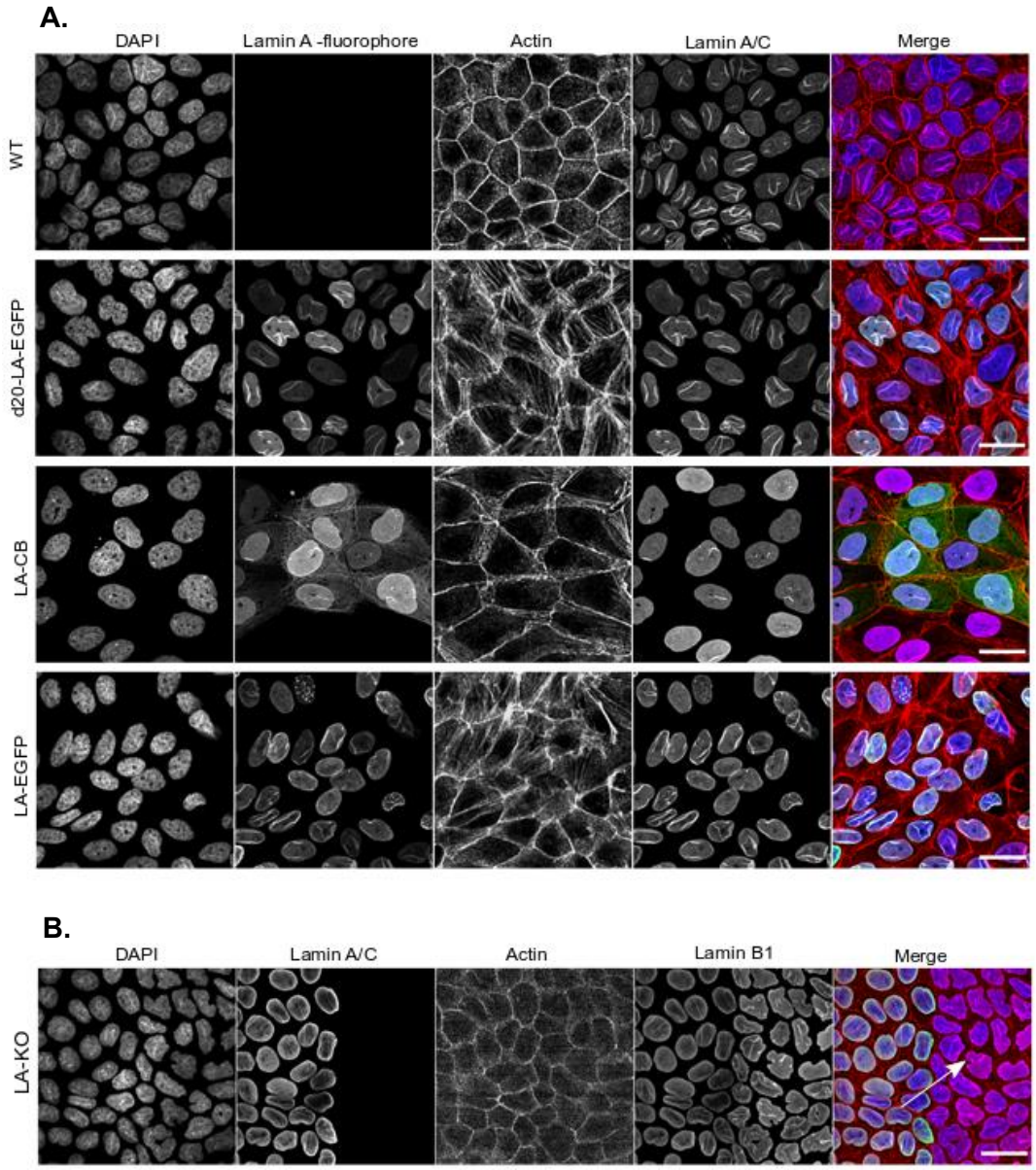

Figure 7. Lamin A/C expression in different cell lines. All cell lines were stained with Lamin A/C antibody to visualize lamin A/C expression. Additionally, LA-KO cells were stained with lamin B1 antibody to detect the KO cells. **A.** In dN20-LA-EGFP, LA-CB and LA-EGFP cell lines, lamin A is stably expressed with a green fluorophore, either GFP (dN20-LA-EGFP and LA-EGFP) or chromobody (LA-CB). GFP expression is restricted into the nucleus, whereas chromobody is also expressed in a filamentous structure within the cytoplasm. **B.** In LA-KO cell line, the morphology of knockout cells (indicated by an arrow) differed clearly from that of the wt controls (cells on the left). The scale bar is 10 μm long.

In LA-EGFP, LA-CB and dN20-LA-EGFP cells, actin cytoskeleton was stretched compared to the WT cells, possibly indicating less dense growth density than in the WT cells (**Figure 7A**). In the WT cells, the nuclei appeared strictly next to one another. There was slightly more space between the nuclei in LA-EGFP and dN20-LA-EGFP cells, and the actin cytoskeleton appeared a bit stretched. This may reflect the maturity of the epithelium: epithelial cells undergo a mesenchymal-to-epithelial transition (MET) during their maturation leading to the acquirement of the typical epithelial cell morphology (Puliafito et al. 2012). Thus, the immature epithelium consists of mesenchymal spindle-shaped cells, instead of having mature, cuboidal cells. The differences in epithelial morphology between the cell lines may result from differences in the epithelial maturity.

There were not clearly visible differences between nuclei size in WT, LA-EGFP and dN20-LA-EGFP cells (**Figure 7A**). In addition, the epithelial morphology seemed similar in LA-EGFP and dN20-LA-EGFP cells based on the microscopy. All cells in the LA-EGFP and dN20-LA-EGFP cell lines seemed more or less fluorescent, indicating that the GFP-tagged lamin was expressed in all cells.

LA-CB cells appeared more different from the WT cells than LA-EGFP and dN20-LA-EGFP both in nuclei size and epithelial maturity. The nuclei seemed to be larger and seemed to have less folds than in any of the other cell lines (**Figure 7A**). The actin cytoskeleton was even more stretched that those of the LA-EGFP and dN20-LA-EGFP cells, and the nuclei appeared far from each other. This indicates that the epithelium was possibly the most immature in these cells. In the LA-CB cell line, all cells didn't exhibit fluorescence at all, and some cells were only slightly fluorescent, indicating that the chromobody (CB)-tagged lamin was not present in all cells. The expression of CB was determined to be 77.07 % of all cells (**Figure 7A, LA-CB panel**). Notably, the cells with bright LMNA-CB signal seemed to have less bright lamin A/C staining signal (**Figure 7A, LA-CB panel**), while the cells without or with low CB expression seemed to have brighter lamin A/C signal. This suggests that either lamin A/C is underexpressed in CB-positive

cells or the lamin A/C antibody binds to the same area with the CB causing antibody blocking in high CB expression levels.

In LA-KO cell line, the nuclei appear near each other like in the WT cells (**Figure 7B**). The lamin A/C expression was restricted only to some cells, indicating the presence of pre-lamin A KO cells in the cell line. The nuclei of KO cells were irregularly shaped, but their density seemed to be similar to that of the wt controls. The actin cytoskeleton appeared less stretched than those of the LA-EGFP, LA-CB and dN20-LA-EGFP cells. Based on the microscopy, LA-KO cells resembled the WT cells more than the other cell lines in their growth density and epithelial maturity (**Figure 7B**).

Most of the nuclei in all the cell lines appeared as folded (**Figure 7**), the percentage of nuclear folding ranging from around 89% to 99% depending on the cell line (**Table 4**). Nuclear folds or invaginations have been detected in several cell lines, but their function remains somewhat unclear, although they may be involved in nucleo-cytoplasmic transport (Abe et al. 2004). Based on the microscopy, LA-CB cells exhibited the smoothest nuclear surface with less folds than the other cell lines (**Figure 7**). The KO cells in LA-KO cell line appeared as highly folded, but clear folds were also visible in the LA-EGFP, dN20-LA-EGFP and WT cells (**Figure 7**).

Table 4. The total and folded nuclei in the cell lines. The number of nuclei (total and folded) were calculated manually from the field images. An example of the calculation is shown in **Appendix 2.** The percentages of folded and unfolded nuclei were calculated for each cell line from the 15 field images. Nuclei/field indicates the average number of nuclei in one field, displayed graphically in **Figure 9**. The percentage of nuclei/WT shows the total nuclei counts divided by the nuclei count of the WT cells. The numbers of total nuclei of LA-EGFP, LA-CB and dN20-LA-EGFP cells are lower than that of the WT, whereas the nuclei count of LA-KO cells is remarkable higher than those of the other cell lines.

Cell line	Total nuclei	Folded nuclei	Nuclei/field	Unfolded nuclei	Percentage of folded nuclei	Percentage of unfolded nuclei	Percentage of nuclei/WT
WT	529	518	35.2	11	97.92 %	2.08 %	100.00 %
LA-EGFP	335	307	22.3	28	91.64 %	8.36 %	63.33 %
LA-CB	200	178	13.3	22	89.00 %	11.00 %	37.81 %
d20-LA-EGFP	410	402	27.3	8	98.05 %	1.95 %	77.50 %
LA-KO	818	807	54.5	11	98.66 %	1.34 %	154.63 %

The effect of the depletion of A-type lamins or LMNA modifications on nucleus morphology were studied in more detail by taking z-stack images of the nuclei and analysing

them using a customized ImageJ macro. The macro calculated several morphological features of the nuclei in both XY and YZ direction, including nucleus area, circularity, AR, roundness and solidity (**Figure 8**). In the morphology analysis, the knockout cells and wt cells of the LA-KO cell line (referred as LA-KO KO and LA-KO ctrl, respectively) were analysed separately. The LA-KO ctrl cells were not pooled with the WT cells as they differed from these cells in several features in the YZ direction.

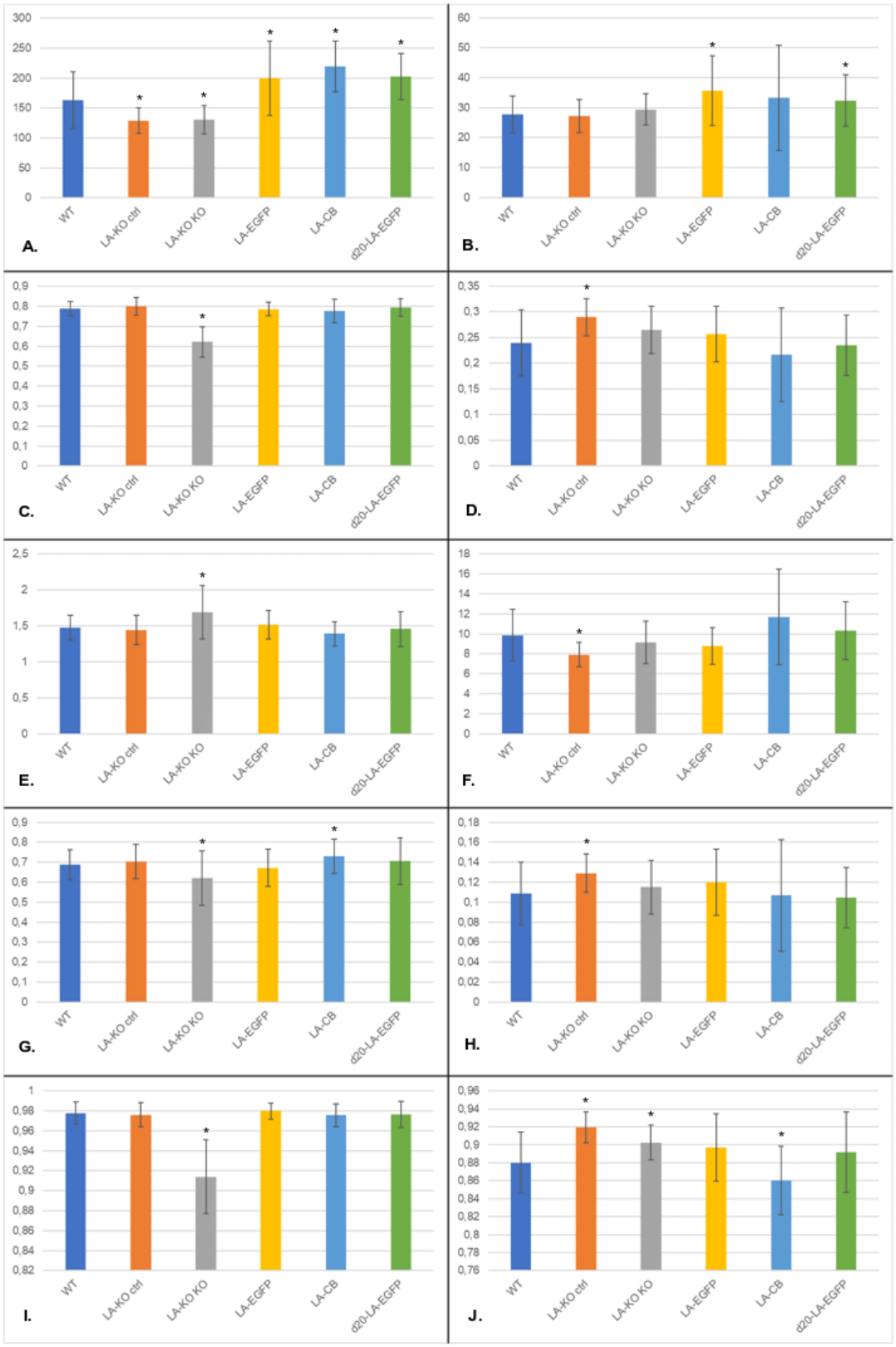

Figure 8. The morphological features of the nuclei. The morphological features of nuclei were measured in both XY and YZ direction in the selected z-stack images with the customized ImageJ macro. The bars represent the means calculated from the 30 values/cell line, and the error bars represent the standard deviations. LA-KO KO and LA-KO ctrl refer to the KO and the wt cells of the LA-KO cell line, respectively. The measured features are as follows: XY area (A.), YZ area (B.), XY circularity (C.), YZ circularity

(D.), XY aspect ratio (AR, E.), YZ aspect ratio (F.), XY round (G.), YZ round (H.), XY solidity (I.), and YZ solidity (J.). The mark (*) indicates significant difference from the WT cells ($p<0.005$, Student's T-test, 2-tailed).

Nucleus area in XY plane differed significantly between the WT cells and all the other cell lines (**Figure 8A**), even though significant differences in the nucleus size were not visually observed between the WT and the EGFP-tagged cell lines (**Figure 7A**). The nuclei of LA-KO KO and LA-KO ctrl cells had smaller XY area than the WT cells, while the nuclei of LA-EGFP, LA-CB and dN20-LA-EGFP cells were larger in size compared to the WT cells. Consequently, the nuclei of LA-KO KO and LA-KO ctrl cells also differed significantly from those of the LA-EGFP, LA-CB and dN20-LA-EGFP cells in their XY area. In addition, the nuclei of LA-EGFP and dN20-LA-EGFP cells had significantly larger area than those of the WT cells in the YZ plane (**Figure 8B**). The YZ area of the nuclei in LA-CB cells also seemed to be larger than that of the WT cells, but the difference was not significant, probably due to the high deviation between individual LA-CB samples indicated by the high error bar. These results indicate that the nucleus size is affected by the LMNA-tagging or LMNA mutations in LA-EGFP, LA-CB and dN20-LA-EGFP cell lines, resulting in greater nucleus size. This is compatible with previous studies demonstrating the correlation between nuclear size and lamin expression (Jevtić et al. 2015, Mukherjee et al. 2016). However, nucleus area between the knockout cells (LA-KO KO) and their wt controls (LA-KO ctrl) didn't significantly differ from each other in either direction, indicating that the nucleus size is unaffected by the LMNA knock-out. The cell lines with the largest nucleus area had the most immature epithelium (**Figure 7**), indicating that that the epithelial maturity may be more crucial determinant of the nucleus size than the lamin A/C expression.

The XY circularity of nuclei in LA-KO KO cells is significantly smaller than in any of the other cell lines (**Figure 8C**). This is compatible with previous studies indicating that lamin A deficiency leads to decreased nuclear circularity (Takaki et al. 2017). There were no differences in XY circularity between any other cell lines, indicating that the XY circularity is unaffected by the LMNA modifications if the gene is still functional. The overexpression or tagging doesn't disturb the ability of A-type lamins to maintain nuclear circularity. In the YZ direction, the nuclei of LA-KO ctrl cells have significantly higher circularity than any of the other cell lines (**Figure 8D**). The difference in YZ circularity between the LA-KO KO and WT cells is not significant; however, the nuclei of LA-KO

KO cells have significantly higher YZ circularity than the LA-CB and dN20-LA-EGFP cells. Also, the nuclei of LA-EGFP cells have significantly high circularity in YZ direction compared to the LA-CB cells. In ImageJ, circularity is measured by the formula *circularity = 4pi(area/perimeter^2)*, and 1.0 indicates perfect circle, whereas values near 0.0 resemble elongated polygon (https://imagej.nih.gov/ij/plugins/circularity.html). In LA-KO KO cells, the mean XY circularity is between 0.6 and 0.7, while it's close to 0.8 in all other cell lines (**Figure 8C**), and this difference is statistically significant (Student's T-test, p-value 0.05). This denotes that the mean circularity of the KO cells is lower than those of the other cells.

The nuclei of LA-KO KO cells have significantly higher XY AR than in any of the other cell lines (**Figure 8E**). The other cell lines don't significantly differ from the WT cells in their XY AR, although LA-CB and LA-EGFP cells differ significantly from each other. In the YZ direction, LA-KO ctrl cells differ significantly from all other cell lines, having the smallest AR (**Figure 8F**). The nuclei of LA-CB cells exhibit the highest AR in YZ direction, significantly higher than that of the LA-KO ctrl, LA-KO KO and LA-EGFP cells. In addition, the YZ AR of dN20-LA-EGFP is significantly higher than that of the LA-EGFP. Again, deviation between the individual LA-CB samples is high, indicated by the considerably high error bar (**Figure 8F**). The high AR seems to correlate with low circularity and vice versa (**Figure 8C-F.**) Again, the LA-EGFP, LA-CB and dN20-LA-EGFP cell lines doesn't significantly differ from the WT cells, demonstrating that the AR is unaffected by the LMNA modifications of these cells.

The nuclei of LA-KO KO and LA-CB cells have significantly lower or higher XY roundness than the WT cells, respectively (**Figure 8G**). In addition, LA-CB has significantly higher nuclear roundness than the LA-EGFP, and LA-KO KO has significantly lower nuclear roundness than the dN20-LA-EGFP, LA-KO ctrl and LA-CB cells. Roundness is another way to measure how spherical an object is in ImageJ, and it is measured by the formula *roundness = 4pi(area/major axis^2)* (https://imagej.nih.gov/ij/docs/guide/146-30.html). It differs from the circularity in that it compares the object area with its major axis and doesn't take the perimeter of the object into account. This explains the differences between the roundness and circularity graphs. For the LA-KO KO cells, the differences in roundness are not as significant as those in circularity. In the YZ direction, LA-KO ctrl cells have significantly higher roundness than all the other cell lines (**Figure 8H**). Based on the results, nuclear roundness is not affected by

the GFP-tagging or the elimination of 20 N-terminal amino acids of the pre-lamin A protein. However, the XY roundness of LA-CB cells is significantly high, indicating that the CB influences nuclear shape.

The XY solidity is significantly smaller in the nuclei of LA-KO KO cells than in any of the other cell lines (**Figure 8I**). In ImageJ, solidity is defined as the object area divided by the convex area (*https://imagej.nih.gov/ij/docs/guide/146-30.html*). The more the convex area resembles the true area of the object, the closer to 1 the solidity value. In the nuclei of LA-EGFP, LA-CB, dN20-LA-EGFP, WT and LA-KO ctrl cells, the solidity is around 0.98, indicating that the convex area is very close to the real nucleus area. In the nuclei of LA-KO KO cells, the XY solidity is around 0.91, indicating that the convex area is somewhat bigger than the real area of the nucleus, i.e. the nuclei have more irregular shape than in the other cell lines. This seems plausible as the KO nuclei in LA-KO cells often appeared as crescent-shaped or "donut"-shaped, having a hole in the middle of the otherwise circular nucleus. The convex hull of these nuclei is circular, which causes the differences in the solidity. In YZ direction, the nuclei of LA-KO ctrl cells have significantly higher and those of LA-CB cells have significantly lower solidity than every other cell line (**Figure 8J**). In addition, the YZ solidity of the nuclei of LA-KO KO cells is significantly higher than that of the WT.

Based on the results, the nuclei of LA-CB cells have the highest variation between individual samples in YZ direction, indicating that the height of the nuclei differ from each other more than in the other cell lines. The differences between WT and LA-KO ctrl cells are also significant in several YZ features, indicating that these nuclei mainly differ in height, not in shape. Also, LA-EGFP and dN20-LA-EGFP don't usually differ remarkable from each other, only in the YZ AR. This suggests that the removal of 20 N-terminal amino acids from the pre-lamin A protein in dN20-LA-EGFP cells doesn't remarkable affect the ability of lamin A to maintain nucleus morphology. Furthermore, LA-EGFP and dN20-LA-EGFP only differ from the WT cells in nucleus area, but not in nucleus shape. This indicates that lamin A overexpression increases nucleus area but doesn't affect nucleus morphology. The nuclei of LA-KO KO cells have the most significant differences between other cell lines in nucleus morphology, including XY circularity, XY AR and XY solidity, in which they differ from all other cell lines, and XY roundness, in which they differ from several cell lines. It seems clear that pre-lamin A knockout have significant effects on nucleus morphology. However, there are no significant differences

between the areas of the nuclei in LA-KO KO and LA-KO ctrl cells, indicating that the LMNA knock-out has no effect on the nucleus area.

5.4 Effects of lamin A modifications on cell growth density

The growth density and environment are known to influence the nucleus morphology in cells (Skinner & Johnson 2017). Based on the microscopy results, there seemed to possibly be differences in cell density (**Figure 7**). Thus, the cell density was studied by calculating the total number of nuclei in each field image (15 pcs/cell line) and comparing the nuclei counts between the cell lines. The number of folded nuclei was also calculated to study whether the differences in lamin A expression influence nuclear envelope folding. In LA-KO field images, around half of the cells were pre-lamin A knockouts and the other half wt controls. In addition to the nuclei counts, the percentages of folded and unfolded nuclei were calculated for each cell line as well as the percentage of nuclei compared to the WT cells (**Table 4**).

The number of nuclei in 15 field images varied remarkably between the cell lines. There were only 200 nuclei in LA-CB images in total, while the number of WT nuclei was 529. The number of total nuclei in LA-EGFP and dN20-LA-EGFP cells were between those of LA-CB and WT cells, being 335 and 410 for the LA-EGFP and dN20-LA-EGFP, respectively. In LA-KO cells, the total nuclei count, 818, was clearly higher than in any of the other cell lines. Statistically, the number of total nuclei significantly differed between the WT and all the other cell lines (Student's T-test, p-value 0.05). In addition, all modified cell lines but LA-EGFP and dN20-LA-EGFP differed significantly from each other in their total nuclei counts (**Appendix 3A**).

In all cell lines, the nuclei were mostly folded. The percentage of folded nuclei ranged from 89.00 % to 98.66 %, depending on the cell line. The highest percentage of folded nuclei was obtained from LA-KO cells, and especially most of the knockout cells were highly folded (**Figure 7B**). In dN20-LA-EGFP cells, the percentage of folded nuclei was almost the same as in the WT cells, near 98 %. The lowest counts for folded nuclei were obtained in LA-CB (89.00 %) and LA-EGFP (91.64 %) cells. The smoothness of the nuclei in LA-CB cells was also visible in microscopy results (**Figure 7A, LA-CB panel**).

To study the significance of differences in nuclei folding between the cell lines, the counts of folded nuclei in each field were divided by the total number of nuclei in the cell

line to normalize the counts. Student's T-test with a significance level 0.05 was used to compare these normalized counts between the cell lines (**Appendix 3B**). Based on the T-test, there were no significant differences in the number of folded nuclei between any of the cell lines. This indicates that differences in lamin A expression have no effect on the formation of nuclear folds.

The average number of nuclei in a field was calculated for each cell line together with the standard deviations (**Figure 9**). The deviation between samples was the highest in dN20-LA-EGFP cells and LA-KO cells and lower in the other cell lines. Particularly in the dN20-LA-EGFP cells, the standard error is almost as big as the average number of cells in a field. An example image of nuclei markings and calculations is shown in **Appendix 2**.

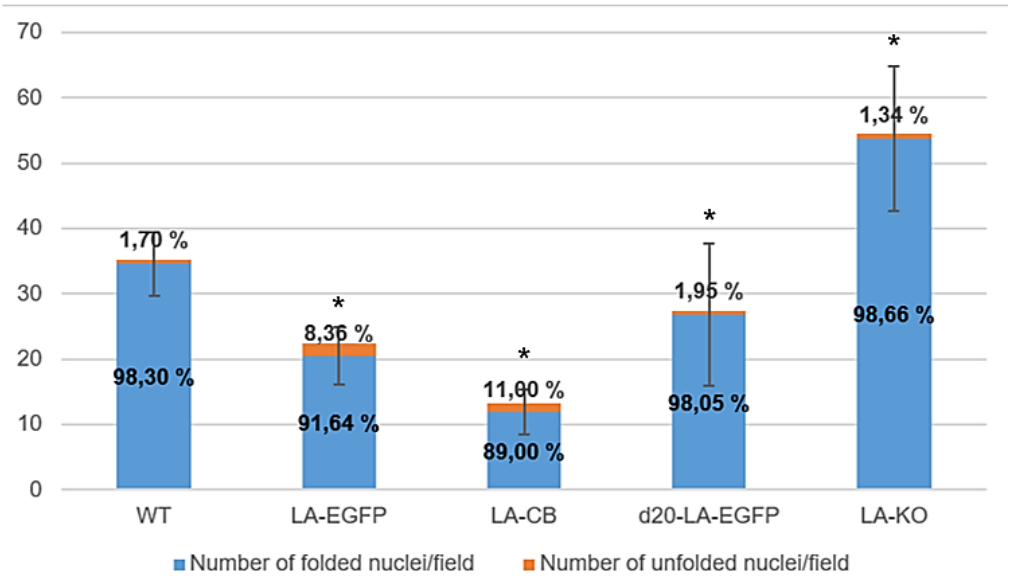

Figure 9. Average number of folded and total nuclei in different cell lines. The average number of nuclei (total and folded) in a field was calculated manually from the field images. The number of folded nuclei is indicated in blue bars and the number of unfolded nuclei in orange bars. Together, they comprise the total nuclei count per field. The percentages of folded and unfolded nuclei are also shown. The asterix (*) indicates the statistically significant difference from the WT cells ($p<0.05$, Student's T-test, 2-tailed).

The percentage differences in the total number of nuclei in modified cell lines compared to the WT cells were also remarkably high. There were 36.7 % and 22.5 % fewer nuclei in LA-EGFP and dN20-LA-EGFP cells compared to the WT cells, respectively. The most drastic difference in the number of total nuclei was obtained between the LA-CB and WT cells: the number of nuclei in LA-CB cells was 62.2 % smaller than that of

the WT cells. Contrary to the other cell lines, the number of nuclei in LA-KO cell line was 54.6 % higher than that of the WT cells.

5.5 Effects of lamin A modifications on cell growth

As the nucleus morphology is dependent on cell density and growth environment (Skinner & Johnson 2017), the growth rates of different cell lines were studied to check whether the cells acquire the same confluency during the growth period. The growth rate of LA-EGFP, LA-CB, dN20-LA-EGFP and WT cells was studied by growing equal numbers of cells in a similar manner for 7 days and counting them. Two parallel samples of each cell line were included. The average number of cells after the 7-day growth period were calculated from the parallel samples (**Figure 10**).

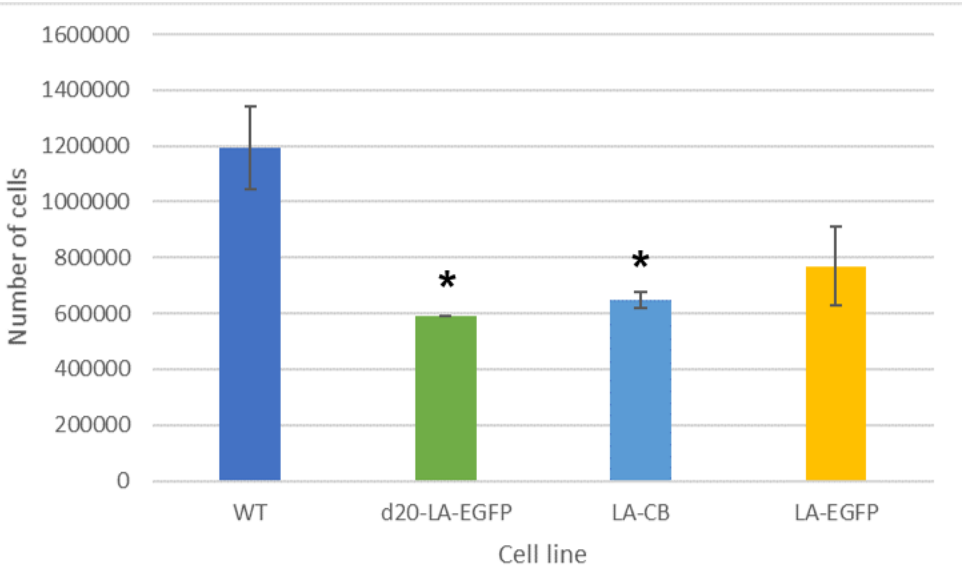

Figure 10. The average number of cells after the 7-day growth. The WT, dN20-LA-EGFP, LA-CB and LA-EGFP cells were grown in a similar manner for 7 days and counted. The bars indicate the means of two parallel samples, and the error bars represent the standard deviations. In dN20-LA-EGFP cell line, the number of cells was equal between the parallel samples, and the standard deviation is zero. The mark (*) indicates the statistically significant difference from the WT cells ($p<0.005$, Student's T-test, 2-tailed).

The confluency of all cell lines was approximately 100 % after the 7-day growth period. However, the number of LA-EGFP, LA-CB and dN20-LA-EGFP cells seemed smaller than that of the WT cells (**Figure 10**). By comparing the cell counts of LA-EGFP, LA-CB and dN20-LA-EGFP with the WT, clear percentage differences were obtained.

The number of LA-EGFP cells was around 30.6 % smaller than that of the WT cells, and in the LA-CB and dN20-LA-EGFP lines, the cell counts were 45.6 % and 50.6 % smaller than that of the WT cells, respectively.

Student's T-test with the significance level 0.05 was as a statistical measure. Despite the percentage difference in cell counts between the LA-EGFP and WT cells, the difference was not significant (**Appendix 3C**). Instead, the number of cells was significantly smaller in both the LA-CB and dN20-LA-EGFP cells compared to the WT cells. There were no significant differences in cell counts between any of the modified cell lines. This indicates that the lamin mutations or tagging in LA-EGFP, LA-CB and dN20-LA-EGFP cells somehow delay cell growth. However, as there were no significant differences in the growth between these modified cell lines, the exact type of the LMNA modification doesn't seem to affect the growth delay.

6. DISCUSSION

Nuclear lamina is an important component of the nucleus, suggested to participate in enabling external force transmission from and to regulate nucleus shape (Dahl et al. 2008, Osmanagic-Myers et al. 2015, Skinner & Johnson 2017). A-type lamins are critical components of the lamina primarily responsible for the nuclear stiffness, and defects in lamin A function leads to disturbances in nuclear stiffness and several cellular processes, causing different tissue-specific diseases (Dahl et al. 2008, Hah & Kim 2019). Still, the structural organization of nuclear lamina and the role of A-type lamins in cellular mechanoresponses is unclear (Burke & Stewart 2013, Osmanagic-Myers et al. 2015). CRISPR/Cas9 is a novel and versatile tool to study gene function e.g. by generating knockout cell lines and organisms to study the function of specific genes and to model diseases (Wang et al. 2016, Chira et al. 2017, Khan et al. 2018). In this thesis, LMNA-knockout MDCK II cell line was successfully established using the CRISPR/Cas9 system to study the effects of the depletion of A-type lamins on nucleus morphology. The CRISPR/Cas9 system was delivered to the cells via electroporation which has been proven useful and efficient method in generating gene knockouts (Wang et al. 2016, Brunetti et al. 2018). The effects of A-type lamins on nucleus morphology were studied by comparing the morphological features of the nuclei in cell lines with different lamin A/C expression. The cell lines with LMNA knock-out (LA-KO), overexpression (LA-EGFP), chromobody-tagging of A-type lamins (LA-CB) and N-terminal mutation (dN20-LA-EGFP) were compared to the wt cells. Also, the growth density and growth rate of these cell lines were analysed.

Off-target activity is still one of the main problems in CRISPR/Cas9 and needs to be carefully considered whenever CRISPR/Cas9 system is utilized (Wang et al. 2016, Zhang et al. 2016, Hryhorowicz et al. 2017, Khan et al. 2018). In this study, the possibility of off-target activity of the Cas9 was minimized by gRNA design and optimisation of the transfection. Several possible gRNAs were analysed in silico and those with minimal off-target sites were chosen for this study. Transfection was performed by electroporation, which is an efficient method with low off-target activity compared to some other delivery methods (Wang et al. 2016). By limiting the active time of the Cas9, off-target activity

can further be reduced (Campenhout et al. 2019). Thus, the Cas9 with transient endonuclease activity was used in this study. Transfection efficiency was increased by optimising gRNA and Cas9 concentrations. CRISPR/Cas9 proved successful method in gene knockout, as demonstrated by previous studies (Simoff et al. 2016, Karlgren et al. 2017, Brunetti et al. 2018).

LMNA knockout cells remained viable and could be cultured as normal cells. The reports of the necessity of A-type lamins on cell viability remain somewhat controversial. In some studies, LMNA knockout has led to decreased cell viability compared to the wt cells (Earle et al. 2020). This seems plausible as A-type lamins are involved in many cellular processes, such as DNA repair (Méjat 2010, Osmanagic-Myers et al. 2015, Adam 2017), cell cycle regulation (Méjat 2010) and apoptosis (Méjat 2010, Hah & Kim 2019). However, some studies have demonstrated that fibroblasts can proliferate and stay viable without any nuclear lamins (Jung et al. 2014), indicating that they may not be critical for cell survival. This was also the case in this study.

Even though the importance of A-type lamins in cell viability is somewhat unclear, they play an essential role in the maintenance of nuclear morphology, as demonstrated by several studies (Capo-chichi et al. 2011, Jung et al. 2014, Hah & Kim 2019). In my study, LA-KO knock-out cells appeared as highly irregular and often as crescent-shaped or "donut-shaped". Similar phenotypes have been observed by *Arias-Garcia et al.* in the absence of the cell-cell adhesion molecule called JAM3. Based on their study, depletion of JAM3 leads to epithelial-to-mesenchymal transition (EMT) and disruption of the lamina structure following the reorganization of microtubules. A critical feature behind this phenomenon seems to be the altered LMNA:LMNB ratio in cells, leading to relatively higher levels of B type lamins (Arias-Garcia et al. 2019). Another study has also suggested that the irregular shape observed in lamin negative cells is caused by cytoskeletal forces and is particularly dependent on lamin A, not lamin B (Chen et al. 2018).

There is also some evidence that actomyosin at least partly determines nuclear morphology (Takaki et al. 2017). However, other studies highlight the role of microtubules in nuclear shaping (Tariq et al. 2017, Arias-Garcia et al. 2019). Anyhow, it seems probable that the irregular nuclear shape caused by pre-lamin A depletion results from the cytoskeletal activity. A-type lamins are mainly responsible for nuclear stiffness (Osmanagic-Myers et al. 2015, Thorpe & Lee 2017, Hah & Kim 2019) and maintain nuclear shape, structure and stability (Dahl et al. 2008). The lamina has been suggested to act as a "fence" that prevents incursion of cytoplasmic components inside the nucleus (Jung et

al. 2014). *Tariq et al.* reported that gamma tubulin is localized to the arc of the crescent shaped nuclei in lamin A negative fibroblasts. Gamma tubulin is involved in microtubule assembly (Wiese & Zheng 2006), giving the researches reason to assume that microtubules cause nuclear abnormalities in lamin A negative cells (Tariq et al. 2017). *Arias-Garcia et al.* observed that the microtubule-organizing center (MTOC) was typically positioned in the hole of the donut-shaped nuclei or at the invagination of the crescent-shaped nuclei, compatible with the study by *Tariq et al*. In this thesis, gamma tubulin localization or microtubule positioning were not studied, but gamma tubulin is probably present in the arc or hole of the nuclei in LA-KO cells. Gamma tubulin staining could be done to verify this assumption.

The lamina and especially the A-type lamins interact both directly and indirectly with the chromatin (Martino et al. 2018, Ranade et al. 2019). A-type lamins are also essential determinants of the chromatin distribution and mobility (Janin & Gache 2018). Therefore, LMNA KO probably alters chromatin organization which can further influence gene expression. Importantly, the A-type lamins interact with both the silent heterochromatin and the active euchromatin (Adam 2017, Shevelyov & Ulianov 2019, Ranade et al. 2019), and the LADs associated with A-type lamins are present both at the nuclear interior and periphery (Ranade et al. 2019). Chromatin organization has been observed to significantly change if the mechanical properties of the A-type lamins are altered, leading to heterochromatin detachment and altered chromatin regulation, among others (Osmanagic-Myers et al. 2015, Shevelyov & Ulianov 2019).

The depletion of A-type lamins has probably consequences in the functionality of the whole nucleus. In addition to storing the genome of the cell, the nucleus is involved in cellular signalling, migration and other processes (Lammerding 2011). Previous studies have reported that LMNA deficiency causes abnormal gene expression in cells (Lammerding 2011, Ranade et al. 2019) and in mice models (Lammerding 2011). Gene expression analysis was not performed in my study, but it could be done in the future to see whether there are any differences between the cell lines.

Lamin A is critical for the correct positioning of SUN proteins (Hah & Kim 2019) and emerin (Osmanagic-Myers et al. 2015). The Sun 2 proteins further position nesprin-1, indicating that lamin A depletion may disturb the positioning of both SUN proteins and nesprins (Méjat 2010, Martino et al. 2018). As lamins are in a close contact with the other LINC components, the effects of lamin A/C depletion are not restricted to the nucleus

only. Instead, LMNA knockout probably affects the whole nucleo-cytoskeletal connectivity and force transmission between the nucleus and cell exterior. Indeed, disturbations in nucleo-cytoskeletal connections in LMNA knockout cells have been demonstrated (Schwartz et al. 2017, Hah & Kim 2019), causing e.g. aberrant nesprin positioning (Houben et al. 2009, Schwartz et al. 2017) and changes in cell migration (Houben et al. 2009, Helvert et al. 2018).

Some features of the LMNA KO cells seemed to resemble those of the cancer cells. Based on the increased growth density of LA-KO cells, contact inhibition signalling seems to be absent or disturbed. Contact inhibition is an important feature of non-cancerous cells as it controls cell growth, and disturbances in contact inhibition cause uncontrolled cell growth typical for cancer cells (Pavel et al. 2018). The depletion of A-type lamins leads to microtubule driven EMT and enhanced cellular migration which is also a typical feature of tumor cells (Arias-Garcia et al. 2019). Generally, lower lamin A levels correlate with higher cellular migration rate and reduced DNA repair (Helvert et al. 2018), indicating that the depletion of A-type lamins probably increases the mutational rate of the cells. High mutation rate is again typical for cancer cells.

LA-KO knock-out cells exhibited remarkably different nucleus morphology from the WT cells, but the morphological differences between the WT cells and the other cell lines were less obvious. LA-EGFP, LA-CB and dN20-LA-EGFP mainly differed from the WT cells in size, and this can be possibly explained by the different epithelial maturity (Puliafito et al. 2012). During longer culture period, the LA-EGFP, LA-CB and dN20-LA-EGFP could have acquired similar maturity state and nuclear size to the WT cells. The morphological differences between the LA-KO ctrl and WT cells were probably caused by different cell densities as there were no morphological differences between these cells in the XY plane. In some studies, mutations in the LMNA gene have led to the failure of lamina assembly causing disease-like phenotypes (Bank et al. 2011). Based on this, there could have been morphological differences between the dN20-LA-EGFP and WT cells, but these were not observed. In this study, LA-EGFP and dN20-LA-EGFP didn't differ in cell proliferation rate or epithelial density, and they only differed in YZ AR in the morphology analysis. Based on a previous study, the removal of the first 20 amino acids from the N-terminus of the LMNA gene in dN20-LA-EGFP cell line prevents the linear polymerization of lamin A but doesn't affect the dimerization or C-terminal activity of the lamin A (Ihalainen et al. 2015). However, the amino acid removal didn't seem to affect nucleus morphology in this study. Still, one should note that the endogeneous lamin

A expression was unaffected by the mutated lamin form which may explain the similar results of the LA-EGFP and dN20-LA-EGFP cell lines.

The morphology analysis was done for the 30 Z-stack images for each cell line. The nuclei to be imaged were chosen randomly, and the measurements were done automatically by using the ImageJ macro. This automatization of the measurements minimizes the possibility of measurement errors. If more than one nucleus was involved in one image, the nucleus at the middle of the image was chosen for the analysis. Sometimes, two or more cells were grown very close to each other and were partially overlapping in the image. This might have caused some minor errors in the calculations if the macro has not properly distinguished between the different nuclei. However, as 30 images per the cell line were analysed, the possible errors have not probably been significant.

As was observed in confocal microscopy, LA-CB cells had high variability in their CB expression, and some cells didn't express the fluorophore at all. To be able to reliably compare LA-CB with the other cell lines, the line should be purified e.g. by FACS sorting as the presence of wt cells may shift the results. Still, based on the confocal microscopy observations, the CB-negative and CB-positive cells seem to exhibit similar nucleus morphology and size, but this can't be undoubtedly evidenced without separating these cells in morphological studies. The nuclei chosen for the z-stack imaging followed by morphological analysis were all CB-positive, but both CB-positive and -negative cells were present in the cell growth density and growth rate analyses. The camelid antibodies of the LA-CB cell line have been suggested to interfere cellular processes less than traditional antibodies and should not disturb the re-distribution of nuclear lamina (Traenkle & Rothbauer 2017).

In the morphological analysis, the XY roundness and YZ solidity of LA-CB were significantly increased and decreased, respectively, compared to the WT cells, indicating that the CB expression may somehow affect the nucleus morphology. However, the epithelial maturity of the LA-CB cells was clearly lower than in any of the other cell lines, which may at least partly explain the differences in nucleus shape. Cytoskeleton-mediated phosphorylation of lamins has been suggested to regulate lamin activity and causing the softening of the NE which increases nuclear roundness (Skinner & Johnson 2017). Depletion of several NE proteins can also round the nucleus (Jevtić et al. 2014). However, the nuclei of LA-CB cells were considerably round only in the XY plane, and this may

simply result from the immatureness of the epithelium. This seems plausible as the nucleus shape is dependent on the cytoskeletal tension and growth environment (Jevtić et al. 2014, Skinner & Johnson 2017).

The effect of lamins on nuclear size is somewhat controversial. A previous study has demonstrated that the size of the nucleus is dependent on the total lamin concentration, regardless of the lamin type (Jevtić et al. 2015). Based on that study, high total lamin concentration tends to decrease nuclear size, while low concentration increases the size of the nucleus. However, the effect of lamin concentration on nuclear size were not as straightforward in the study as the increase in lamin concentration initially increased the nuclear size up to some limit and even higher concentrations of nuclear lamins led to decreased nuclear size (Jevtić et al. 2015).

In this study, the nuclei of LA-EGFP, LA-CB and dN20-LA-EGFP were larger in size than those of the WT cells, whereas in the LA-KO cell line, both the nuclei of KO cells and those of the LA-KO ctrl cells were smaller in size. The reason for the smaller size of the nuclei in LA-KO cells may be explained by their increased cellular density. A previous study has demonstrated that cell size is reduced in higher cell density in the MDCK II culture (Puliafito 2012). On the other hand, the cell size often correlates with the size of the nucleus (Mukherjee et al. 2016). This may explain why the nucleus size of LA-KO cells was smaller than that of the LA-EGFP, LA-CB and dN20-LA-EGFP although A-type lamins were expressed in these cells. The correlation between the cell size and the nucleus size was also observed in my study: particularly the LA-EGFP cells seemed larger in size than the WT cells when observed with the light microscope during the cell culture.

Despite the differences in lamin A expression, the nuclei were mostly folded in all cell lines. The functional significance of nuclear folds is still unclear, but as the folds increase nuclear area, they are suggested to participate in nucleo-cytoplasmic transport (Abe et al. 2004), and they seem to be involved in calcium metabolism (Abe et al. 2004, Mauger 2012, Drozdz & Vaux 2017) and determination of the nucleus morphology (Mauger 2012). Thus, it is not surprising that some lamin mutations have been shown to alter nuclear folding (Drozdz & Vaux 2017), although this was not observed in my study. The actin cap seems to prevent nuclear folding as it organises the lamina (J. Kim, Louhghalam, Lee, Schafer et al. 2017), and the cap is absent in LMNA KO cells (Khatau et al. 2009), which may explain why the LA-KO knock-out cells appeared the most folded in my study.

The classification of nuclei into folded and unfolded was done by hand based on the field images. There were differences in the overall image quality between both the cell lines and the individual images, and sometimes it was difficult to be sure whether some nuclei were folded or not. The nuclei were usually classified as unfolded if no clear folds were seen. In this study, most of the nuclei were folded in all cell lines, and the differences between the cell lines were not significant, indicating that problems in detecting folds in some images have not affected the results. However, cells were classified as folded even if only a single fold was observed, and the number of folds in nuclei were not analysed. Even though most of the nuclei were folded in all cell lines, some nuclei were only minimally folded, while the others had several clearly visible folds. There may have been differences between the cell lines in the number of folds/nuclei, but this was not studied here.

LMNA modifications resulted in delayed cell growth in LA-CB and dN20-LA-EGFP cells, while differences in cell number after the 7-day growth were not observed between LA-EGFP and WT cells. Based on my study, LA-EGFP and dN20-LA-EGFP behaved quite similarly, and differences between these two cell lines were not observed in most of the analyses. One possible explanation for the difference in cell number is in the re-suspension of dN20-LA-EGFP cells. They were strongly attached to each other and would have needed longer time to properly detach. Thus, the cells detached as large layers which were difficult to properly disperse, which may have resulted in miscalculations of the cell number.

However, some lamin A mutations have an effect on cellular proliferation rate (Piekarowicz et al. 2017), indicating that the removal of amino acids in dN20-LA-EGFP may have delayed cellular growth. Remarkably, the dN20-LA-EGFP cells seemed to be more strongly attached to each other and to the substrate than the LA-EGFP cells, indicating that the prevention of lamin A polymerization may somehow increase the adhesion properties of the cells. There is actually some evidence that specific LMNA mutations can increase the adhesiveness of the cells (Emerson et al. 2009). Lamins are involved in the activation of extracellular signal-regulated kinase (ERK) signalling (Osmanagic-Myers et al. 2015), and the cells with deficient ERK signalling display increased adhesion and decreased spreading (Emerson et al. 2009). In addition, the N-terminal domain of lamins is suggested to act as a phosphorylation target of several kinases, including Cdks and ERKs (Machowska et al. 2015). Thus, it may be possible that the removal of amino acids from the N-terminus of the LMNA gene in the dN20-LA-EGFP cells causes changes in

cellular signalling, which in turn increases cell adhesion e.g. by increasing the recruitment of focal adhesions. However, this needs further studies to be verified.

Differences in cell size may explain at least partly the differences in cell number after the 7-day growth. As LA-EGFP, LA-CB and dN20-LA-EGFP cells are all larger in size than the WT cells, they need more space to grow. But, as the cell size often decreases with the increased cell density (Puliafito et al. 2012), prolonged growth period could have led to the increased cell density and decreased cell size in LA-EGFP, LA-CB and dN20-LA-EGFP cells.

There may also be differences in the contact inhibition between the cell lines. As lamin A is important in force transmission from the outside of the cell to the nucleus (Osmanagic-Myers et al. 2015, Adam 2017, Hah & Kim 2019), there may be disturbances in the force transmission between neighbouring cells in LMNA mutant or KO cells. This might cause differences in contact inhibition leading to differences in cell proliferation (N. Kim et al. 2011, Pavel et al. 2018). The number of LA-KO cells in a field was significantly higher than in any of the other cell lines, indicating that the LMNA knockout may somehow increase cell density. At least some LMNA mutations seem to increase the accumulation of yes-associated protein (YAP) into the nucleus (Owens et al. 2020), and YAP is a component of the Hippo signalling pathway involved in contact inhibition (N. Kim et al. 2011). In this study, LMNA knockout seemed to cause increase in cell density in LA-KO cells, possibly due to changes in contact inhibition. Similar effects were not seen in LA-EGFP, LA-CB and dN20-LA-EGFP cells, but the slower proliferation rate of these cells may explain the lower cell density, and longer culture period could have increased the cell density.

The 7-day growth study was performed only once with two parallel samples of each cell line. To increase the reliability of the results, the growth study should be repeated at least once. The growth of LA-KO cells was not studied in this thesis. As A-type lamins are involved in centrosome polarization during cell division (Osmanagic-Myers et al. 2015) and probably stabilize the replication fork during DNA replication (Adam 2017), their loss could affect the cell growth. There is some evidence that LMNA knockout may slow cellular proliferation rate (Piekarowicz et al. 2017). The cellular growth rate seems to be dependent on the lamina-associated polypeptide 2α (LAP2α), which promotes cell growth in the absence of nucleoplasmic lamins and prevents it in the presence of these lamins (Vidak et al. 2018). Nucleoplasmic lamins are absent in LA-KO knock-out cells, but the distribution of A-type lamins between the lamina and the nucleoplasm is unknown

in the other cell lines. In the future, LAP2α staining could be done to study whether its expression correlates with the growth rate of the cells. In addition, the interactions between lamin A and other NE proteins could be investigated e.g. by proximity ligation assay (PLA), which utilizes antibody-labeling and PCR amplification of the proteins of interest to detect their interactions (Alam 2018).

The delayed growth seen in LA-CB cells seems plausible as it was also observed during cell culturing when cells were grown for e.g. immunostaining or western analysis. Perhaps the distributions of A-type lamins between the lamina and the nucleoplasm differed from the other cell lines. Little seems to be known about the effects of CBs on cellular processes. Stable CB expression in cells has been suggested to possibly affect cellular processes if CB transgenes are randomly introduced into the genome (Keller et al. 2019), but there is a lack of evidence about the specific effects. In my study, the LA-CB cells seemed to have the largest and smoothest nuclei, and the smallest number of nuclei/field. This suggests that the stable CB expression influences cell growth density, nuclear size and proliferation rate. However, the mechanisms remain unknown.

A previous study has demonstrated that the production of hydrogen peroxide (H_2O_2) in a cell line stably expressing eGFP is remarkably higher than that of the non-eGFP cells, indicating that fluorescent proteins cause oxidative stress in cells (Ganini et al. 2017). H_2O_2 is an important cellular signalling molecule, contributing to several cellular processes including metabolism, immunity and cell fate (Ganini et al. 2017). Based on this, one might expect that LA-EGFP cells behave differently to WT cells or have different nuclear morphology. Apart from the nucleus size, major differences between the LA-EGFP and WT cells were not observed in most of the analyses in my study. However, the average number of cells in a field was decreased in LA-EGFP cells compared to the WT cells, and the epithelium was less mature, indicating that the GFP-tagging may somehow delay the cell growth. The effects of stable GFP expression on cells need further studies.

Even though visible differences in nucleus morphology between the WT and LA-EGFP, LA-CB and dN20-LA-EGFP cells were rarely observed, the modifications of the LMNA gene may have influenced the composition of the lamina. Fluorescence microscopy analysis revealed that EGFP- tagged lamin is expressed in virtually all LA-EGFP and dN20-LA-EGFP cells, indicating that the composition of the lamina is probably different from that of the wt cells. The nuclear lamina of the dN20-LA-EGFP cells is probably somewhat weaker than that of the wt cells, although this was not studied here. The contribution of A-type lamins on nuclear stiffness can be investigated e.g. by isolating

the nuclei and using atomic force microscopy (AFM) to measure the stiffness (Schäpe et al. 2009).

The aims of this study were to establish the LMNA knock-out cell line and to study the effects of the depletion of A-type lamins on nucleus morphology. The knock-out cell line was successfully established by CRISPR/Cas9 as was verified by western blotting, and the knock-out cells remained viable. The depletion of A-type lamins was hypothesized to cause irregular nucleus morphology, and, according to the hypothesis, LMNA knockout led to significant alterations in the nucleus shape. The EGFP tags or mutations of the LMNA gene delayed cell proliferation and epithelial maturation, but they didn't cause major differences in nucleus morphology, except the increased nucleus area which is probably explained by the epithelial immaturity. The CB caused additional changes in the roundness and solidity of the nuclei, but the reason for these alterations remain unknown. In LA-CB cells, the proliferation rate seemed to be the slowest, which may explain the clearer differences in nucleus morphology and cell density. Contrary to the expectations, the endogenous lamin A expression was unaffected in LA-EGFP cells and dN20-LA-EGFP cells despite the lamin A overexpression, which probably explains the small differences between these cell lines and the WT cells in the nucleus morphology analysis.

Further studies are needed to elucidate the far-reaching effects of LMNA knockout, including changes in the overall force transmission in the cell and the localization of LINC components and possible alterations in gene expression. The LA-KO cell line generated here may serve as a model for laminopathies and shed light on the structural and functional abnormalities leading to disease conditions. By studying the nucleo-cytoskeletal connectivity in these LMNA-deficient cells, the complex interplay between cytoskeleton and nucleus can be further deciphered.

7. CONCLUSION

The aims of this study were to establish the LMNA knock-out MDCK II cell line by CRISPR/Cas9 and to study the effects of the depletion of A-type lamins on nucleus morphology. The knock-out cell line was successfully established by delivering the Cas9 and previously designed gRNAs into the cells via electroporation. Off-target activity was minimized by in silico analysis of the gRNA sequences and by using Cas9 with transient endonuclease activity. The presence of KO cells was verified by western blot and immunostaining. The established LA-KO cell line contained around equal number of wt and LMNA KO cells.

The effect of LMNA KO or modifications on nucleus morphology were studied by immunostaining, confocal microscopy imaging and data analysis in ImageJ and Microsoft Excel. A customized ImageJ macro was used to measure morphological features of the nuclei. This demonstrated the critical effects of A-type lamins on nucleus morphology as the nuclei of LA-KO knock-out cells exhibited remarkable differences in several morphological features compared to the other cell lines. On the other hand, differences between the WT cells and LA-EGFP, LA-CB and dN20-LA-EGFP cells were rarely observed, except in the nuclear size. This probably resulted from the endogenous LMNA expression which was basically unaffected by the modifications of the LMNA gene.

Immunostaining and microscopy were also used to assess the effects of lamin A/C expression differences on cell growth density and nuclear folding, and cell proliferation rate was evaluated by culturing the same number of cells and counting them after the culture period. These studies revealed the delayed growth in LA-EGFP, LA-CB and dN20-LA-EGFP cells, which was coincident with the epithelial maturity observations. Also, the growth density was significantly lower in these cell lines and higher in LA-KO cell line compared to the WT cells, suggesting possible differences in contact inhibition.

The LMNA KO cell line established in this thesis can serve as a model to study the importance of A-type lamins in several cellular processes. The depletion of A-type lamins revealed their critical effect on nucleus morphology. Further studies are still needed to clarify the far-reaching effects of LMNA knockout, including changes in the overall force transmission in the cell and possible alterations in gene expression. The effects of GFP tagging or mutations of the LMNA gene also need further studies to be elucidated.

REFERENCES

Abe T., Takano K., Suzuki A., Shimada Y., Inagaki M., Sato N., Obinata T. & Endo T. (2004) Myocyte differentiation generates nuclear invaginations traversed by myofibrils associating with sarcomeric protein mRNAs. *Journal of Cell Science* **117**(Pt 26), 6523-6534.

Adam S.A. (2017) The Nucleoskeleton. *Cold Spring Harbor Perspectives in Biology* **9**(2), a023556.

Alam M.S. (2018) Proximity Ligation Assay (PLA). *Current Protocols in Immunology* **123**(1), e58.

Al-Qahtani W.S., Abduljabbar M., AlSuhaibani E.S., Abdel Rahman A. & Aljada A. (2019) Quantification of the Lamin A/C Transcript Variants in Cancer Cell Lines by Targeted Absolute Quantitative Proteomics and Correlation with mRNA Expression. *International Journal of Molecular Sciences* **20**(8).

Arias-Garcia M., Rickman R., Sero J., Yuan Y. & Bakal C. (2019) *Microtubule-mediated nuclear deformation drives the Epithelial-to-Mesenchymal Transition and breast cancer.*

Arora L. & Narula A. (2017) Gene Editing and Crop Improvement Using CRISPR-Cas9 System. *Frontiers in Plant Science* **8**, 1932.

Bank E.M., Ben-Harush K., Wiesel-Motiuk N., Barkan R., Feinstein N., Lotan O., Medalia O. & Gruenbaum Y. (2011) A laminopathic mutation disrupting lamin filament assembly causes disease-like phenotypes in Caenorhabditis elegans. *Molecular Biology of the Cell* **22**(15), 2716-2728.

Beyret E., Liao H., Yamamoto M., Hernandez-Benitez R., Fu Y., Erikson G., Reddy P. & Izpisua Belmonte J.C. (2019) Single-dose CRISPR-Cas9 therapy extends lifespan of mice with Hutchinson-Gilford progeria syndrome. *Nature Medicine* **25**(3), 419-422.

Boyle S.T. & Samuel M.S. (2016) Mechano-reciprocity is maintained between physiological boundaries by tuning signal flux through the Rho-associated protein kinase. *Small GTPases* **7**(3), 139-146.

Brunetti L., Gundry M.C., Kitano A., Nakada D. & Goodell M.A. (2018) Highly Efficient Gene Disruption of Murine and Human Hematopoietic Progenitor Cells by CRISPR/Cas9. *Journal of Visualized Experiments : JoVE* (134).

Burke B. & Stewart C.L. (2013) The nuclear lamins: flexibility in function. *Nature Reviews. Molecular Cell Biology* **14**(1), 13-24.

Campenhout C.V., Cabochette P., Veillard A., Laczik M., Zelisko-Schmidt A., Sabatel C., Dhainaut M., Vanhollebeke B., Gueydan C. & Kruys V. (2019) Guidelines for optimized gene knockout using CRISPR/Cas9. *BioTechniques* **66**(6), 295-302.

Capo-chichi C.D., Cai K.Q., Smedberg J., Ganjei-Azar P., Godwin A.K. & Xu X. (2011) Loss of A-type lamin expression compromises nuclear envelope integrity in breast cancer. *Chinese Journal of Cancer* **30**(6), 415-425.

Carroll D. (2017) Genome Editing: Past, Present, and Future. *The Yale Journal of Biology and Medicine* **90**(4), 653-659.

Chen N.Y., Kim P., Weston T.A., Edillo L., Tu Y., Fong L.G. & Young S.G. (2018) Fibroblasts lacking nuclear lamins do not have nuclear blebs or protrusions but nevertheless have frequent nuclear membrane ruptures. *Proceedings of the National Academy of Sciences of the United States of America* **115**(40), 10100-10105.

Chiang T.W., le Sage C., Larrieu D., Demir M. & Jackson S.P. (2016) CRISPR-Cas9D10A nickase-based genotypic and phenotypic screening to enhance genome editing. *Scientific Reports* **6**(1), 24356.

Chira S., Gulei D., Hajitou A., Zimta A., Cordelier P. & Berindan-Neagoe I. (2017) CRISPR/Cas9: Transcending the Reality of Genome Editing. *Molecular Therapy - Nucleic Acids* **7**(C), 211-222.

Cornelison G.L., Levy S.A., Jenson T. & Frost B. (2019) Tau-induced nuclear envelope invagination causes a toxic accumulation of mRNA in Drosophila. *Aging Cell* **18**(1), e12847-n/a.

Dahl K.N., Ribeiro A.J.S. & Lammerding J. (2008) Nuclear Shape, Mechanics, and Mechanotransduction. *Circulation Research* **102**(11), 1307-1318.

Dittmer T.A. & Misteli T. (2011) The lamin protein family. *Genome Biology* **12**(5), 222.

Drozdz M.M. & Vaux D.J. (2017) Shared mechanisms in physiological and pathological nucleoplasmic reticulum formation. *Nucleus: SEB Brighton 2016: Dynamic Organization of the Nucleus, Pt. 1 of 2* **8**(1), 34-45.

DuFort C.C., Weaver V.M. & Paszek M.J. (2011) Balancing forces: architectural control of mechanotransduction. *Nature Reviews Molecular Cell Biology* **12**(5), 308-319.

Earle A.J., Kirby T.J., Fedorchak G.R., Isermann P., Patel J., Iruvanti S., Moore S.A., Bonne G., Wallrath L.L. & Lammerding J. (2020) Mutant lamins cause nuclear envelope rupture and DNA damage in skeletal muscle cells. *Nature Materials* **19**(4), 464-473.

Emerson L.J., Holt M.R., Wheeler M.A., Wehnert M., Parsons M. & Ellis J.A. (2009) Defects in cell spreading and ERK1/2 activation in fibroblasts with lamin A/C mutations. *Biochimica Et Biophysica Acta* **1792**(8), 810-821.

Engler A.J., Sen S., Sweeney H.L. & Discher D.E. (2006) Matrix elasticity directs stem cell lineage specification. *Cell* **126**(4), 677-689.

Ganini D., Leinisch F., Kumar A., Jiang J., Tokar E.J., Malone C.C., Petrovich R.M. & Mason R.P. (2017) Fluorescent proteins such as eGFP lead to catalytic oxidative stress in cells. *Redox Biology* **12**, 462-468.

Giuliano C.J., Lin A., Girish V. & Sheltzer J.M. (2019) Generating Single Cell–Derived Knockout Clones in Mammalian Cells with CRISPR/Cas9. *Current Protocols in Molecular Biology* **128**(1), e100.

González-Cruz R.D., Dahl K.N. & Darling E.M. (2018) The Emerging Role of Lamin C as an Important LMNA Isoform in Mechanophenotype. *Frontiers in Cell and Developmental Biology* **6**.

Hah J. & Kim D. (2019) Deciphering Nuclear Mechanobiology in Laminopathy. *Cells* **8**(3), 231.

Hahn C. & Schwartz M.A. (2009) Mechanotransduction in vascular physiology and atherogenesis. *Nature Reviews. Molecular Cell Biology* **10**(1), 53-62.

Harris A.R., Jreij P. & Fletcher D.A. (2018) Mechanotransduction by the Actin Cytoskeleton: Converting Mechanical Stimuli into Biochemical Signals. *Annual Review of Biophysics* **47**(1), 617-631.

Helvert S.v., Storm C. & Friedl P. (2018) Mechanoreciprocity in cell migration. *Nature Cell Biology* **20**(1), 8-20.

Holaska J.M. (2016) Diseases of the nucleoskeleton. *Comprehensive Physiology* **6**(4), 1655-1674.

Houben F., Willems, C. H. M. P., Declercq I.L.J., Hochstenbach K., Kamps M.A., Snoeckx, L. H. E. H., Ramaekers F.C.S. & Broers J.L.V. (2009) Disturbed nuclear orientation and cellular migration in A-type lamin deficient cells. *Biochimica Et Biophysica Acta* **1793**(2), 312-324.

Hryhorowicz M., Lipiński D., Zeyland J. & Słomski R. (2017) CRISPR/Cas9 Immune System as a Tool for Genome Engineering. *Archivum Immunologiae Et Therapiae Experimentalis* **65**(3), 233-240.

Hsu P.D., Lander E.S. & Zhang F. (2014) Development and Applications of CRISPR-Cas9 for Genome Engineering. *Cell* **157**(6), 1262-1278.

Ihalainen T.O., Aires L., Herzog F.A., Schwartlander R., Moeller J. & Vogel V. (2015) Differential basal-to-apical accessibility of lamin A/C epitopes in the nuclear lamina regulated by changes in cytoskeletal tension. *Nature Materials* **14**(12), 1252-1261.

Janin A. & Gache V. (2018) Nesprins and Lamins in Health and Diseases of Cardiac and Skeletal Muscles. *Frontiers in Physiology* **9**.

Jevtić P., Edens L.J., Li X., Nguyen T., Chen P. & Levy D.L. (2015) Concentration-dependent Effects of Nuclear Lamins on Nuclear Size in Xenopus and Mammalian Cells. *The Journal of Biological Chemistry* **290**(46), 27557-27571.

Jevtić P., Edens L.J., Vuković L.D. & Levy D.L. (2014) Sizing and shaping the nucleus: mechanisms and significance. *Current Opinion in Cell Biology* **0**, 16-27.

Jorgens D.M., Inman J.L., Wojcik M., Robertson C., Palsdottir H., Tsai W., Huang H., Bruni-Cardoso A., López C.S., Bissell M.J., Xu K. & Auer M. (2017) Deep nuclear invaginations are linked to cytoskeletal filaments - integrated bioimaging of epithelial cells in 3D culture. *Journal of Cell Science* **130**(1), 177-189.

Jung H., Tatar A., Tu Y., Nobumori C., Yang S.H., Goulbourne C.N., Herrmann H., Fong L.G. & Young S.G. (2014) An Absence of Nuclear Lamins in Keratinocytes Leads to Ichthyosis, Defective Epidermal Barrier Function, and Intrusion of Nuclear Membranes and Endoplasmic Reticulum into the Nuclear Chromatin. *Molecular and Cellular Biology* **34**(24), 4534-4544.

Kang S., Yoon M. & Park B. (2018) Laminopathies; Mutations on single gene and various human genetic diseases. *BMB Reports* **51**(7), 327-337.

Karlgren M., Simoff I., Backlund M., Wegler C., Keiser M., Handin N., Müller J., Lundquist P., Jareborg A., Oswald S. & Artursson P. (2017) A CRISPR-Cas9 Generated MDCK Cell Line Expressing Human MDR1 Without Endogenous Canine MDR1 (cABCB1): An Improved Tool for Drug Efflux Studies. *Journal of Pharmaceutical Sciences* **106**(9), 2909-2913.

Keller B., Maier J., Weldle M., Segan S., Traenkle B. & Rothbauer U. (2019) A Strategy to Optimize the Generation of Stable Chromobody Cell Lines for Visualization and Quantification of Endogenous Proteins in Living Cells. *Antibodies* **8**(1).

Khan S., Mahmood M.S., Rahman S.U., Zafar H., Habibullah S., Khan Z. & Ahmad A. (2018) CRISPR/Cas9: the Jedi against the dark empire of diseases. *Journal of Biomedical Science* **25**(1), 29.

Khatau S.B., Hale C.M., Stewart-Hutchinson P.J., Patel M.S., Stewart C.L., Searson P.C., Hodzic D. & Wirtz D. (2009) A perinuclear actin cap regulates nuclear shape. *Proceedings of the National Academy of Sciences of the United States of America* **106**(45), 19017-19022.

Khatau S.B., Bloom R.J., Bajpai S., Razafsky D., Zang S., Giri A., Wu P., Marchand J., Celedon A., Hale C.M., Sun S.X., Hodzic D. & Wirtz D. (2012) The distinct roles of the nucleus and nucleus-cytoskeleton connections in three-dimensional cell migration. *Scientific Reports* **2**(1), 488.

Kim J., Louhghalam A., Lee G., Schafer B.W., Wirtz D. & Kim D. (2017a) Nuclear lamin A/C harnesses the perinuclear apical actin cables to protect nuclear morphology. *Nature Communications* **8**(1), 2123.

Kim N., Koh E., Chen X. & Gumbiner B.M. (2011) E-cadherin mediates contact inhibition of proliferation through Hippo signaling-pathway components. *Proceedings of the National Academy of Sciences of the United States of America* **108**(29), 11930-11935.

Kristiani L., Kim M. & Kim Y. (2020) Role of the Nuclear Lamina in Age-Associated Nuclear Reorganization and Inflammation. *Cells* **9**(3), 718.

Lammerding J. (2011) Mechanics of the Nucleus. *Comprehensive Physiology* **1**(2), 783-807.

Lammerding J., Fong L.G., Ji J.Y., Reue K., Stewart C.L., Young S.G. & Lee R.T. (2006) Lamins A and C but not lamin B1 regulate nuclear mechanics. *The Journal of Biological Chemistry* **281**(35), 25768-25780.

Lele T.P., Dickinson R.B. & Gundersen G.G. (2018) Mechanical principles of nuclear shaping and positioning. *The Journal of Cell Biology* **217**(10), 3330-3342.

Lelièvre S.A. (2009) Contributions of extracellular matrix signaling and tissue architecture to nuclear mechanisms and spatial organization of gene expression control. *BBA - General Subjects* **1790**(9), 925-935.

Lim C., Jang J. & Kim C. (2018) Cellular machinery for sensing mechanical force. *BMB Reports* **51**(12), 623-629.

Lin Y., Guo Y.R., Miyagi A., Levring J., MacKinnon R. & Scheuring S. (2019) Force-induced conformational changes in PIEZO1. *Nature* **573**(7773), 230-234.

Liu L., Luo Q., Sun J. & Song G. (2016) Nucleus and nucleus-cytoskeleton connections in 3D cell migration. *Experimental Cell Research* **348**(1), 56-65.

Machowska M., Piekarowicz K. & Rzepecki R. (2015) Regulation of lamin properties and functions: does phosphorylation do it all? *Open Biology* **5**(11), 150094.

Martino F., Perestrelo A.R., Vinarský V., Pagliari S. & Forte G. (2018) Cellular Mechanotransduction: From Tension to Function. *Frontiers in Physiology* **9**, 824.

Martins R.P., Finan J.D., Farshid G. & Lee D.A. (2012) Mechanical Regulation of Nuclear Structure and Function. *Annual Review of Biomedical Engineering* **14**(1), 431-455.

Mattioli E., Andrenacci D., Mai A., Valente S., Robijns J., De Vos W.H., Capanni C. & Lattanzi G. (2019) Statins and Histone Deacetylase Inhibitors Affect Lamin A/C - Histone Deacetylase 2 Interaction in Human Cells. *Frontiers in Cell and Developmental Biology* **7**, 6.

Mauger J. (2012) Role of the nuclear envelope in calcium signalling. *Biology of the Cell* **104**(2), 70-83.

Méjat A. (2010) LINC complexes in health and disease. *Nucleus* **1**(1), 40-52.

Miroshnikova Y.A., Nava M.M. & Wickström S.A. (2017) Emerging roles of mechanical forces in chromatin regulation. *Journal of Cell Science* **130**(14), 2243-2250.

Mukherjee R.N., Chen P. & Levy D.L. (2016) Recent advances in understanding nuclear size and shape. *Nucleus (Austin, Tex.)* **7**(2), 167-186.

Nicolas H.A., Akimenko M. & Tesson F. (2019) Cellular and Animal Models of Striated Muscle Laminopathies. *Cells* **8**(4).

Nmezi B., Xu J., Fu R., Armiger T.J., Rodriguez-Bey G., Powell J.S., Ma H., Sullivan M., Tu Y., Chen N.Y., Young S.G., Stolz D.B., Dahl K.N., Liu Y. & Padiath Q.S. (2019) Concentric organization of A- and B-type lamins predicts their distinct roles in the spatial organization and stability of the nuclear lamina. *Proceedings of the National Academy of Sciences of the United States of America* **116**(10), 4307-4315.

Osmanagic-Myers S., Dechat T. & Foisner R. (2015) Lamins at the crossroads of mechanosignaling. *Genes & Development* **29**(3), 225-237.

Osmanagic-Myers S. & Foisner R. (2019) The structural and gene expression hypotheses in laminopathic diseases-not so different after all. *Molecular Biology of the Cell* **30**(15), 1786-1790.

Owens D.J., Fischer M., Jabre S., Moog S., Mamchaoui K., Butler-Browne G. & Coirault C. (2020) Lamin Mutations Cause Increased YAP Nuclear Entry in Muscle Stem Cells. *Cells* **9**(4).

Paszek M.J., Zahir N., Johnson K.R., Lakins J.N., Rozenberg G.I., Gefen A., Reinhart-King C.A., Margulies S.S., Dembo M., Boettiger D., Hammer D.A. & Weaver V.M. (2005) Tensional homeostasis and the malignant phenotype. *Cancer Cell* **8**(3), 241-254.

Pavel M., Renna M., Park S.J., Menzies F.M., Ricketts T., Füllgrabe J., Ashkenazi A., Frake R.A., Lombarte A.C., Bento C.F., Franze K. & Rubinsztein D.C. (2018) Contact inhibition controls cell survival and proliferation via YAP/TAZ-autophagy axis. *Nature Communications* **9**(1), 1-18.

Piekarowicz K., Piekarowicz K., Machowska M., Machowska M., Dratkiewicz E., Dratkiewicz E., Lorek D., Lorek D., Madej-Pilarczyk A., Madej-Pilarczyk A., Rzepecki R. & Rzepecki R. (2017) The effect of the lamin A and its mutants on nuclear structure, cell proliferation, protein stability, and mobility in embryonic cells. *Chromosoma* **126**(4), 501-517.

Puliafito A., Hufnagel L., Neveu P., Streichan S., Sigal A., Fygenson D.K. & Shraiman B.I. (2012) Collective and single cell behavior in epithelial contact inhibition. *Proceedings of the National Academy of Sciences of the United States of America* **109**(3), 739-744.

Ranade D., Pradhan R., Jayakrishnan M., Hegde S. & Sengupta K. (2019) Lamin A/C and Emerin depletion impacts chromatin organization and dynamics in the interphase nucleus. *BMC Molecular and Cell Biology* **20**(1), 11.

Roy A., Goodman J.H., Begum G., Donnelly B.F., Pittman G., Weinman E.J., Sun D. & Subramanya A.R. (2014) Generation of WNK1 knockout cell lines by CRISPR/Cas-mediated genome editing. *American Journal of Physiology-Renal Physiology* **308**(4), F366-F376.

Santiago-Fernández O., Osorio F.G., Quesada V., Rodríguez F., Basso S., Maeso D., Rolas L., Barkaway A., Nourshargh S., Folgueras A.R., Freije J.M.P. & López-Otín C. (2019) Development of a CRISPR/Cas9-based therapy for Hutchinson-Gilford progeria syndrome. *Nature Medicine* **25**(3), 423-426.

Sawyer I.A., Sturgill D., Sung M., Hager G.L. & Dundr M. (2016) Cajal body function in genome organization and transcriptome diversity. *BioEssays : News and Reviews in Molecular, Cellular and Developmental Biology* **38**(12), 1197-1208.

Schäpe J., Prauße S., Radmacher M. & Stick R. (2009) Influence of Lamin A on the Mechanical Properties of Amphibian Oocyte Nuclei Measured by Atomic Force Microscopy. *Biophysical Journal* **96**(10), 4319-4325.

Schwartz C., Fischer M., Mamchaoui K., Bigot A., Lok T., Verdier C., Duperray A., Michel R., Holt I., Voit T., Quijano-Roy S., Bonne G. & Coirault C. (2017) Lamins and nesprin-1 mediate inside-out mechanical coupling in muscle cell precursors through FHOD1. *Scientific Reports* **7**(1), 1253.

Shevelyov Y.Y. & Ulianov S.V. (2019) The Nuclear Lamina as an Organizer of Chromosome Architecture. *Cells* **8**(2).

Shinmyo Y., Tanaka S., Tsunoda S., Hosomichi K., Tajima A. & Kawasaki H. (2016) CRISPR/Cas9-mediated gene knockout in the mouse brain using in utero electroporation. *Scientific Reports* **6**(1), 20611.

Simoff I., Karlgren M., Backlund M., Lindström A., Gaugaz F.Z., Matsson P. & Artursson P. (2016) Complete Knockout of Endogenous Mdr1 (Abcb1) in MDCK Cells by CRISPR-Cas9. *Journal of Pharmaceutical Sciences* **105**(2), 1017-1021.

Skinner B.M. & Johnson E.E.P. (2017) Nuclear morphologies: their diversity and functional relevance. *Chromosoma* **126**(2), 195-212.

Sui T., Liu D., Liu T., Deng J., Chen M., Xu Y., Song Y., Ouyang H., Lai L. & Li Z. (2019) LMNA-mutated Rabbits: A Model of Premature Aging Syndrome with Muscular Dystrophy and Dilated Cardiomyopathy. *Aging and Disease* **10**(1), 102-115.

Takaki T., Montagner M., Serres M.P., Le Berre M., Russell M., Collinson L., Szuhai K., Howell M., Boulton S.J., Sahai E. & Petronczki M. (2017) Actomyosin drives cancer cell nuclear dysmorphia and threatens genome stability. *Nature Communications* **8**(1), 16013.

Tariq Z., Zhang H., Chia-Liu A., Shen Y., Gete Y., Xiong Z., Xiong Z., Tocheny C., Campanello L., Wu D., Losert W. & Cao K. (2017) Lamin A and microtubules collaborate to maintain nuclear morphology. *Nucleus* **8**(4), 433-446.

Thorpe S.D. & Lee D.A. (2017) Dynamic regulation of nuclear architecture and mechanics-a rheostatic role for the nucleus in tailoring cellular mechanosensitivity. *Nucleus: SEB Brighton 2016: Dynamic Organization of the Nucleus, Pt. 2 of 2* **8**(3), 287-300.

Traenkle B. & Rothbauer U. (2017) Under the Microscope: Single-Domain Antibodies for Live-Cell Imaging and Super-Resolution Microscopy. *Frontiers in Immunology* **8**, 1030.

Tytell J.D., Ingber D.E. & Wang N. (2009) Mechanotransduction at a distance: mechanically coupling the extracellular matrix with the nucleus. *Nature Reviews Molecular Cell Biology* **10**(1), 75-82.

Uhler C. & Shivashankar G.V. (2018) Nuclear Mechanopathology and Cancer Diagnosis. *Trends in Cancer* **4**(4), 320-331.

Urciuoli E., Petrini S., D'Oria V., Leopizzi M., Della Rocca C. & Peruzzi B. (2020) Nuclear Lamins and Emerin Are Differentially Expressed in Osteosarcoma Cells and Scale with Tumor Aggressiveness. *Cancers* **12**(2).

Van Itallie C.M., Tietgens A.J., Aponte A., Gucek M., Cartagena-Rivera A.X., Chadwick R.S. & Anderson J.M. (2018) MARCKS-related protein regulates cytoskeletal organization at cell-cell and cell-substrate contacts in epithelial cells. *Journal of Cell Science* **131**(3).

Vidak S., Georgiou K., Fichtinger P., Naetar N., Dechat T. & Foisner R. (2018) Nucleoplasmic lamins define growth-regulating functions of lamina-associated polypeptide 2α in progeria cells. *Journal of Cell Science* **131**(3).

Wang H., La Russa M. & Qi L.S. (2016) CRISPR Cas9 in Genome Editing and Beyond. *Annual Review of Biochemistry* **85**(1), 227-264.

Weaver V.M., Alliston T. & Butcher D.T. (2009) A tense situation: forcing tumour progression. *Nature Reviews Cancer* **9**(2), 108-122.

Webster M., Witkin K.L. & Cohen-Fix O. (2009) Sizing up the nucleus: nuclear shape, size and nuclear-envelope assembly. *Journal of Cell Science* **122**(Pt 10), 1477-1486.

Wiese C. & Zheng Y. (2006) Microtubule nucleation: gamma-tubulin and beyond. *Journal of Cell Science* **119**(Pt 20), 4143-4153.

Yuen G., Khan F.J., Gao S., Stommel J.M., Batchelor E., Wu X. & Luo J. (2017) CRISPR/Cas9-mediated gene knockout is insensitive to target copy number but is dependent on guide RNA potency and Cas9/sgRNA threshold expression level. *Nucleic Acids Research* **45**(20), 12039-12053.

Zhang J., Adikaram P., Pandey M., Genis A. & Simonds W.F. (2016) Optimization of genome editing through CRISPR-Cas9 engineering. *Bioengineered* **7**(3), 166-174.

Zhou T., Gao B., Fan Y., Liu Y., Feng S., Cong Q., Zhang X., Zhou Y., Yadav P.S., Lin J., Wu N., Zhao L., Huang D., Zhou S., Su P. & Yang Y. (2020) Piezo1/2 mediate mechanotransduction essential for bone formation through concerted activation of NFAT-YAP1-ß-catenin. *eLife* **9**.

APPENDIX 1. THE LAMIN A INTENSITY VALUES OF WT, DN20-LA-EGFP, LA-CB AND LA-EGFP CELL LINES.

A. The normalized lamin A intensities for each sample. The intensities have been normalized as described in Materials and Methods. Two parallel samples of each cell line were included in each of the three replicates. For the EGFP-tagged cell lines, the intensities of EGFP-lamin A bands were also measured, but these were not included in **Figure 6.** The EGFP-Lamin A bands are highlighted with red in the table. **B. The mean normalized intensities and the corresponding standard deviations for each cell line** (displayed in **Figure 6**) **C. Student's T-test table of the intensity differences.** Two-tailed Student's T-test with the significance level 0.05 was used as a statistical measure to compare differences in lamin A expression between the cell lines. None of the values is smaller than the p value (0.05), indicating that there were no significant differences in lamin A expression between any of the cell lines.

A.

Cell sample	Replicate 1	Replicate 2	Replicate 3	Mean intensity	Stdev
WT2	95,6931008	88,85	76,83673638	87,12723593	9,545753
WT1	128,0880584	113,96	62,17830076	101,4072544	34,70038
d20-LA-EGFP 2	147,7852634	58,93	79,93784181	95,54970172	46,44125
d20-LA-EGFP 1	141,3046209	64,48	86,4849491	97,42464123	39,56129
LA-CB 2	98,40728837	63,89	56,11828519	72,80652244	22,50922
LA-CB 1	114,1995562	54,29	46,48735849	71,6596605	37,04673
LA-EGFP 2	115,8764907	57,14	71,88642458	81,63504332	30,55659
LA_EGFP 1	111,5762639	54,69	56,962	74,4095319	32,20737
EGFP d20-LA-EGFP 2	1638,522884	47,94	140,839		
EGFP d20-LA-EGFP 1	1292,69452	38,733	115,613		
EGFP LA-EGFP 2	137,855	72,774	48,038		
EGFP LA-EGFP 1	124,145	81,037	47,919		

B.

Cell line	Mean intensity	Stdev
WT	94,26724517	24,06804248
d20-LA-EGFP	96,48717148	38,59804325
LA-CB	72,23309147	27,42343309
LA-EGFP	78,02228761	28,35613568

C.

Cell line	WT	d20-LA-EGFP	LA-CB	LA-EGFP
WT	1	0,907212384	0,169879638	0,309822834
d20-LA-EGFP	0,907212384	1	0,238102257	0,367243717
LA-CB	0,169879638	0,238102257	1	0,726712171
LA-EGFP	0,309822834	0,367243717	0,726712171	1

APPENDIX 2. EXAMPLE OF THE CALCULATION OF FOLDED AND UNFOLDED NUCLEI

The number of total and folded nuclei were calculated by marking the folded nuclei with dots and utilising the Measure-tool in ImageJ (**Appendix figure 1**). Nuclei were classified as folded if even in the presence of a single visible fold, and most of the nuclei were classified as folded in all cell lines.

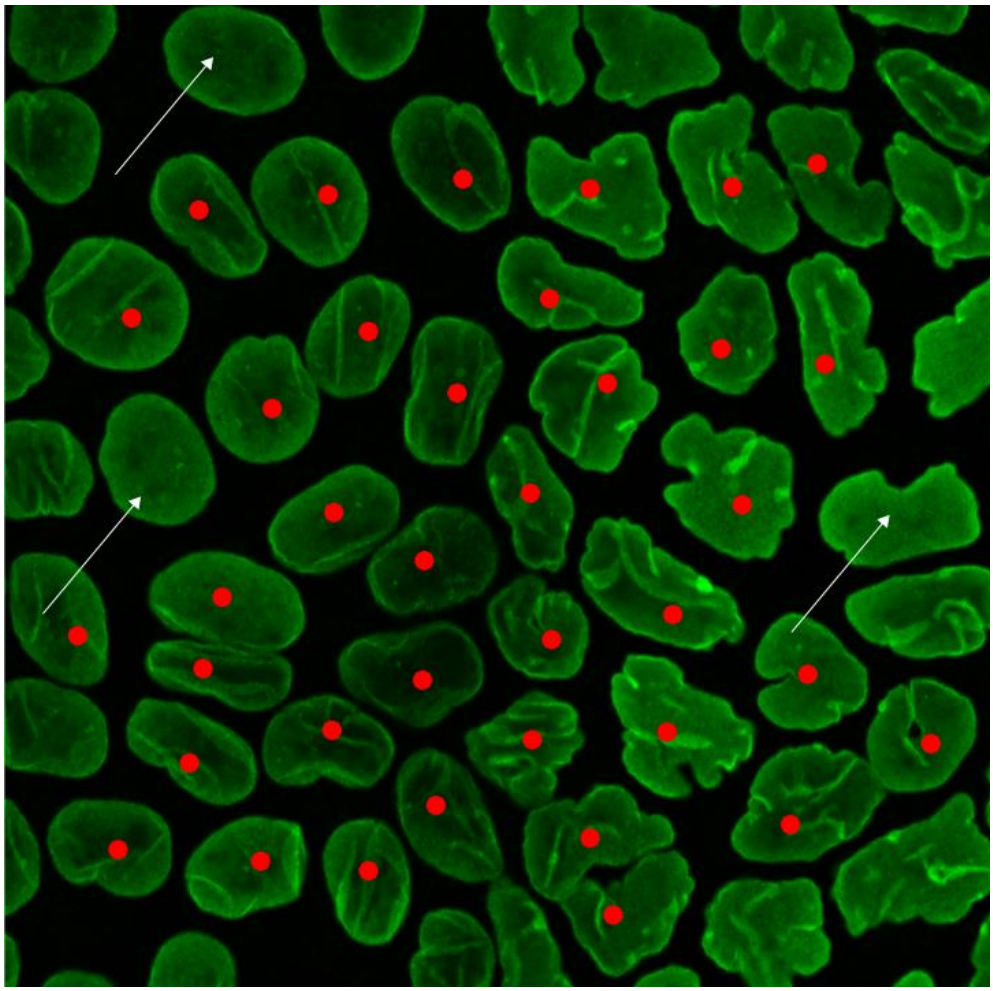

Appendix figure 1. The calculation of total and folded nuclei. The total nuclei and folded nuclei in each cell line were calculated from the field images. The folded nuclei are marked with red dots and were counted with ImageJ using the Measure tool. Only the nuclei that are entirely included in the image were calculated. The unfolded nuclei (indicated here with arrows) were not marked and were counted manually. The image shows one of the LA-KO samples.

APPENDIX 3. STUDENT'S T-TEST TABLES OF NUCLEI COUNTS AND 7D GROWTH

Two-tailed Student's T-test with the significance level 0.05 was used as a statistical measure to compare differences in nuclei counts and cell growth. The significant differences are highlighted in red. **A. The total nuclei counts** (shown in **Figure 9** and **Table 4**) **B. The counts of folded nuclei** (**Figure 9** and **Table 4**). The counts of the folded nuclei were normalized for each cell line by dividing by the total nuclei count of the cell line before applying the T-test. **C. The number of cells after the 7-day growth period.**

A.

Cell line	WT	LA-EGFP	LA-CB	d20-LA-EGFP	LA-KO
WT	1	2,70869E-08	2,4103E-14	0,016266923	1,07971E-06
LA-EGFP	2,70869E-08	1	8,53751E-07	0,109614998	3,32002E-11
LA-CB	2,4103E-14	8,53751E-07	1	5,3846E-05	5,26093E-14
d20-LA-EGFP	0,016266923	0,109614998	5,3846E-05	1	2,22995E-07
LA-KO	1,07971E-06	3,32002E-11	5,26093E-14	2,22995E-07	1

B.

Cell line	WT	LA-EGFP	LA-CB	d20-LA-EGFP	LA-KO
WT	1	0,35453151	0,267367	0,98287892	0,955324
LA-EGFP	0,35453151	1	0,785801	0,61087929	0,394411
LA-CB	0,26736686	0,78580102	1	0,49656285	0,299042
d20-LA-EGFP	0,98287892	0,61087929	0,496563	1	0,960269
LA-KO	0,95532401	0,39441085	0,299042	0,96026919	1

C.

Cell line	WT	LA-EGFP	LA-CB	d20-LA-EGFP
WT	1	0,09935592	0,036378785	0,028824894
LA-EGFP	0,099355918	1	0,360397851	0,213666349
LA-CB	0,036378785	0,36039785	1	0,095465966
d20-LA-EGFP	0,028824894	0,21366635	0,095465966	1

APPENDIX 4. STUDENT'S T-TEST TABLES FOR THE MORPHOLOGICAL FEATURES OF THE NUCLEUS

Two-tailed Student's T-test with the significance level 0.05 was used as a statistical measure to compare differences in nucleus morphology between the cell lines. All significant differences are highlighted in red. Notably, nucleus area in XY direction significantly differs between the WT cells and all other cell lines. In addition, LA-KO KO cells differs significantly from all other cell lines in XY circularity, XY aspect ratio (AR) and XY solidity, whereas their endogenous controls differ from all other cell lines in all YZ features except the area. Also, LA-CB cells significantly differ from other cell lines in YZ solidity.

A.

Cell line	WT	d20-LA-EGFP	LA-CB	LA-EGFP	LA-KO KO	LA-KO-ctrl
WT	1	0,000795139	1,08247E-05	0,012937161	0,001359097	0,000582751
d20-LA-EGFP	0,000795139	1	0,123609051	0,828386099	4,77447E-12	6,7866E-13
LA-CB	1,08247E-05	0,123609051	1	0,165470891	4,03873E-14	6,525E-15
LA-EGFP	0,012937161	0,828386099	0,165470891	1	4,57781E-07	1,87321E-07
LA-KO	0,001359097	4,77447E-12	4,03873E-14	4,57781E-07	1	0,755777814
LA-KO-ctrl	0,000582751	6,7866E-13	6,525E-15	1,87321E-07	0,755777814	1

B.

Cell line	WT	d20-LA-EGFP	LA-CB	LA-EGFP	LA-KO KO	LA-KO-ctrl
WT	1	0,018542256	0,10320603	0,00154927	0,250757404	0,737462802
d20-LA-EGFP	0,018542256	1	0,792526096	0,21365321	0,113177581	0,007607931
LA-CB	0,10320603	0,792526096	1	0,537565659	0,247875765	0,073460468
LA-EGFP	0,00154927	0,21365321	0,537565659	1	0,009329681	0,000661685
LA-KO	0,250757404	0,113177581	0,247875765	0,009329681	1	0,118908411
LA-KO-ctrl	0,737462802	0,007607931	0,073460468	0,000661685	0,118908411	1

C.

Cell line	WT	d20-LA-EGFP	LA-CB	LA-EGFP	LA-KO KO	LA-KO-ctrl
WT	1	0,548092779	0,336685566	0,848450477	9,39322E-16	0,318951075
d20-LA-EGFP	0,548092779	1	0,171213602	0,426519705	1,16631E-15	0,716700158
LA-CB	0,336685566	0,171213602	1	0,395925419	1,8789E-12	0,094153084
LA-EGFP	0,848450477	0,426519705	0,395925419	1	6,63476E-16	0,227314836
LA-KO	9,39322E-16	1,16631E-15	1,8789E-12	6,63476E-16	1	4,11681E-16
LA-KO-ctrl	0,318951075	0,716700158	0,094153084	0,227314836	4,11681E-16	1

D.

Cell line	WT	d20-LA-EGFP	LA-CB	LA-EGFP	LA-KO KO	LA-KO-ctrl
WT	1	0,788325661	0,262151321	0,25865388	0,08090357	0,000414629
d20-LA-EGFP	0,788325661	1	0,347628253	0,1410532	0,032330403	5,81209E-05
LA-CB	0,262151321	0,347628253	1	0,04037622	0,011373233	0,000125746
LA-EGFP	0,258653876	0,141053197	0,040376215	1	0,532603818	0,007500693
LA-KO	0,08090357	0,032330403	0,011373233	0,53260382	1	0,024076877
LA-KO-ctrl	0,000414629	5,81209E-05	0,000125746	0,00750069	0,024076877	1

E.

Cell line	WT	d20-LA-EGFP	LA-CB	LA-EGFP	LA-KO KO	LA-KO-ctrl
WT	1	0,754933387	0,068522953	0,37343616	0,00545194	0,553640566
d20-LA-EGFP	0,754933387	1	0,227462036	0,29412146	0,00543371	0,832590181
LA-CB	0,068522953	0,227462036	1	0,0110585	0,000180272	0,27678485
LA-EGFP	0,373436155	0,294121463	0,011058498	1	0,028640161	0,169613413
LA-KO	0,005451942	0,00543371	0,000180272	0,02864016	1	0,002431646
LA-KO-ctrl	0,553640566	0,832590181	0,27678485	0,16961341	0,002431646	1

F.

Cell line	WT	d20-LA-EGFP	LA-CB	LA-EGFP	LA-KO KO	LA-KO-ctrl
WT	1	0,527735326	0,073150819	0,06358607	0,24407805	0,000353031
d20-LA-EGFP	0,527735326	1	0,188589242	0,01742791	0,081892113	9,51194E-05
LA-CB	0,073150819	0,188589242	1	0,00306581	0,010713693	0,000100957
LA-EGFP	0,063586067	0,017427909	0,003065812	1	0,468574324	0,033526145
LA-KO	0,24407805	0,081892113	0,010713693	0,46857432	1	0,006923298
LA-KO-ctrl	0,000353031	9,51194E-05	0,000100957	0,03352615	0,006923298	1

G.

Cell line	WT	d20-LA-EGFP	LA-CB	LA-EGFP	LA-KO KO	LA-KO-ctrl
WT	1	0,483976198	0,049497427	0,46327369	0,022191254	0,422467049
d20-LA-EGFP	0,483976198	1	0,364546725	0,217391359	0,01224377	0,973915646
LA-CB	0,049497427	0,364546725	1	0,015281525	0,000505655	0,267638616
LA-EGFP	0,46327369	0,217391359	0,015281525	1	0,098325977	0,160683603
LA-KO	0,022191254	0,01224377	0,000505655	0,098325977	1	0,006287875
LA-KO-ctrl	0,422467049	0,973915646	0,267638616	0,160683603	0,006287875	1

H.

Cell line	WT	d20-LA-EGFP	LA-CB	LA-EGFP	LA-KO KO	LA-KO-ctrl
WT	1	0,589771373	0,859784121	0,177498509	0,41153278	0,003545554
d20-LA-EGFP	0,589771373	1	0,847618737	0,061140118	0,159911221	0,000400621
LA-CB	0,859784121	0,847618737	1	0,262415181	0,466458542	0,041561652
LA-EGFP	0,177498509	0,061140118	0,262415181	1	0,512957443	0,199104692
LA-KO	0,41153278	0,159911221	0,466458542	0,512957443	1	0,022265317
LA-KO-ctrl	0,003545554	0,000400621	0,041561652	0,199104692	0,022265317	1

I.

Cell line	WT	d20-LA-EGFP	LA-CB	LA-EGFP	LA-KO KO	LA-KO-ctrl
WT	1	0,685697854	0,480911641	0,391902807	9,13845E-13	0,587052668
d20-LA-EGFP	0,685697854	1	0,803814656	0,231493432	3,30153E-12	0,911274794
LA-CB	0,480911641	0,803814656	1	0,109959019	3,39872E-12	0,888807479
LA-EGFP	0,391902807	0,231493432	0,109959019	1	1,5016E-13	0,164318348
LA-KO	9,13845E-13	3,30153E-12	3,39872E-12	1,5016E-13	1	3,13352E-12
LA-KO-ctrl	0,587052668	0,911274794	0,888807479	0,164318348	3,13352E-12	1

J.

Cell line	WT	d20-LA-EGFP	LA-CB	LA-EGFP	LA-KO KO	LA-KO-ctrl
WT	1	0,261134793	0,035218393	0,073592301	0,002872478	5,6115E-07
d20-LA-EGFP	0,261134793	1	0,004473878	0,625833647	0,238727015	0,002655568
LA-CB	0,035218393	0,004473878	1	0,000370019	1,14453E-06	1,45985E-10
LA-EGFP	0,073592301	0,625833647	0,000370019	1	0,490732502	0,004678622
LA-KO	0,002872478	0,238727015	1,14453E-06	0,490732502	1	0,000759049
LA-KO-ctrl	5,6115E-07	0,002655568	1,45985E-10	0,004678622	0,000759049	1

APPENDIX 5. LIST OF USED BUFFERS

Buffer	Composition
Permeabilization buffer in immunostaining	0.5% BSA (Sigma-Aldrich, #A8022-100G, pH 5.2, ≥96%) 0.5% Triton™ X-100 (Sigma-Aldrich, #T8787-100ML) 1X PBS (10X DPBS, #14200-067, dilution 1:10)
Blocking buffer in western blot	3% BSA (Sigma-Aldrich, #A8022-100G, pH 5.2, ≥96%) 0.1% Tween® 20 (Sigma-Aldrich, #P9416-50ML) 1X TBS (10X TBS, VWR (Radnor, Pennsylvania, USA), #CAYM600232, pH 7.4, dilution 1:10)